

Noise Reduction in an Axisymmetric Supersonic Inlet using Trailing Edge Blowing

by

Christopher A. Saunders

Thesis submitted to the Faculty of the
Virginia Polytechnic Institute and State University
in partial fulfillment of the requirements for the degree of

Master of Science

in

Mechanical Engineering

Wing F. Ng, Chair
Ricardo D. Burdisso
Clint L Dancey
Jonathan L. Fleming

January 1998

Blacksburg, Virginia

Key words: Turbomachinery, Noise, Aeroacoustics, Struts

Copyright 1998, Christopher Saunders

Noise Reduction in an Axisymmetric Supersonic Inlet using Trailing Edge Blowing

by

Christopher A. Saunders
Dr. W. F. Ng, Chairman
Mechanical Engineering

(ABSTRACT)

Acoustic experiments were conducted in an anechoic chamber with a 1/14th scale model of a supersonic aircraft engine inlet using Trailing Edge Blowing (TEB) to reduce the engine fan noise from a turbofan propulsion simulator (TPS). The TPS is 4.1 in. (10.4 cm) in diameter and is powered by compressed air. The supersonic inlet is connected to the TPS and is geometrically and acoustically scaled from a working design. The supersonic inlet is operated in a takeoff or landing operating condition where the inlet core flow is subsonic. TEB is the process of ejecting high pressure air to re-energize the wakes of upstream fan disturbances such as struts or inlet guide vanes (IGV). The elimination of the wakes will provide a uniform flow field at the engine fan face and reduce noise at the blade passing frequency. The TEB was implemented on six non-uniformly spaced support struts in the inlet. Acoustic tests were then performed at 40%, 60% and 88% of the fan design speed (PNC) to measure the reduction in the blade passing tone (BPT) due to TEB from the struts with and without the presence of IGV.

The noise reductions without IGV at 40 PNC show the best results with the blade passing tone (BPT) being reduced by an average of 3.1 dB. The first harmonic of the BPT and the overall Sound Pressure Level (SPL) were also reduced by 1 dB. The addition of the IGV in the inlet reduced the effectiveness of the TEB. The addition of IGV changed the reduction in BPT at 40 PNC by 0.5 dB and the overall SPL was unchanged. At 60 PNC the addition of IGV reduced the reduction due to TEB in the BPT from an average of 2 dB to an average of 1 dB. The tests performed at 88 PNC showed negligible effects due to TEB. Aerodynamic experiments performed on the inlet that showed that the wakes of the IGV have a larger velocity defect than the struts, thus making the IGV a greater noise source.

Table of Contents

1.0	Introduction	1
2.0	Background.....	4
2.1	Previous Research	4
2.1.1	Fan Noise Theory	4
2.1.2	Virginia Tech Aircraft Inlet Noise Program	5
2.1.3	Applications of Trailing Edge Blowing	6
2.2	Understanding Fan Noise and the Effect of Inlet Aerodynamics.....	9
2.2.1	Understanding Fan Noise	9
2.2.1.1	Understanding Spectral Components of Fan Noise	9
2.2.1.2	Fan Noise Generation.....	10
2.2.1.3	Fan Noise Propagation and Radiation in an Aircraft Inlet	14
2.2.2	Understanding Strut and Inlet Guide Vane Wakes	16
3.0	The Experiment	20
3.1	Turbofan Propulsion Simulator.....	20
3.2	Supersonic Mixed Compression Inlet	23
3.2.1	Original Configurations.....	23
3.2.2	Modifications to Inlet for TEB	24

3.3 Research Facility	33
3.3.1 Bench Test	33
3.3.1.1 Strut Design Test Setup with Aerodynamic Measurements	33
3.3.1.2 Inlet Bench Test Setup	34
3.3.2 Anechoic Chamber	34
4.0 Results and Discussion.....	43
4.1 Acoustic Results	45
4.1.1 Acoustic Test at 30,000 RPM	45
4.1.1.1 30,000 RPM Tests without IG V	45
4.1.1.2 30,000 RPM Tests with IG V	49
4.1.2 Acoustic Tests at 50,000 RPM.....	52
4.1.2.1 50,000 RPM Tests without IG V	52
4.1.2.2 50,000 RPM Tests with IG V	55
4.1.3 Acoustic Tests at 70,000 RPM.....	57
4.1.3.1 70,000 RPM Tests without IG V	58
4.1.3.2 70,000 RPM Tests with IG V	61
4.1.4 Discussion of Acoustic Results.....	64
4.1.5 Comparison with Previous Research.....	68
4.2 Acoustic Analysis of the Boeing Translating Inlet	71
4.2.1 Analysis of the Rotor / Stator Interaction.....	71
4.2.2 Analysis of the Rotor / IG V Interaction	72
4.2.3 Analysis of the Rotor / Strut Interaction.....	75
4.3 Aerodynamic Test Results.....	75
5.0 Conclusions	79
References.....	82
Appendix A: Comparison of Strut Shapes and their Effects on Far Field Noise Levels	85

Appendix B: The Acoustic Effects of Struts and IGV Rotational Clocking.....91

**Appendix C: Comparison of Symmetric Strut Patterns to Asymmetric Strut
Patterns98**

Appendix D: Anechoic Chamber Aerodynamic Measurements..... 102

Appendix E: Bench Design Tests 108

Vita..... 115

List of Illustrations

Figure 2.1: Comparison of the Experimental Blowing Inlet with an Axisymmetric Supersonic Inlet.....	8
Figure 2.2: Typical Compressor Frequency Spectrum.....	12
Figure 2.3: Rotating Pressure Patterns in a 3 blade, 4 vane compressor	13
Figure 2.4: Typical Acoustic Radiation Pattern (Johnson and Fleeter, 1995).....	18
Figure 2.5 Typical Strut or IGV Wake.....	19
Figure 3.1: Turbofan Propulsion Simulator	22
Figure 3.2: Boeing Translating Inlet under wing of HSCT Aircraft.....	25
Figure 3.3 Isometric View of Boeing Translating Inlet	26
Figure 3.4: Boeing Translating Inlet Side and Front View	27
Figure 3.5: Boeing Translating Inlet during Testing.....	28
Figure 3.6: Boeing Strut Modified for Trailing Edge Blowing	29
Figure 3.7: Schematic of TEB Supply Piping	30
Figure 3.8: TEB Supply Air Plenum.....	31
Figure 3.9: Strut Air Supply Tubing Entering the Inlet Body	32
Figure 3.10 Experimental Setup for Blowing Strut Design Tests	37
Figure 3.11: Measurement Positions for Strut Design Test on Bench Blower.....	38
Figure 3.12: Testing of Inlet with Bench Test Blower.....	39
Figure 3.13: Test Locations for Inlet Tests on Bench Blower.....	40
Figure 3.14: The Virginia Tech Anechoic Chamber.....	41
Figure 3.15: Acoustic Measurement Locations	42

Figure 4.1: Directivity Plots of the Boeing Translating Inlet at 30,000 RPM without IGV	48
Figure 4.2 Directivity Plots of the Boeing Translating Inlet at 30,000 RPM with IGV ...	51
Figure 4.3: Directivity Plots of the Boeing Translating Inlet at 50,000 RPM without IGV	54
Figure 4.4: Directivity Plots of the Boeing Translating Inlet at 50,000 RPM with IGV ..	57
Figure 4.5: Directivity Plots of the Boeing Translating Inlet at 70,000 RPM without IGV	60
Figure 4.6: Directivity Plots of the Boeing Translating Inlet at 70,000 RPM with IGV ..	63
Figure 4.7: Comparison of the effect of IGV on TEB	66
Figure 4.8: Impact of IGV on the 1 st harmonic of the BPT at 70,000 RPM	67
Figure 4.9: Comparison of reductions in the BPT due to TEB with previous research....	69
Figure 4.10: Comparison of the wakes of blunt and sharp strut trailing edges	70
Figure 4.11: Acoustic Comparison of the influence of IGV on Acoustic Radiation Patterns	74
Figure 4.12: Acoustic Radiation Pattern of Rotor / Strut Noise	77
Figure 4.13: Contour Plot of Fan Face Velocity.....	78
Figure A.1: Isometric views of the VPI Faceted Strut and the Boeing Airfoil Strut.....	88
Figure A.2: Radiation Directivity of Faceted and Airfoil Struts at 50,000 RPM (60 PNC)	89
Figure A.3: Radiation Directivity of Faceted and Airfoil Struts at 70,000 RPM (88 PNC)	90
Figure B.1: Inlet Guide Vane / Strut Clocking positions	95
Figure B.2: Acoustic Radiation Directivity of Aligned and Offset IGVs at 50,000 RPM	96
Figure B.3: Acoustic Radiation Directivity of Aligned and Offset IGVs at 70,000 RPM	97
Figure C.1: Symmetric and Asymmetric Strut Patterns.....	100
Figure C.2: Acoustic Comparison of Asymmetric and Symmetric Strut Patterns	101
Figure D.1: Aerodynamic Measurement Locations.....	104
Figure D.2: Circumferential Aerodynamic Measurement Positions.....	105
Figure D.3: Aerodynamic Radial Traverses	106
Figure D.4: Circumferential Aerodynamic Traverses.....	107

Figure E.1: Previous Strut Designs for TEB	110
Figure E.2: Radial Traverse	111
Figure E.3: Tip Circumferential Traverse	112
Figure E.4: Midspan Circumferential Traverse	113
Figure E.5: Hub Circumferential Traverse	114

List of Tables

(ABSTRACT).....	2
Table 3.1 Experimental s^2 values for Acoustic Measurements.....	36
Table 4.1: Blowing Pressure used in acoustic tests.....	44
Table 4.2 Tone SPL Reductions for 30,000 RPM (40 PNC) without IGV	47
Table 4.3: 1 st Harmonic SPL Reductions for 30,000 RPM without IGV.....	47
Table 4.4: Tone Sound Pressure Level Reductions at 30,000 RPM (40 PNC) with IGV.....	49
Table 4.5: 1 st Harmonic SPL Reductions for 30,000 RPM (40 PNC) with IGV	50
Table 4.6: Tone SPL Reductions for 50,000 RPM (60 PNC) without IGV	53
Table 4.7: 1 st Harmonic SPL Reductions for 50,000 RPM (60 PNC) without IGV.....	53
Table 4.8: Tone SPL Reductions for 50,000 RPM (60 PNC) with IGV	55
Table 4.9: 1 st Harmonic SPL Reductions for 50,000 RPM (60 PNC) with IGV	56
Table 4.10: Tone SPL Reductions for 70,000 RPM (88 PNC) without IGV	59
Table 4.11: 1 st Harmonic SPL Reductions for 70,000 RPM (88 PNC) without IGV.....	59
Table 4.12: Tone SPL Reductions for 70,000 RPM (88 PNC) with IGV	61
Table 4.13: 1 st Harmonic SPL Reductions for 70,000 RPM (88 PNC) with IGV	62
Table 4.14: Comparison of the effects of IGV on the 1 st harmonic at 70,000 RPM	65
Table 4.15: Modal Analysis of Rotor / Stator Interaction	72
Table 4.16: Modal Analysis of the Rotor / IGV Interaction.....	73
Table 5.1: SPL Reductions due to TEB.....	80
Table A.1: Acoustic comparison of Faceted and Airfoil Struts at 50,000 RPM	86
Table A.2: Acoustic comparison of Faceted and Airfoil Struts at 70,000 RPM	87

Table B.1: BPT SPL increases at 50,000 RPM due to strut and IGV aligning	92
Table B.2: 1 st Harmonic SPL increases at 50,000 RPM due to strut and IGV aligning ...	93
Table B.3: BPT SPL increases at 70,000 RPM due to strut and IGV aligning	94
Table B.4: 1 st Harmonic of BPT SPL increases at 70,000 RPM due to strut and IGV aligning	94
Table C.1: Summary of Acoustic Analysis of the Symmetric Strut Pattern	99

Nomenclature

q	angular position (rad)
S	hub to tip ratio
W	shaft rotational speed (rad/sec)
W_m	mode rotational speed (rad/sec)
w	frequency (rad/sec)
dB	Decibel, sound pressure level, reference pressure 20×10^{-6} Pa
BPF	blade passing frequency
n	harmonic of BPF
B	number of rotors
N	shaft rotational speed (RPM)
r	radius
m	number of lobes or cycles of circumferential pressure variation
k	index
V	number of stators
k_{xm}	axial wave number
k_{mm}	characteristic number associated with E-functions
k	wave number of standing wave
c	speed of sound

m	radial nodes in the pressure patterns
f	frequency (Hz)
f_{mm}	cut-off frequency (Hz)
PNC	percent corrected fan speed
P_t	total pressure
SPL	sound pressure level

1.0 Introduction

In 1976, British Airways and Air France introduced the Concorde, the world's most successful commercial supersonic aircraft. The Concorde showed signs of great promise, but was ultimately doomed from the beginning because of two factors that were unforeseen. The first was the energy crises of the 1970's which drastically increased jet fuel costs. The second was the backlash against the environmental noise generated by the Concorde's four supersonic aircraft engines. Even during the first test flights, complaints were made about the takeoff and landing noise generated by the Concorde. This noise caused many countries to restrict the frequency of landings and takeoffs, which greatly hampered the Concorde's usefulness.

With the drop in oil prices in the 1990's, NASA, Boeing/McDonnell Douglas, General Electric Aircraft Engines, and Pratt and Whitney combined resources to research, design and eventually build a High Speed Civil Transport (HSCT). The HSCT aircraft will be an attempt to correct the problems of the Concorde design and take full advantage of the benefits of civilian supersonic travel. Foremost on the list of design criteria for the HSCT aircraft is the reduction in environmental noise, particularly at takeoff and landing. This thesis investigates the application of trailing edge blowing (TEB) to a HSCT candidate inlet to evaluate the potential benefits of TEB for the reduction of noise at takeoff and approach.

There are two major sources of noise generated by gas turbine aircraft engines. The first and loudest is exhaust noise generated by the jet of an engine. The second source is fan noise, which is caused by the interaction between the fan rotor and stationary vanes. Through the past thirty years, advances in the reduction of exhaust noise have made fan noise a much more noticeable component of the sound pressure levels that are heard by ground observers. Although exhaust is dominant during flight conditions, Trefny and Wessenbauer (1985) showed that "forward propagating fan noise is a significant component during takeoff and approach." The purpose of the experiments performed with Trailing Edge Blowing is to reduce the radiated fan noise.

The design of an aircraft inlet determines many of the properties of the radiated fan noise. Supersonic aircraft engines in particular are very sensitive to the inlet design because they have a much more complicated inlet geometry due to the demands placed on the inlet. While a subsonic inlet attempts to obtain the highest pressure recovery only in subsonic conditions, a supersonic inlet must do the same task in subsonic, transonic and supersonic flight conditions. This necessitates a translating centerbody or collapsible bifurcation ram to create the conditions for both supersonic and subsonic flight. In order for the HSCT program to be a success, the aircraft engine inlet must be designed to optimally limit fan noise. This thesis will focus on modifications to a candidate HSCT supersonic inlet to reduce the radiated fan noise by reducing the noise generation caused by the inlet during takeoff and landing when the inlet is in a sub operating position.

Leitch (1997) used an experimental blowing inlet to determine the effectiveness of trailing edge blowing in re-energizing the wakes of upstream fan disturbances at subsonic speeds and thus reducing the blade passing tone of an aircraft gas turbine. The experimental blowing inlet was neither subsonic nor supersonic but was designed to evaluate the viability of TEB in a lab environment. His experiments showed great promise for the application of TEB to HSCT inlet design.

Trailing edge blowing itself is not a new idea. For example, it has been used for decades as a part of turbine blade cooling schemes. The current research is unique because the application of TEB to the compressor side of the gas turbine with the goal of

reducing the flow distortions to the subsequent rotor and the resulting noise reduction is a new application. The research documented in this thesis applies TEB to an industry designed aircraft engine inlet to evaluate the acoustic benefits.

Several years ago, the Virginia Tech Supersonic Inlet Aeroacoustic Program was initiated to provide support to engine manufacturers in the design of potential inlets in the HSCT program. The purpose of the program is to analyze the generation and radiation of fan noise in candidate supersonic inlets. Experiments are performed with a small turbofan propulsion simulator (TPS) as a noise source and geometric models of the potential inlets. Previous studies have been documented by Nuckolls, Detwiler, Pande, Wagner, and Miller under this research program and will be reviewed in Chapter 2.

This thesis is organized in five chapters. Chapter 2 describes the research previously published and background information on fan noise and strut and inlet guide vane wakes. Chapter 3 details the experimental setups used for the thesis work, including the bench test and anechoic chamber. Chapter 4 presents and discusses the results of the experiments. Chapter 5 discusses the findings of the research and draws some conclusions.

2.0 Background

Chapter 2 is divided into two sections: The first will cover the previous research on the topic of fan noise, trailing edge blowing and the aeroacoustic research program at Virginia Tech. The second will explain the mechanisms of generation, propagation and radiation of fan noise in an axial compressor and how the inlet design effects the fan noise.

2.1 Previous Research

The previous research is divided into three categories. The first is previous research into fan noise theory. The second is a short description of the work completed by the aeroacoustic program at Virginia Tech. The third is published research in the area of wake filling using trailing edge blowing.

2.1.1 Fan Noise Theory

Tyler and Sofrin (1962) performed experiments the 1960's to explain the generating mechanisms of compressor noise. They focused on two aspects of noise generation. The first was the noise generated by the rotor alone. The second was the noise generated by the interaction of the rotor blades and the stator vanes. They also

gave predictions for the directivity of the noise radiated from the inlet opening. Their findings are considered the benchmark for modal analysis of the acoustics of aircraft compressors and will be explained in detail later in this chapter. Homicz and Lordi (1974) refined the radiation predictions of Tyler and Sofrin and included the effects of mean flow and a centerbody in the inlet.

Tyler and Sofrin performed their experiments using a uniform cylindrical duct without a centerbody in their inlet. While this inlet design is valid for understanding the acoustics of compressors, a supersonic aircraft inlet typically has a centerbody. The addition of a variable centerbody affects the modal shapes and acoustic propagation. As the hub and tip of the supersonic inlet changes, the modal wave changes shape also. Since the directivity of the radiation pattern is caused by the acoustic wave modal shape, the directivity will change as the acoustic wave propagates down the inlet. Research has shown that the radiation directivity formulae is acceptable for inlets with a hub to tip ratio less than 0.5.

2.1.2 Virginia Tech Aircraft Inlet Noise Program

The Virginia Tech Aircraft Inlet Noise Program was initiated in 1991 to assist the HSCT program in the evaluation of candidate supersonic aircraft inlet designs. The program is based around the use of a Tech Development Incorporated Model 460 Turbofan Propulsion Simulator connected to geometric models of potential HSCT inlets. Nuckolls and Ng (1993) performed experiments comparing two auxiliary door configurations on an axisymmetric supersonic inlet at landing speed. They showed that increasing the inlet distortion caused by opening the doors increases the forward radiated noise. Detwiler and Ng (1993) performed experiments with the same two auxiliary door configurations as well as a closed door configuration on an axisymmetric supersonic inlet at takeoff speed. They showed that the inlet throat Mach number does not have to be sonic in order to receive benefits of choking. Mach numbers greater than 0.50 will show slight reductions in forward propagated noise called "soft choking". Wagner and Ng

(1994) evaluated the acoustic properties of a two dimensional bifurcated supersonic inlet. Pande and Ng (1994) moved the struts of an axisymmetric inlet three chord lengths upstream from the design position to evaluate the effects of struts on the fan noise. By moving struts ahead of the fan face, the wakes of the struts mixed with the core flow giving a more uniform fan face pressure field. Pande's work showed that great acoustic benefit could be obtained by reducing the wakes of the struts. Miller and Ng (1995) compared the acoustics and aerodynamics of the two dimensional inlet with the axisymmetric inlet under static test conditions in an anechoic chamber.

2.1.3 Applications of Trailing Edge Blowing

Corcoran (1992) and Nauman (1992) performed experimental studies of "blowing from the downstream side of a body." The experiments were performed in a large water channel using a trailing edge blowing from a blade profile. Corcoran (1992) showed that trailing edge blowing is effective in reducing the mean wake deficit from the edge of the simulated blade. Nauman's (1992) work used a turbulent boundary layer at separation. He tested single slit, double slit and discrete jet blowing configurations. His research showed that the discrete jet configuration provided the most mixing in the near wake areas and therefore the least turbulence downstream. He also showed that the effect of trailing edge blowing can be greatly enhanced by the addition of vortex generators. Nauman concluded that the fluid characteristics of re-energized wakes were highly dependant on the mechanisms that cause the wakes.

Waitz et al (1995) performed experiments applying trailing edge blowing and boundary layer suction to fan blades in a compressor cascade. The research suggested that a "40% reduction of the steady wake velocity deficit and greater than 35% reduction of the unsteady velocity fluctuations in the wake can be achieved by removal of less than 3% of the fan mass flow through boundary layer suction, or through the addition of less than 1% of the fan mass flow through trailing edge blowing". Using the aerodynamic results, Linsub, a two dimensional linearized panel method, was used to predict the noise

reduction in an actual rotor. A 3 dB reduction in tone noise was estimated for the boundary layer suction and an 11 dB reduction in tone noise was estimated for trailing edge blowing.

Leitch (1997) performed experiments using high pressure blowing from the trailing edge of upstream struts to re-energize the wakes cause by the struts. His research was the first published experimental work using trailing edge blowing in the compressor section of a gas turbine for the purpose of reducing noise. Leitch used a simple inlet geometry consisting of two concentric cylinders and four struts 1.21 chord length upstream of the fan face. The experimental blowing inlet geometry is compared to a supersonic axisymmetric inlet geometry in figure 2.1. The major difference between a supersonic axisymmetric and the experimental inlet is the varying hub and tip values present in the supersonic axisymmetric inlet that are not present in the experimental inlet. The experimental inlet geometry is reasonable for experimental testing, but does not accurately represent a realistic design. Leitch performed his experiments at 40%, 60% and 88% of normal operating speed. His results showed that TEB reduced the tone and overall sound pressure levels at 40 PNC and 60 PNC. The tone sound pressure level was reduced by an average of 6 dB in the far field. Little benefit was shown at 88 PNC.

The research being presented in this thesis is the next step in applying the procedure documented by Leitch to a realistic supersonic inlet. The purpose of this research is to investigate how effective TEB is in reducing the noise radiated from an axisymmetric supersonic inlet.

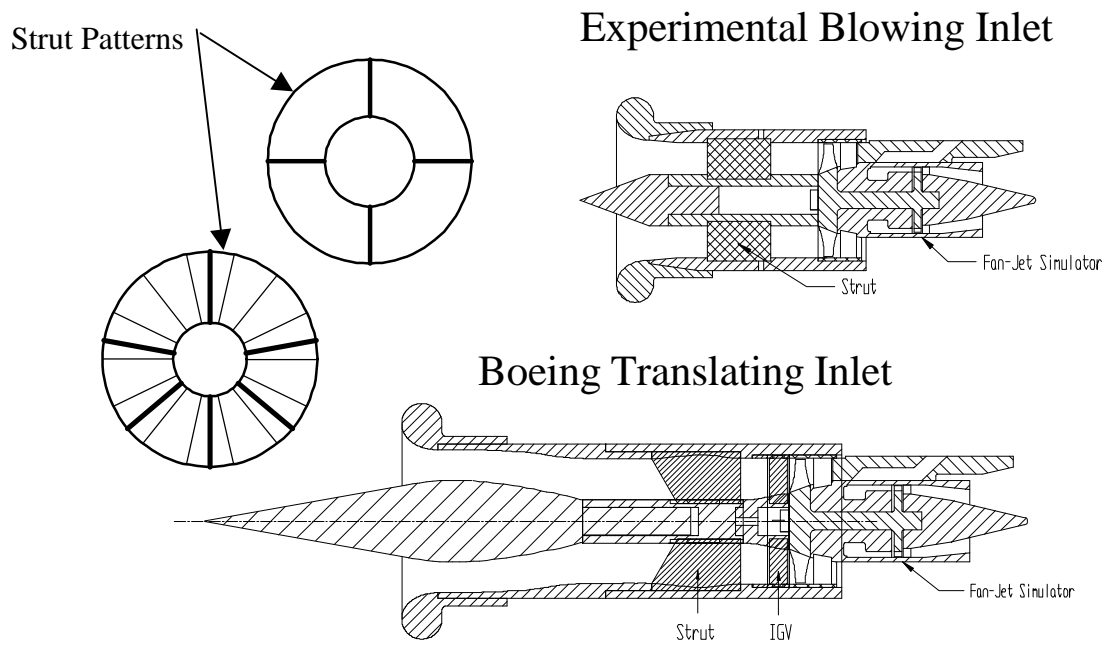


Figure 2.1: Comparison of the Experimental Blowing Inlet with an Axisymmetric Supersonic Inlet

2.2 Understanding Fan Noise and the Effect of Inlet Aerodynamics

In order to understand fan noise in a supersonic inlet, there are two areas which must be explained in more detail. The first is generation of the fan noise, and the second is how the fan noise is affected by the aerodynamics of the inlet.

2.2.1 Understanding Fan Noise

The knowledge of three areas is needed to have a basic understanding of compressor fan noise. The first is an understanding of the spectral components of fan noise. The second is an understanding of how fan noise is generated by the rotor and stator. The third is an understanding of the duct acoustics that govern the propagation of the noise down the inlet and the radiation to the far field.

2.2.1.1 Understanding Spectral Components of Fan Noise

There are three spectral components of compressor fan noise. The first is broadband noise. The broadband noise can be caused by vortex shedding, boundary layer turbulence, interaction of blade pressure fields and interaction between the blade pressure fields and the wall boundary layers. It is seen at every frequency and is typically equally distributed among all frequencies. Broadband noise is sometimes referred to as “white” noise.

The most dominant frequency is the blade passing frequency (BPF). The sound pressure level measured at the BPF is the blade passing tone (BPT). Tyler and Sofrin (1962) have shown that the noise generated at the BPF, also called tone noise, is due to the interaction between the rotor blades and the stator vanes or other flow disturbances.

The BPF is calculated by knowing the geometric properties of the inlet and compressor.

$$BPF = \frac{N}{60} B \quad (2.1)$$

where: N = the rotational speed of the rotor in RPM

B = the number of blades.

For example, the BPF of a 10,000 RPM rotor with three blades is 500 Hz. It should also be noted that the physical mechanism that creates the BPT also creates harmonics of the BPF.

The third component of fan noise is multiple pure tones or "buzz saw" tones. these occur when the blade tip speed surpasses the speed of sound, causing shock waves at the blade tips. Because of small imperfections in the blade as well as the highly non-linear nature of leading edge shocks, noise is generated at multiples of the fan rotational frequency. The frequencies the pure tones appear at are given by

$$f = \frac{N}{60} i \quad \text{where } i = 2, 3, 4, \dots, B-2, B-1 \quad (2.2)$$

where: f = the frequency of the pure tone

N = the rotation speed in RPM

B = the number of rotor blades

Figure 2.2 is a sample frequency spectrum that illustrates all three components of fan noise.

2.2.1.2 Fan Noise Generation

There are two noise generating mechanisms present in aircraft engines. The first is noise generated by the interaction of the rotor blade and stators or other flow disturbances. The second is the noise generated by the rotor itself.

Tyler and Sofrin (1962) examined discrete tone noise in compressors. The first area investigated was the rotor / stator interaction. As the rotor passes a stator, the wake of the rotor passes by the stator causing a modal peak heard as noise. Figure 2.3 illustrates wakes on a 3 blade rotor and a 4 vane stator. Each diagram in figure 2.3 shows

the rotor blade passing a different stator vane. Each time the rotor passes a stator, a peak or acoustic blip is generated. This is called a spinning mode since these blips will rotate at a certain frequency to create the BPF.

While an infinite number of acoustic modes are possible, only certain modes will exist in the inlet. Acoustic modes are determined geometrically by the number of rotor blades and the number of stator vanes. Equation 2.3 is used to determine the acoustic modes that will exist at the fan face of the inlet. In the equation,

$$|m| = nB + kV, \quad \text{where } k = \dots -1, 0, 1, 2, \dots \quad (2.3)$$

where: m = the modal number, which is the number of circumferential pressure lobes

n = the harmonic of the blade passing frequency (1=BPF, 2=1st Harmonic)

B = the number of rotor blades

k = the index

V is the number of stators or IGV

For symmetric geometry, equation 2.3 will give the only spinning modes that will propagate down the inlet. Upon calculation of the mode, the rotational speed of the mode can be calculated by

$$W_m = \frac{nB}{m} W \quad (2.4)$$

where: W_m = the rotational speed of the circumferential pressure lobes

n = the harmonic index

B = the number of rotor blades

m = the acoustic circumferential mode number

W = the shaft rotational speed (rad/sec)

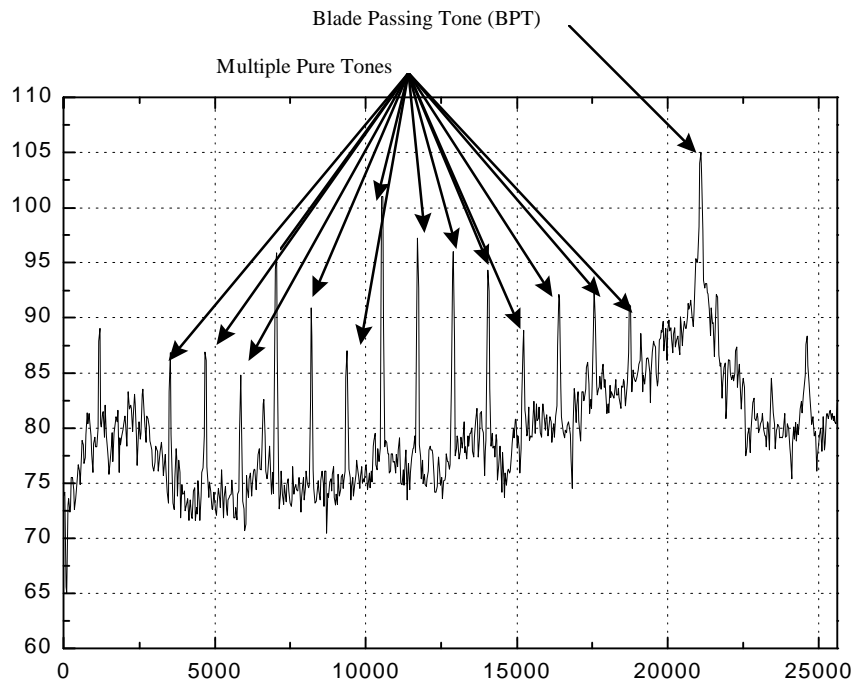


Figure 2.2: Typical Compressor Frequency Spectrum

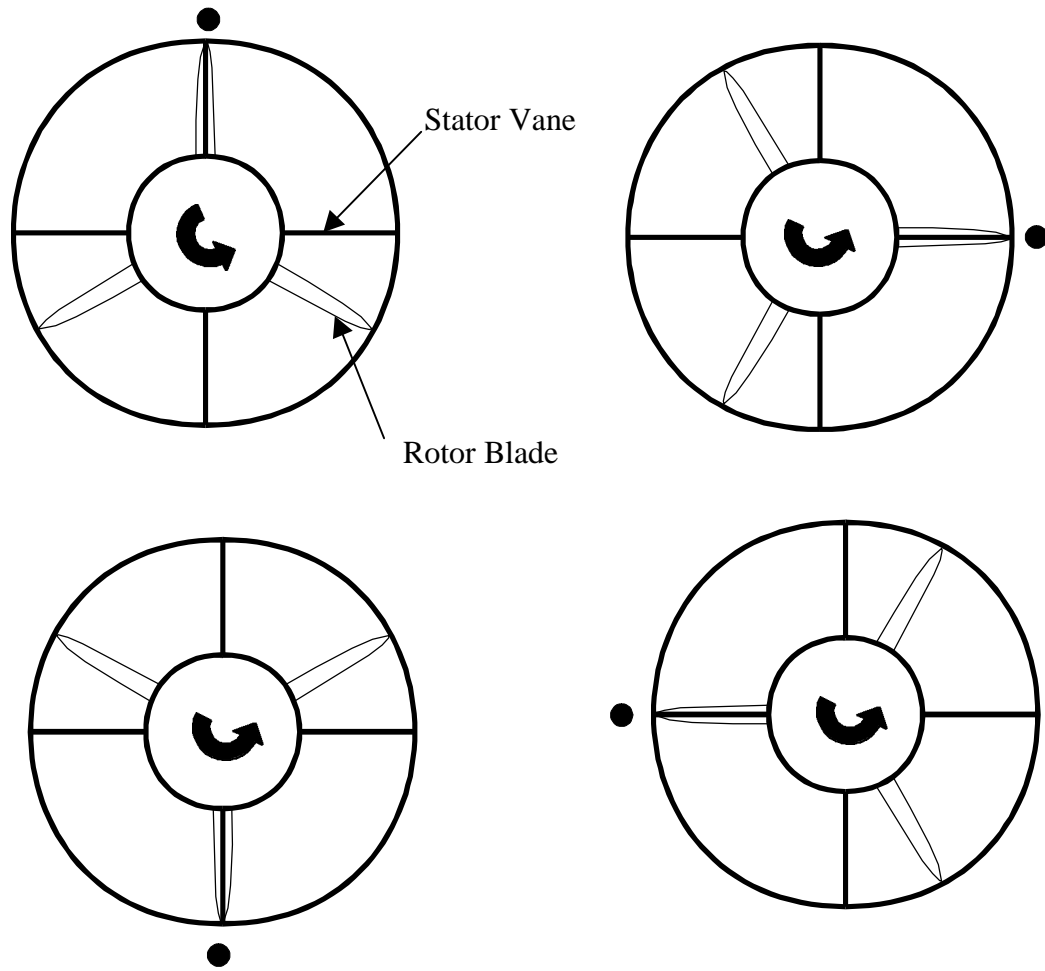


Figure 2.3: Rotating Pressure Patterns in a 3 blade, 4 vane compressor

Any disturbance that is not symmetric with respect to the inlet longitudinal axis can also generate acoustic modes. However, the non-symmetry creates standing modes as opposed to spinning modes. Noise is generated regardless of whether the mode is spinning or stationary.

Another component of aircraft inlet noise is generated only by the rotor when no other flow disturbances are present. This noise can be heard in propeller driven planes and helicopters where the propeller or rotor chops through the turbulence cause by the other blades on the rotor. Although rotor noise is primarily seen in helicopters, it is present in aircraft engine compressors. However, the noise generated by the rotor alone is insignificant in relation to the noise generated by rotor / stator interaction.

2.2.1.3 Fan Noise Propagation and Radiation in an Aircraft Inlet

After the noise has been generated, the next question is if the acoustic mode will propagate down the inlet. The axial wave number for the acoustic mode can be found by

$$k_{x\mu} = \sqrt{k^2 - k_{m\mu}^2} \quad (2.5)$$

where: $k_{x\mu}$ = the axial wave number

$$k = \frac{W}{c}, \text{ the standing wave number created by the rotor}$$

$k_{m\mu}$ = characteristic number associated with the E-functions depending on the hub/tip ratio (σ), the number of circumferential lobes (m) and the number of nodes (zero points) across the annulus (μ)

The cutoff frequency is associated with the zeros of the E-functions of the mode. The E-functions are linear combinations of Bessel Functions of the first and second kind that take into account the fan hub to tip ratio, the number of circumferential lobes and the number of zero pressure points across the annulus. The E-functions are derived directly from the solution of the acoustic wave equation in cylindrical coordinates.

If $k_{m\mu}$ is greater than k then the value of k_x will be imaginary. An imaginary axial wave number indicates that the acoustic wave generated is an evanescent wave.

Evanescent waves decay exponentially as they propagate down the axis of the inlet. If k_x is imaginary, the acoustic mode is considered to be “cut off” and will not propagate to the far field. However, if $k_{m\mu}$ is less than k , then the value of k_x will be real. The acoustic mode is then “cut on” and will propagate down the inlet and radiate to the far field.

When the acoustic waves reach the opening of the inlet, they are free to propagate to the far field. The inlet is assumed to be in an anechoic environment, where there are no reflections of the acoustic waves.

Homicz and Lordi (1974) developed equations for the duct mode radiation patterns of acoustic modes propagating down a cylinder. Each pressure mode will produce a radiation pattern in the far field. When measuring in the far field, the sound pressure level directivity is a composite of all the present acoustic modes. A full radiation directivity can be found, but for the purposes of this thesis, only the principle lobe angle is calculated. Equation 2.6 describes the location of the principle lobe.

$$y_p = \cos^{-1} \left(b \sqrt{\frac{1 - \left(\frac{v_{nm}}{\bar{k}a}\right)^2}{1 - M^2 \left[1 - \left(\frac{v_{nm}}{\bar{k}a}\right)^2\right]}} \right) \quad (2.6)$$

where: y_p = the angle of the principal lobe of the radiation directivity of the acoustic mode

$v_{nm} = k_{m\mu}$ = the characteristic number associated with the E-functions

M = inlet core flow Mach Number

$$b = \sqrt{1 - M^2}$$

$\bar{k} = \frac{k}{b}$ = standing wave number with Mach number effects included

a = the radius of the inlet

These equations are applicable for aircraft engine inlets with a hub to tip ratio of less than 0.5.

While only the principle lobe is calculated for each acoustic mode, a series of lobes actually exists. The radiation pattern is a series of lobe peaks and zeros or lobe

minima. The number of lobes will equal the number of radial acoustic modes. An example of a typical lobe pattern is given in Figure 2.4.

A special case is the $m = 0$ mode. This is referred to as the axisymmetric mode because there is only one pressure lobe. The presence of an $m = 0$ mode is evident by a principle directivity lobe at the 0° measurement angle. This is because all of the acoustic energy propagates straight out the axis of the inlet with no deflection angle.

2.2.2 Understanding Strut and Inlet Guide Vane Wakes

As stated above, fan face flow distortion is a large contributor to blade passing tone noise generation. Supersonic aircraft inlets typically have struts and IGV that create fan face flow distortion. Struts are usually support devices that give structural support to a centerbody. IGV are located directly in front of the fan face and normally turn the core flow into the fan rotor. Since the inlet model uses thin flat plates to simulate the wakes of IGV, the flow turning capabilities of IGV are ignored. The velocity deficits caused by upstream struts and IGV create unsteady flow fields that the rotor must pass through. Those unsteady flow fields cause tone noise in the same way that the rotor and downstream stator interaction causes tone noise. An understanding of the flow distortions that are created by the struts and IGV reveals how TEB can be a viable method of reducing tone noise.

The flow disturbance created by the struts and IGV has two components. The first is a loss due to vortical effects, or viscous effects known as the wake. The wake is created when the boundary layers that are developing along the surface of the strut or IGV meet at the trailing edge creating an area of low velocity compared to the core flow. The wake can be amplified by the separation of the boundary layer from the strut or IGV surface. The second component is potential effects due to the blockage in the flow created by the strut or IGV. The potential effects are located near the strut surface and decay exponentially with axial distance while the wake decays linearly with axial distance. Since the potential effects are small and will decay much quicker than the wake,

they are not an important factor in this research. Figure 2.5 shows a typical strut or IGV wake.

Since the wakes of upstream disturbances interact with the fan rotor to generate tone noise, the reduction or elimination of the wakes will reduce the tone noise associated with the wakes. There are several ways in which this principle has been applied in the past. Since the wake of the strut decays with distance, the greater the distance between the disturbance and the fan face, the less impact the wake has on the fan noise. This principle has led to increasing the distance between rotors and stators. Also, the geometry of the strut or IGV, such as the leading edges, trailing edges and camber, can increase or decrease the width and depth of the wake. Mani (1968) and others are performing research to derive models from experimental data to predict the location of acoustic noise given a fan face distortion. Since most of the predictive tools are under continuing improvement and most are proprietary to the companies that developed them, they were not used in this project. The effect of the geometry on the acoustic sound pressure levels in the Boeing Translating Inlet is documented in appendices A and B. By reducing the wake generated by the strut or inlet guide vane, the tone noise can be reduced. The goal of TEB is to reduce the wake of the upstream flow disturbance thereby reducing the tone noise generated.

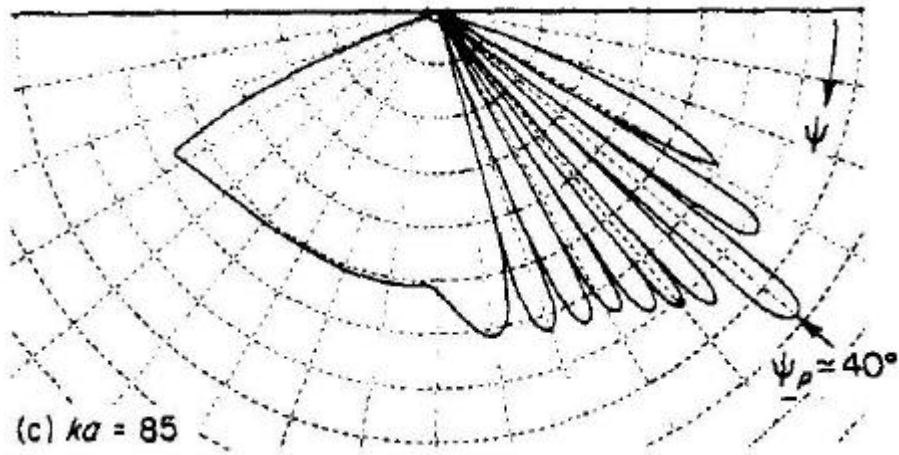


Figure 2.4: Typical Acoustic Radiation Pattern (Johnson and Fleeter, 1995)

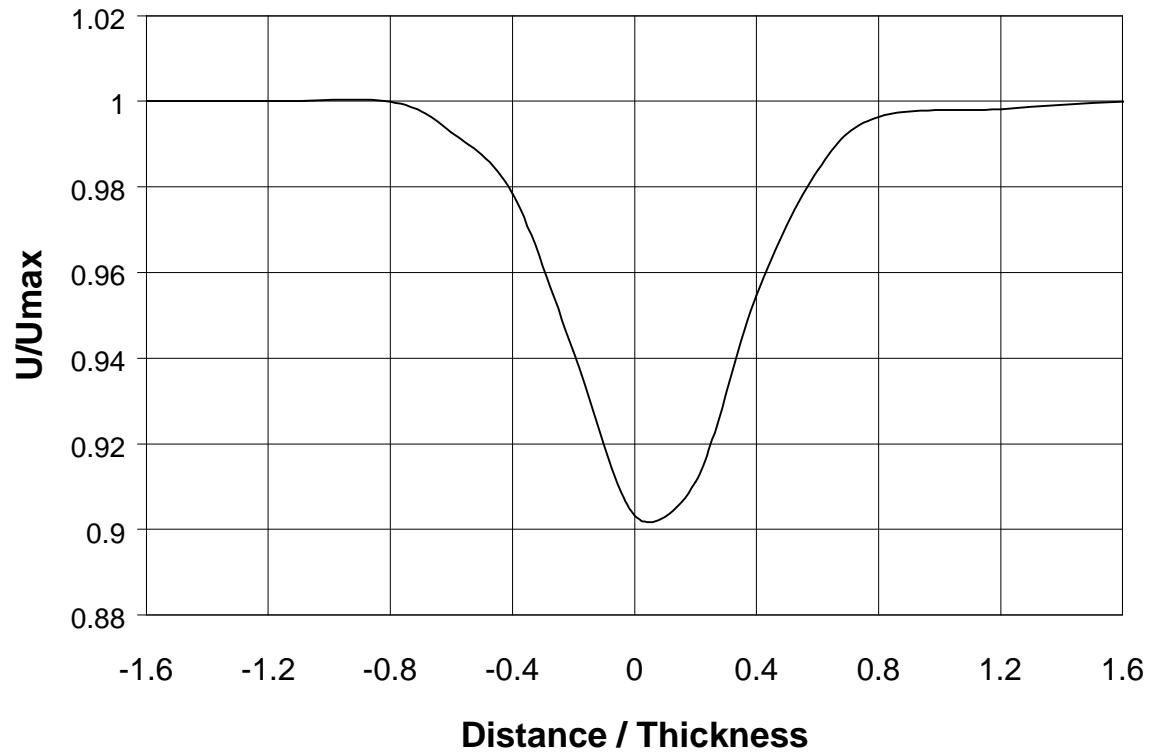


Figure 2.5 Typical Strut or IGV Wake

3.0 The Experiment

The effects of trailing edge blowing (TEB) were evaluated on a 1/14th scale model of the Boeing Translating Inlet with a Turbofan Propulsion Simulator (TPS). The inlet is a geometrically and acoustically scaled model of a working design. A supersonic inlet design was chosen to allow for correlation to needs in the High Speed Civil Transport (HSCT) research program. The inlet model was coupled with a TPS to simulate the bypass fan of an aircraft engine. This equipment was tested in both a bench situation and in an anechoic chamber to evaluate the acoustic benefits of TEB. The goal of the testing is to evaluate the effectiveness of trailing edge blowing on a working aircraft inlet design.

This chapter describes the experimental setup. The first section describes the TPS used in the experiments. The second section details the mixed compression supersonic inlet used with the TPS. The third section covers the research facility, equipment and test procedures used for the experiments.

3.1 Turbofan Propulsion Simulator

The experiments were performed using a Tech Development Incorporated Model 460 Turbofan Propulsion Simulator. The TPS simulates the acoustics and aerodynamics of a high bypass fan in an aircraft gas turbine engine. The TPS works in a fashion similar to an ordinary gas turbine, except without a combustor. High pressure air from an outside

source is fed into a single stage turbine. The turbine is connected on a shaft to a single stage fan. Figure 3.1 shows the TPS with the rotating components removed from the simulator body.

The TPS uses externally compressed air to drive a turbine in the simulator body. The single stage turbine has 29 blades and a maximum mass flow rate of 1.5 lbm/sec (0.68 kg/s). Instrumentation on the TPS turbine includes thermocouples to measure the turbine bearing temperatures and a magnetic speed pickup to measure the rotational speed.

The TPS has a single stage fan which draws air into the TPS. The fan rotor has 18 fan blades and 26 stators. The rotor diameter is 4.1 in. (10.4 cm) with a hub to tip ratio of 0.44 at the fan inlet. The design rotational speed of the TPS is 80,000 RPM where the fan produces a total pressure ratio of 1.6. The maximum fan mass flow is 2.72 lbm/sec (1.23 kg/s) at design speed. Thermocouples are also used on the fan bearings to monitor the performance of the TPS. In the experiments, the speeds measured are 30,000 RPM (40 PNC), 50,000 RPM (60 PNC) and 70,000 RPM (88 PNC), which represent taxiing, landing and takeoff speeds respectively. At 65,000 RPM (80 PNC), the fan blade tip speed becomes supersonic and shock waves produce multiple pure tones. The interaction of the rotor and the exit guide vanes or stators produces fan noise that begins to propagate at 33,500 Hz.

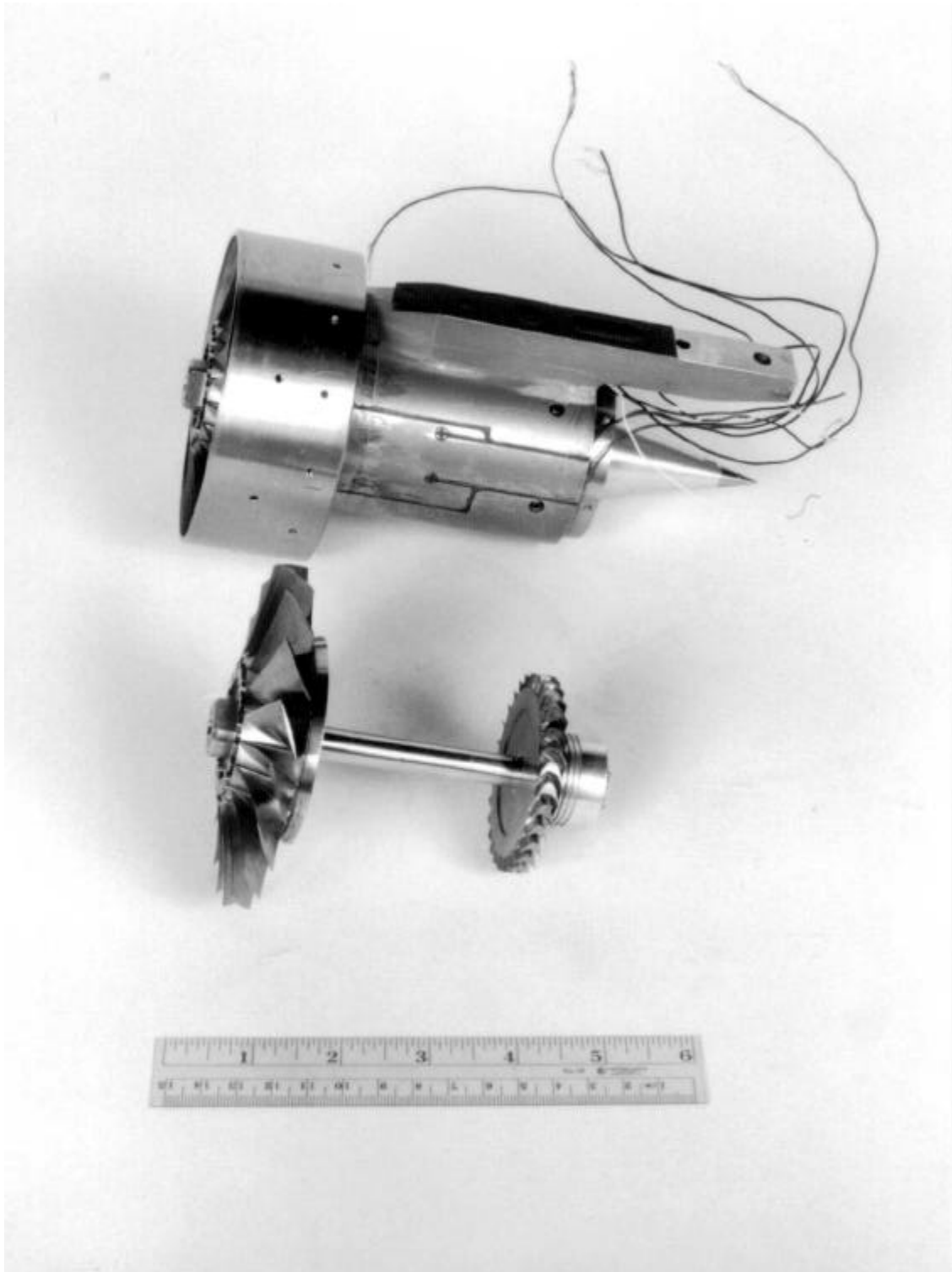


Figure 3.1: Turboprop Propulsion Simulator

3.2 Supersonic Mixed Compression Inlet

A supersonic, mixed compression, axisymmetric aircraft engine inlet model was used in the experiment. Although the inlet geometry and flow fields are not truly symmetric with respect to the inlet axis, the term “axisymmetric” is used to differentiate between cylindrical and two dimensional inlet geometry. Figure 3.2 is a schematic of the inlet attached to an aircraft wing. The inlet will be discussed in two parts. The first section is the original inlet configuration. The second section covers the modifications made to the inlet to allow for TEB in the struts.

3.2.1 Original Configurations

The inlet is a candidate inlet for the HSCT aircraft and has a conical translating centerbody to create the conditions necessary for subsonic and supersonic flight. An isometric view of the inlet is given in figure 3.3. For the purposes of this experiment, the centerbody is fully forward in a subsonic takeoff and landing position. There are six axisymmetric struts located behind the translating section of the inlet, which provide support for the centerbody. Figure 3.4 shows the inlet front a side view along with a view of the strut and IGV patterns. The struts are not uniform in circumferential spacing due to two auxiliary doors located in the two largest gaps between the struts. The auxiliary doors are shown in figure 3.2 with the engine inlet underneath the aircraft wing. For the purposes of this experiment, the doors will remain closed. There are fourteen 0.031 in. (0.79 mm) thick steel plates that generate flow disturbances to simulate IGV. The IGV plates are directly upstream of the fan face and downstream of the struts. The IGV assembly is capable of rotating with respect to the strut locations. In these experiments, the IGV assembly will be offset from the struts such that the wakes of the struts do not impinge on the downstream IGV. This subject is discussed further in appendix B. The Virginia Tech model of this inlet has a bellmouth to prevent flow

separation at the lip due to the static conditions of the tests. This inlet was designed by the Boeing Aircraft Company and will be referred to as the Boeing Translating Inlet.

3.2.2 Modifications to Inlet for TEB

The Boeing Translating Inlet was modified to allow the injection of air into the strut bodies for TEB. Holes were drilled at the junction of the strut with the outer inlet wall to allow high pressure air to enter the strut body through $\frac{1}{4}$ in. (0.635 cm) copper refrigeration tubing. Figure 3.5 shows the Boeing Translating inlet during testing with the blowing tubes attached.

Each strut was designed to allow for the blowing of high pressure air out of the trailing edge of the strut. The details of the design process are given in appendix E. The final strut design is shown in figure 3.6. Air enters a cavity in the strut from the tip junction with the inlet wall. The cavity is a plenum, created in the strut to allow a uniform total pressure field at the exit holes. Six equidistant exit holes were drilled, each with a diameter of 0.031 in. (0.79 mm).

A plumbing system was designed to facilitate the TEB from the struts. Figure 3.7 is a schematic of the plumbing for the blowing air. For these experiments, three breathing air bottles were used as the high pressure air source. All three bottles were connected to a pressure manifold consisting of $\frac{1}{2}$ in. (1.27 cm) copper refrigeration tubing. A needle valve was used to control the mass flow from the manifold. Flexible $\frac{3}{8}$ in. (0.95 cm) 125 psi (863 kPa) air hose was used to bring the blowing air into the anechoic chamber. The air hose connected to a 9 gallon (25 L) air tank that was modified to be a plenum. The plenum is shown without acoustic covering in figure 3.8. The plenum was instrumented with a static pressure transducer and a thermocouple to measure the properties of the air flow. The upstream needle valve was used to control mass flow based on the pressure readings from the plenum. From the plenum, six $\frac{1}{4}$ in. (0.635 cm) (OD) Copper Refrigeration tubes were used to route the air to the inlet.

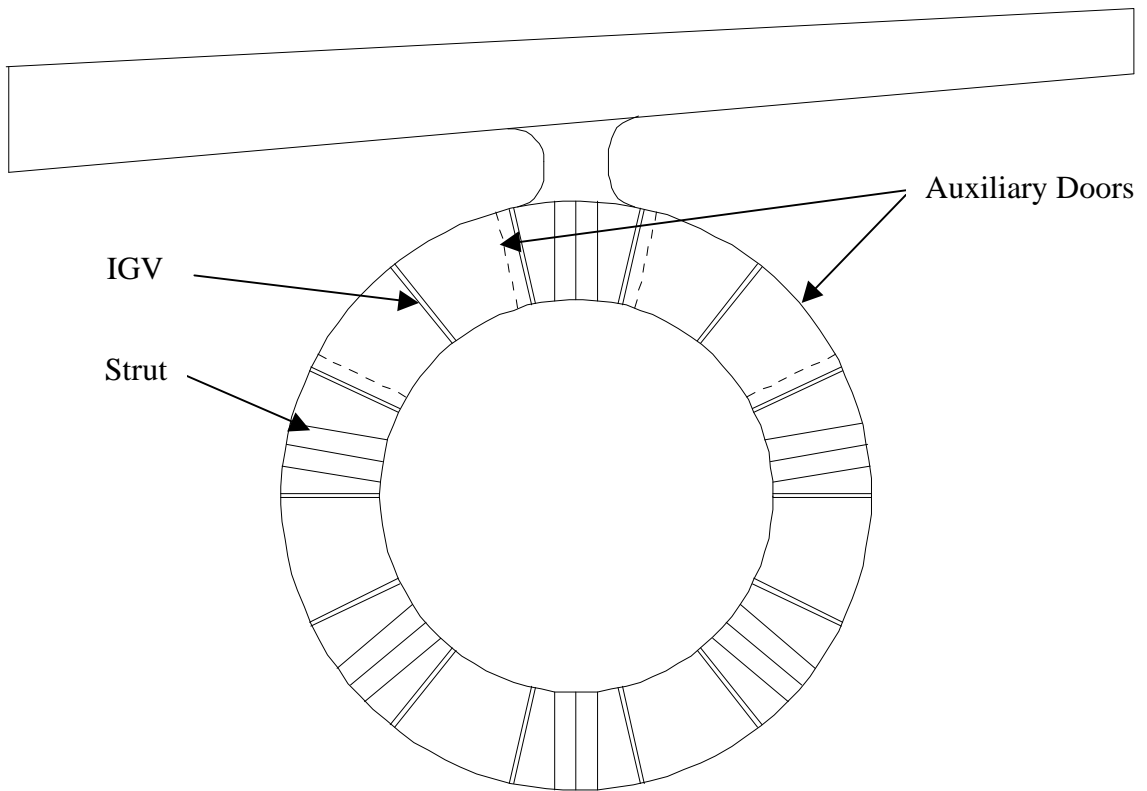


Figure 3.2: Boeing Translating Inlet under wing of HSCT Aircraft

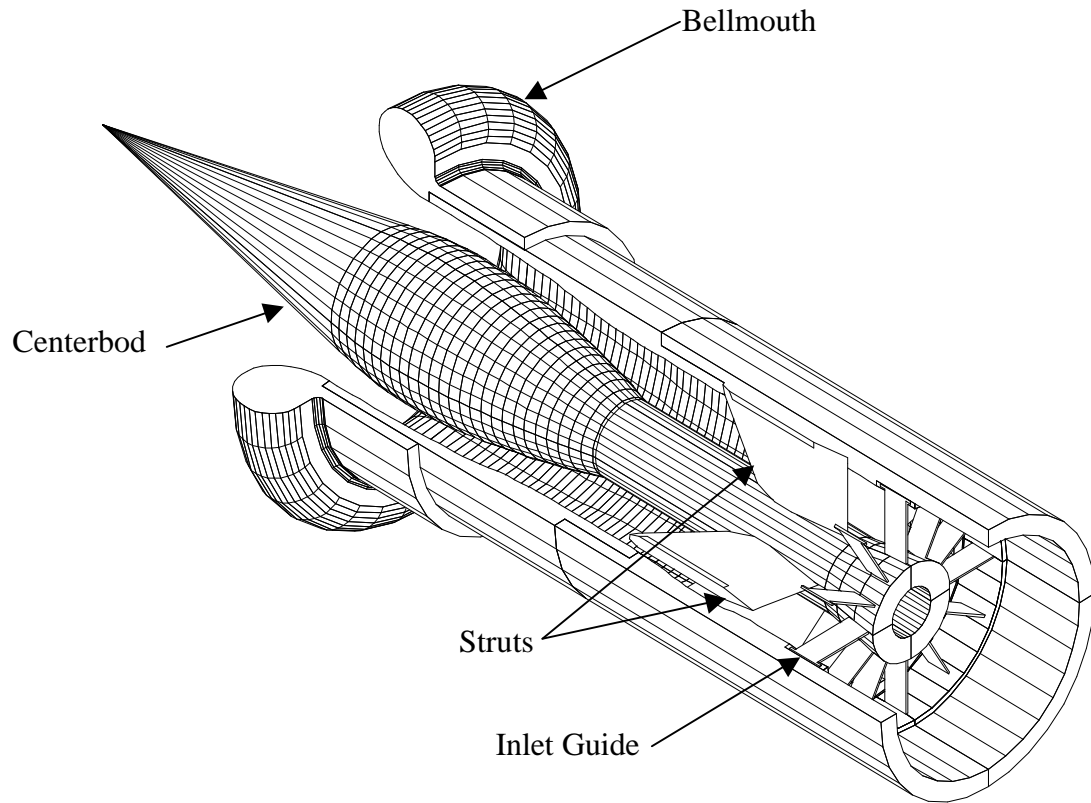


Figure 3.3 Isometric View of Boeing Translating Inlet

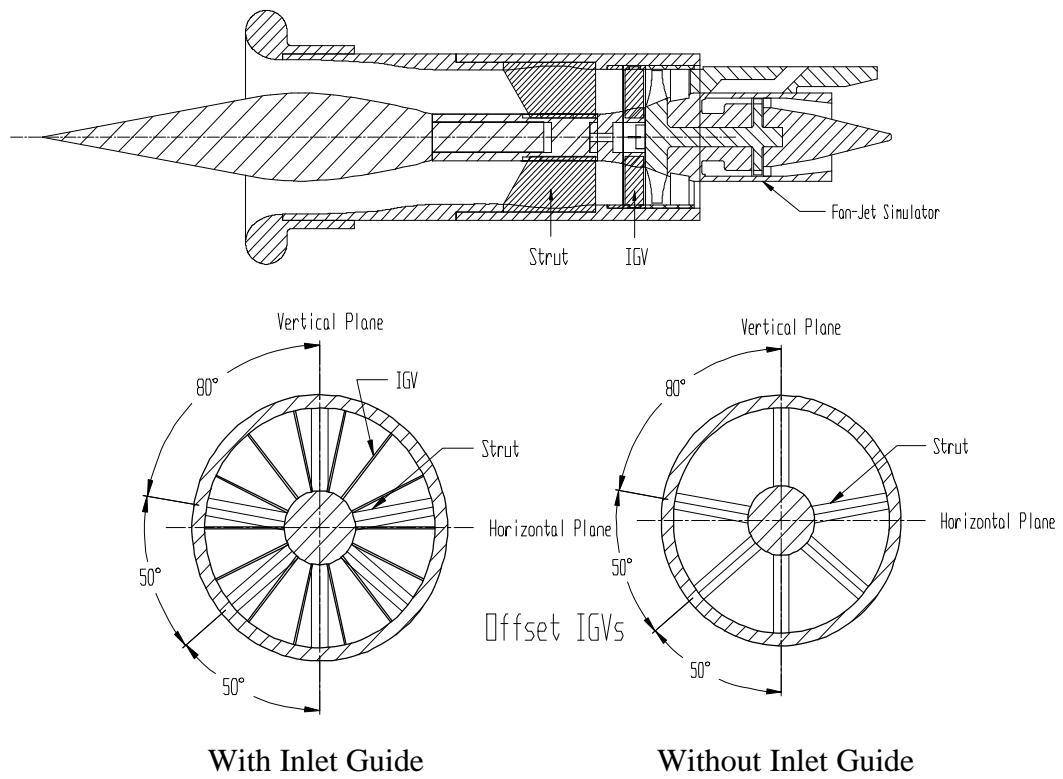


Figure 3.4: Boeing Translating Inlet Side and Front View



Figure 3.5: Boeing Translating Inlet during Testing

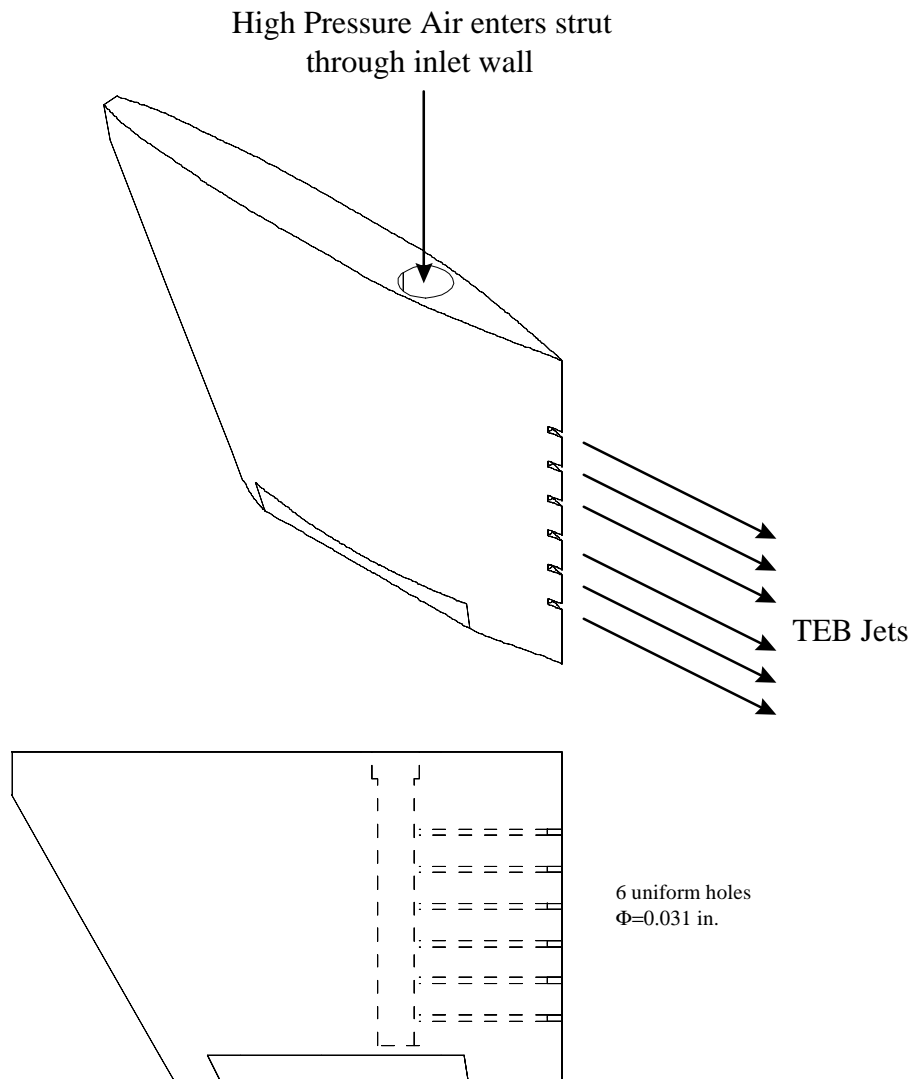


Figure 3.6: Boeing Strut Modified for Trailing Edge Blowing

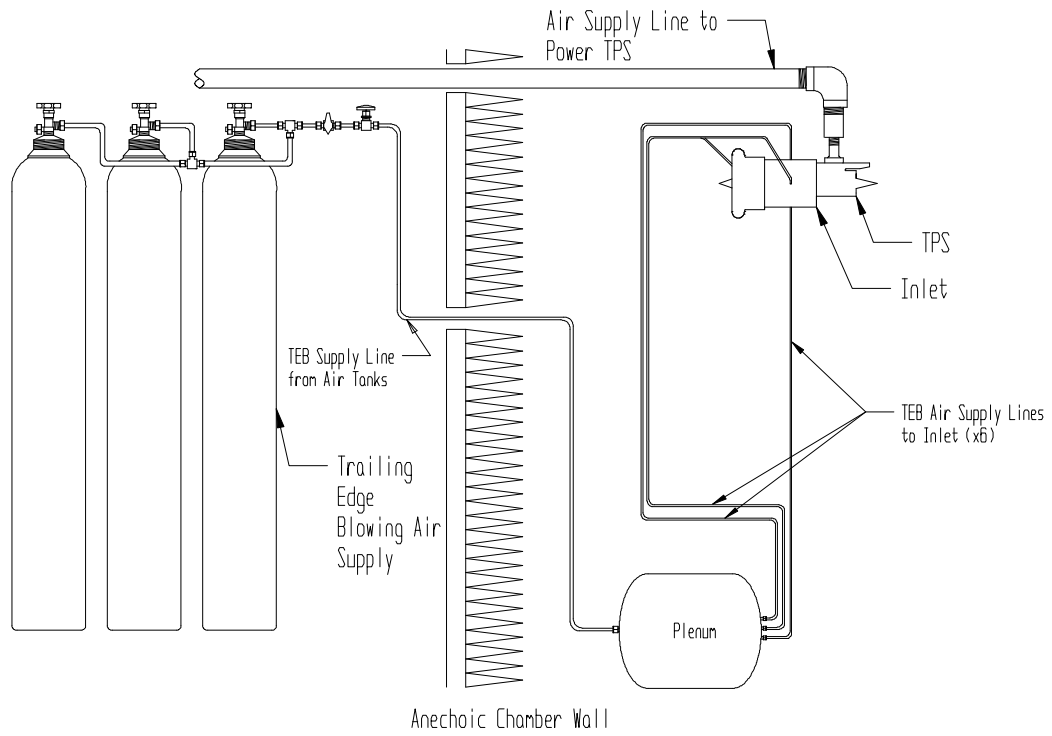


Figure 3.7: Schematic of TEB Supply Piping



Figure 3.8: TEB Supply Air Plenum

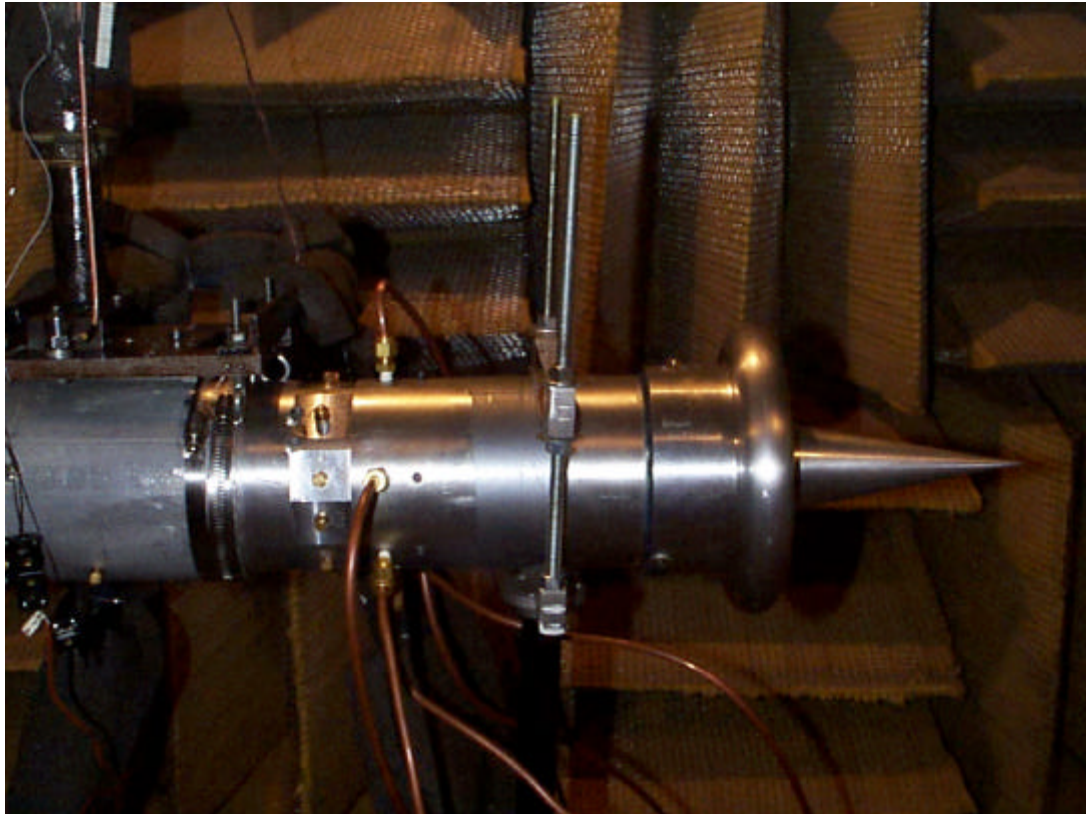


Figure 3.9: Strut Air Supply Tubing Entering the Inlet Body

3.3 Research Facility

There were two research facilities used in the experiments. The first facility used is a low speed blower used for a bench test. The second is the Virginia Tech Anechoic Chamber used to simulate acoustic free space for sound pressure level measurements.

3.3.1 Bench Test

A low speed blower was used for two experiments. The blower is shown in figures 3.10 and 3.12. The centrifugal blower is driven by a 5 HP electric motor and is mounted approximately 12 in. above the lab floor. The first experiment used the blower exhaust to generate a flow field in which to examine the different blowing hole configurations as well as the strut wakes. Figure 3.10 is a picture of the blower exhaust used in the strut design bench test. The second uses the blower inlet with the Boeing Translating Inlet to measure the aerodynamics of the inlet in finer detail than can be accomplished in the anechoic chamber.

3.3.1.1 Strut Design Test Setup with Aerodynamic Measurements

During the blowing strut design phase, it was necessary to examine the wake profiles of different strut blowing arrangements. Since detail in the aerodynamic measurements was needed, a bench setup was used. Figure 3.10 shows the bench setup used with the blower. A test strut was sandwiched between two sheets of Plexiglas to simulate the boundary layers on the hub and tip walls of the inlet. This test assembly is placed at the blower exit for aerodynamic measurements using pitot static probes. Figure 3.10 shows the aerodynamic measurements stations behind the trailing edge of the strut. One radial and three circumferential traverses were used to characterize the flow for each condition. Each radial traverse has a distance of 0.1 in. (2.54 mm) between each position

and each circumferential traverse has 0.05 in. (1.27 mm) between each position. Each strut design was tested under three conditions. First, the wake of the strut was measured with the fan blower on. Second, the jet from TEB was measured with the fan blower off. Last, filling of the strut wake was measured with both the TEB jet from the strut and the fan blower. This strut design bench test allowed for the analysis of several strut blowing designs. Further details of this design process are given in Appendix E.

3.3.1.2 Inlet Bench Test Setup

Although the single strut bench design test was helpful in designing and understanding the fluid mechanics of the Boeing Strut, there was a need to examine in detail the aerodynamics of the Boeing Translating Inlet at the fan face. A flange was connected to the intake of the blower which was specifically made to connect to the Boeing Translating Inlet. Figure 3.12 shows the Boeing Translating Inlet on the bench test blower intake during testing. A pitot-static probe was used to take detailed aerodynamic measurements at seven radial locations. The measurement locations are shown in figure 3.13. Due to the symmetry in the inlet, a span of 25° was measured. The probe was rotated at 1° increments at a fan face of the inlet. The aerodynamic survey started 5° from the centerline of a strut and finished 20° on the opposite side of the strut. This test pattern enabled the measurement of the strut and IGV wakes.

3.3.2 Anechoic Chamber

The Virginia Tech Anechoic Chamber is 4.0 x 2.7 x 2.2 meters in size. The surfaces of the chamber are Owens Corning Type 705 Fiberglass, cut in to wedges 0.91 meters thick. An elevated metal grate floor is installed above the floor fiberglass wedges to provide a working surface for the chamber. The chamber is anechoic above 200 Hz and has a background noise level of 30 dB. This background noise level is 80 dB below the average BPT and 50dB below the average broadband noise level of the TPS.

The simulator is placed 48 in. (122 cm) above the metal grate floor of the anechoic chamber where it is attached to a steel test stand. The test stand is secured to the chamber floor to limit vibration. The turbine supply air enters the room through a 2 in. high-pressure steel pipe which is secured to the chamber floor and bolted by a flange to the inlet test stand. The exhaust from the TPS is directed out of the chamber to the atmosphere through a 12 in. duct. All exposed metal surfaces including the TEB supply air plenum are covered with anechoic foam to limit the acoustic reflection. Figure 3.14 shows the interior of the Virginia Tech Anechoic Chamber during testing.

A Hewlett Packard Model 8360 Signal analyzer is used to process the acoustic signals. The microphone signal is first filtered using a Hanning Window and then converted to a power spectrum using a Fast Fourier Transform. The spectrum analyzer processes the power spectrum between the frequencies of 0 Hz and 102.4 kHz with a bandwidth of 128 Hz. Although the human audible range does not exceed 25 kHz, the harmonics of the blade passing frequency are of interest because several of the harmonics will scale down into the audible range when the TPS model is scaled up to working size.

Five to seven data sets are used when taking an acoustic measurement. Each data set is an average of twenty power spectrums. Every time a data set is taken, the BPT, the first harmonic of the BPT, and the overall SPL is recorded. Data sets are taken and recorded until the BPT of the data sets are within ± 1 dB of each other.

The acoustic microphone used for the experiments is a $\frac{1}{4}$ in. (0.635 cm) Bruel and Kjaer model 4136 condenser microphone. The microphone is calibrated from 0 Hz to 200 kHz, but is only linear below 30 kHz. For the nonlinear range, the manufacturer's calibration is used to correct the reading. The microphone signal is sent to a Bruel and Kjaer model 2639 pre-amps and then to a Bruel and Kjaer model 5935 Power Supply before going to the signal analyzer.

Figure 3.15 shows the measurement locations in relation to the inlet. Acoustic measurements were taken at twelve different far field locations. All measurement stations were 48 in. (189 cm) from the inlet opening and 48 in. (189 cm) from the chamber floor. The inlet can be measured in several acoustic planes due to the asymmetry in the inlet. The major planes are along horizontal and vertical lines of

symmetry. Since noise reductions due to TEB were shown to be present in two planes in Leitch (1997), only the horizontal plane was measured.

Acoustic measurements of fan noise can vary greatly. The microphone signals are measured voltages that are converted into pressures that fluctuate with time. The fluctuation in the magnitude of the pressures is so large that it is helpful to compare the pressure magnitudes in a decibel scale. The acoustic measurements will be given in terms of decibels (dB) with the threshold of human hearing in air as the reference pressure. The conversion from pressures to dB is given by

$$SPL = 10 \log \left(\frac{p_{rms}^2}{p_{ref}^2} \right) \quad (3.1)$$

where: p_{rms}^2 = square of the rms acoustic pressure

p_{ref}^2 = square of the reference pressure for air (2×10^5 Pa)

SPL = Sound Pressure Level in dB

In the decibel scale, a 3 dB difference is a factor of two in the pressure magnitude. Previous acoustic measurements with the TPS in the anechoic chamber are given in Table 3.1. The average value of the blade passing tone will vary by ± 0.6 to 0.7 dB with a 90% confidence range. The 1st harmonic sound and the overall sound pressure level will vary by ± 0.8 to 1.1 dB and ± 0.2 dB, respectively, given the same conditions.

Table 3.1 Experimental s^2 values for Acoustic Measurements

Average Std	30,000 dB	50,000 dB	70,000 dB
Tone	0.61	0.71	0.55
1 st Harmonic	1.13	0.84	0.78
Overall	0.18	0.17	0.18

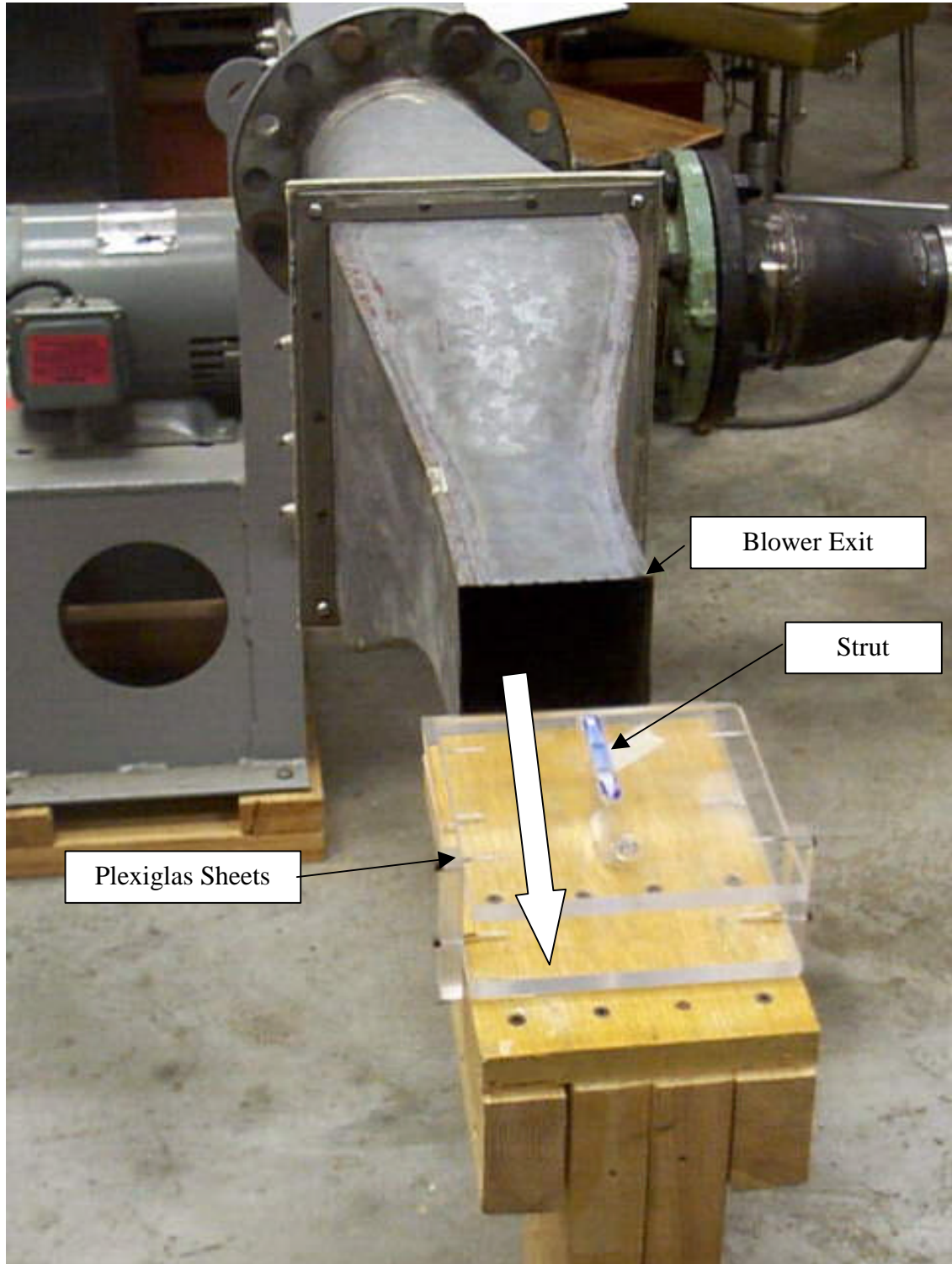


Figure 3.10 Experimental Setup for Blowing Strut Design Tests

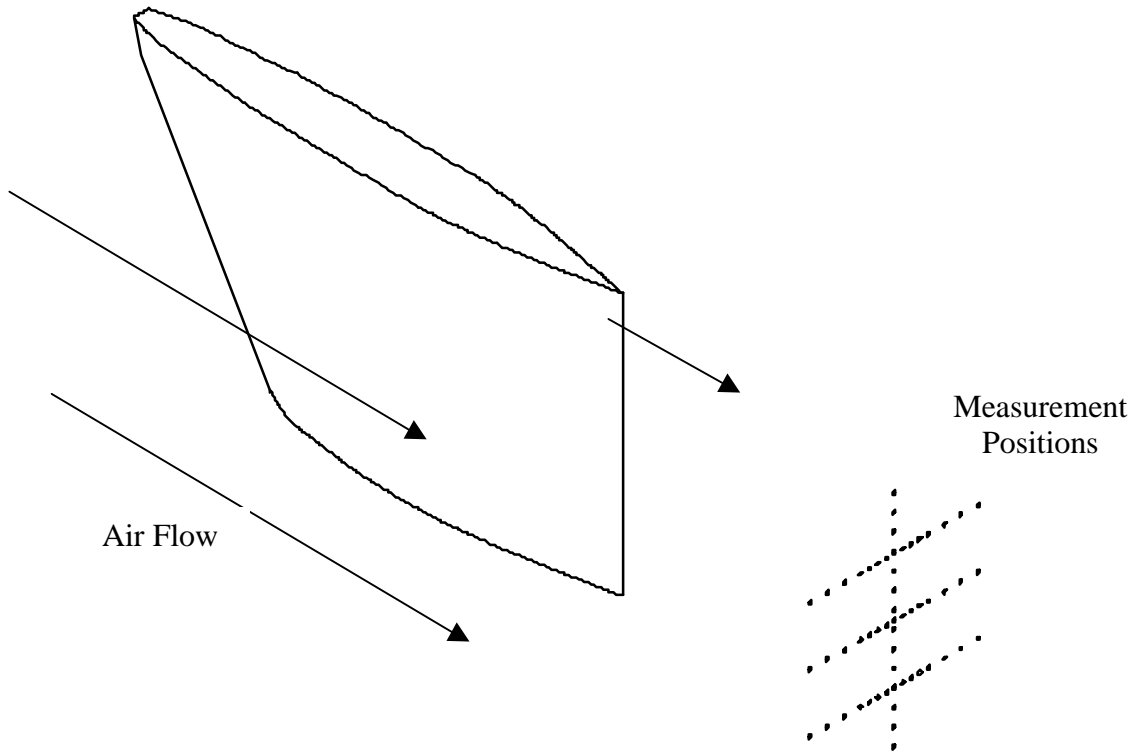


Figure 3.11: Measurement Positions for Strut Design Test on Bench Blower

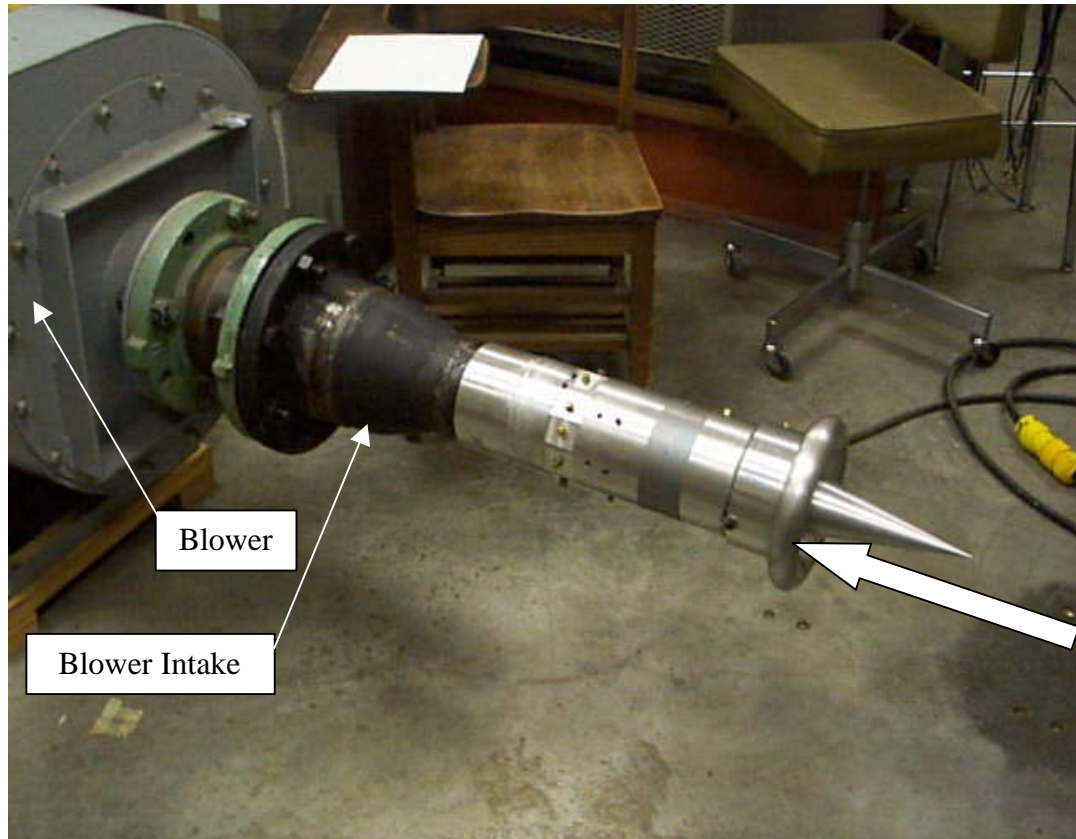


Figure 3.12: Testing of Inlet with Bench Test Blower

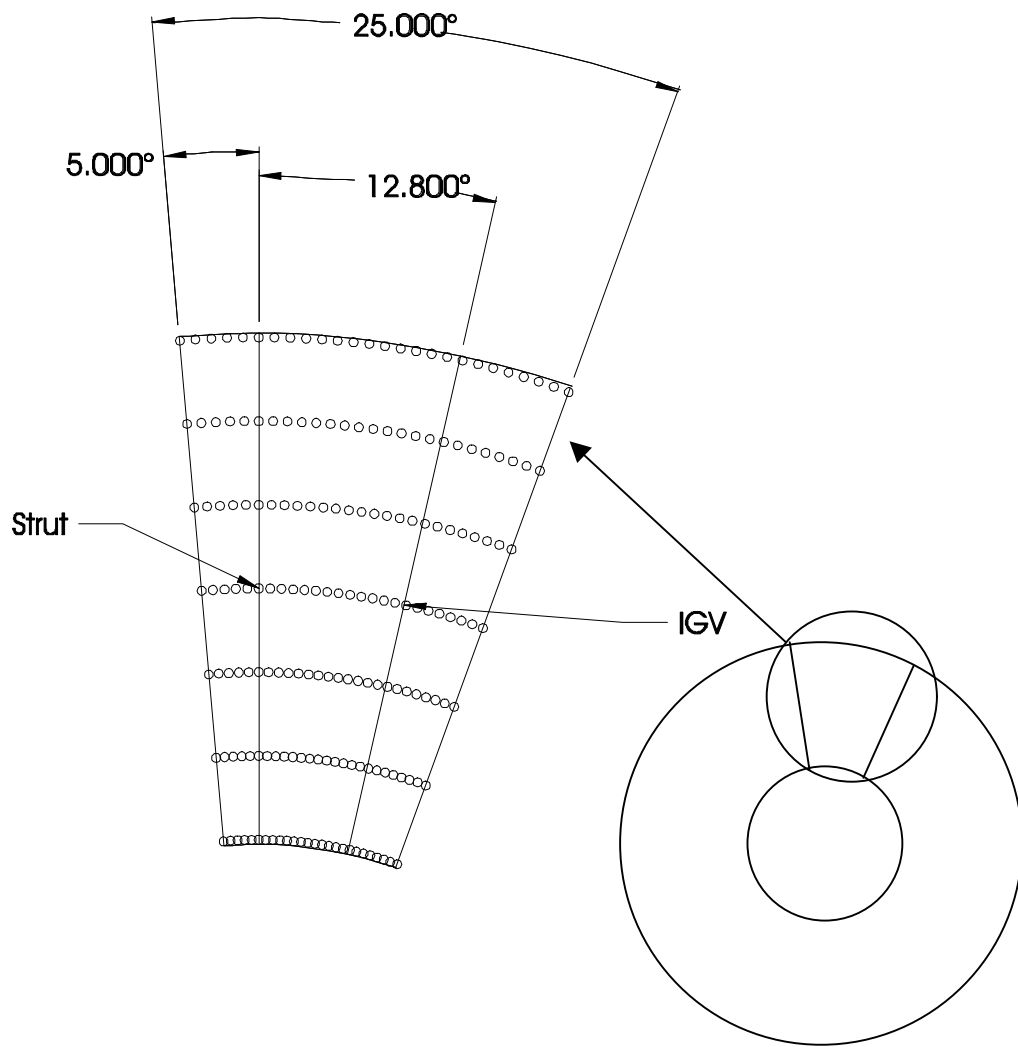


Figure 3.13: Test Locations for Inlet Tests on Bench Blower

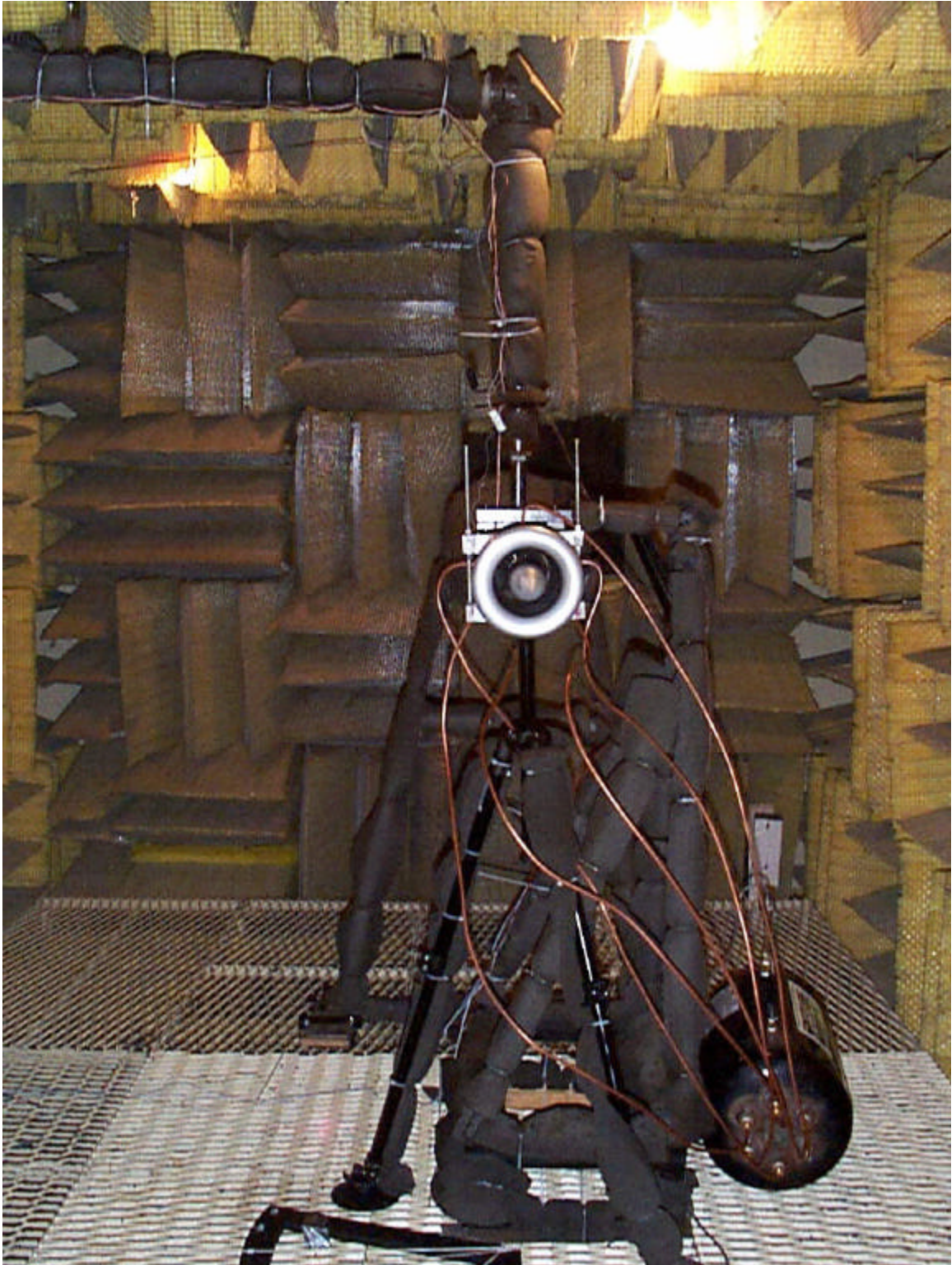


Figure 3.14: The Virginia Tech Anechoic Chamber

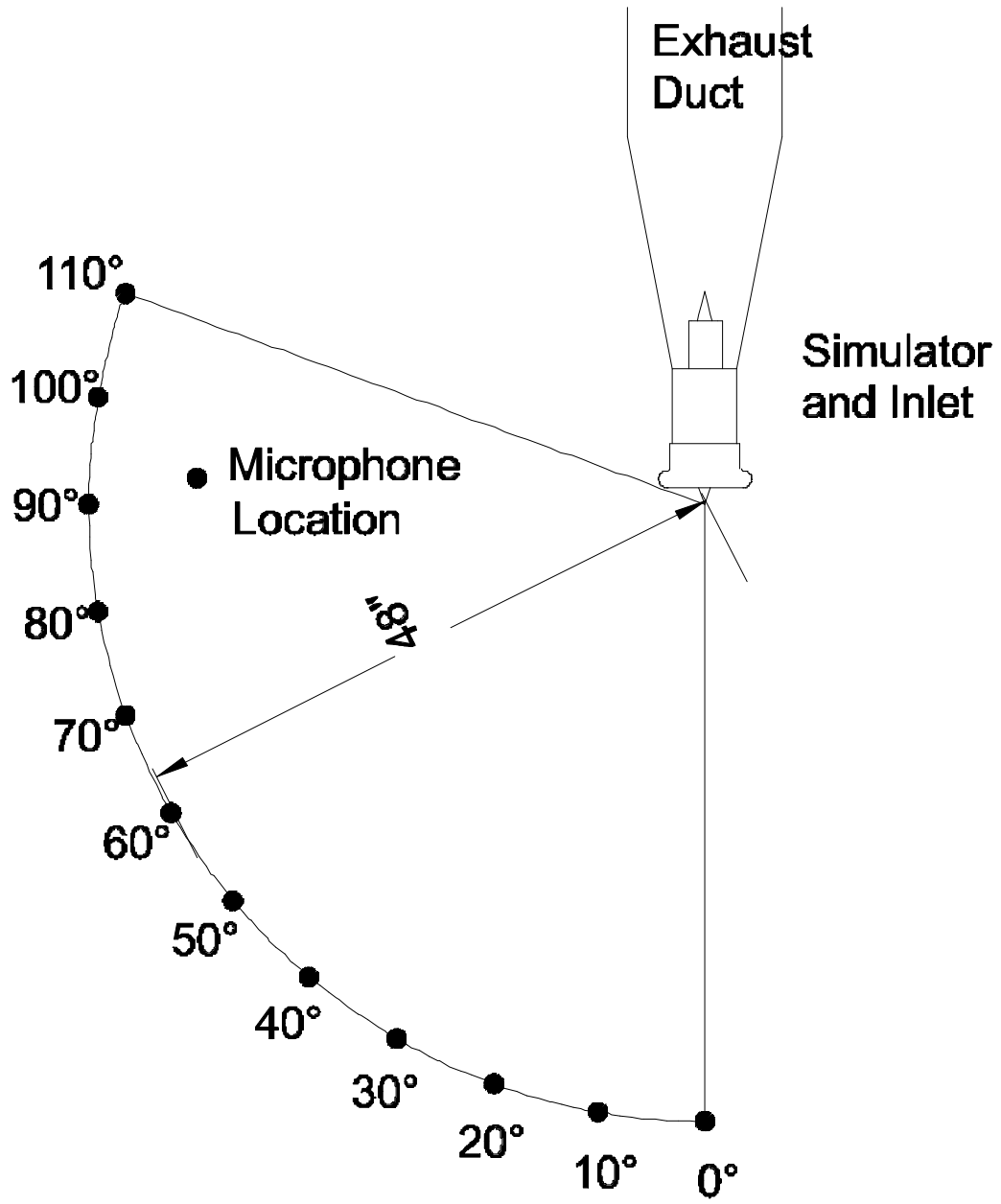


Figure 3.15: Acoustic Measurement Locations

4.0 Results and Discussion

The results discussed in this chapter will focus on the acoustic experiments performed in the Virginia Tech Anechoic Chamber. Appendix A is an acoustic comparison between faceted and airfoil shaped struts. The faceted struts increased both the Blade Passing Tone (BPT) and the 1st harmonic of the BPT at 50,000 RPM (60 PNC), but did not increase the sound substantially at 70,000 RPM (88 PNC). Appendix B details acoustic tests comparing the rotating or clocking of the inlet guide vanes (IGV) to align or offset with the struts. The tests showed that the aligning of the IGV increased the BPT and the 1st harmonic of the BPT at 50,000 RPM, but made insignificant increases at 70,000 RPM. Appendix C details acoustic tests performed to compare the asymmetric strut pattern used in the Boeing Translating Inlet with a symmetric pattern used in the same inlet. Appendix D details aerodynamic measurements in the Boeing Translating Inlet taken in the anechoic chamber. The bench test experiments performed as part of the strut design are discussed in Appendix E.

This chapter is divided into three sections, the first focusing on the acoustic results, the second examining the acoustic analysis of the Turbofan Propulsion Simulator (TPS) and the Boeing Translating Inlet and the third discussing some aerodynamic reasons for the acoustic results. The tests were performed in the anechoic chamber at simulator speeds of 30,000 RPM (40 PNC), 50,000 RPM (60 PNC) and 70,000 RPM (88 PNC). The effectiveness of trailing edge blowing (TEB) was quantified by comparing the noise levels of tests performed with TEB against tests performed without TEB. Instrumentation and test procedures were detailed in chapter 3.

Determination of Blowing Rate

An “optimal” blowing rate for the TEB at each speed was calculated. The blowing rate was changed by controlling the plenum pressure with a needle valve in the air supply line. The blowing rate was determined by finding the largest reduction in BPT in both the forward and side sectors of the far field around the inlet as documented by Leitch (1997). Each sector was represented by a microphone that was placed 48 in. (1.22 m) from the mouth of inlet. One microphone was placed at 30° from the inlet axis and the other at 90° from the inlet axis. A Spectrum Analyzer was used to measure the two microphone signals while the blade passing tone (BPT), the 1st harmonic of the BPT, and the overall sound pressure level were recorded. At each speed, the blowing rate was modified until an optimal noise reduction was established. Table 4.1 gives the blowing pressure used as well as the range of pressures tested where reductions in the BPT were measured.

Table 4.1: Blowing Pressure used in acoustic tests

	Plenum Pressure	
	Pressure Used	Pressure Range
30,000 RPM	18 psia	15-24 psia
50,000 RPM	22 psia	18-25 psia
70,000 RPM	30 psia	25-30 psia

4.1 Acoustic Results

The acoustic results will first discuss the tests without IGV and then with IGV. After the data is presented it will be compared with previous published data. The acoustic plane measured is the horizontal plane, which is the inlet orientation parallel to inlet wing, and was the only plane measured. The horizontal plane is shown in figure 3.2. Previous work by Leitch (1997) has shown that for TEB, the results and therefore the conclusions from those results do not differ greatly in other measurement planes. Each acoustic measurement position can be given a single value for the average BPT, the average 1st harmonic of the BPT and the average overall sound pressure level. An acoustic radiation directivity can be approximated from the position acoustic measurements. The directivity plots are used to examine the effectiveness of the TEB over the angles that an observer would hear during takeoff or landing.

The effectiveness of TEB can be quantified by the sound pressure level reduction of the BPT and harmonics of the BPT. This is due to the TEB reducing or eliminating some of the causes of the tone noise due to the wakes of the struts.

The acoustic modal analysis of the Boeing Translating Inlet and the TPS are important factors in understanding the acoustic results. This data will be presented later in this chapter.

4.1.1 Acoustic Test at 30,000 RPM

The tests performed at 30,000 RPM are evaluated both with and without IGV. The IGV were positioned to offset the strut so as to de-couple the two noise sources. The Boeing Translating Inlet has two noise sources at 30,000 RPM: the IGV and the struts. When the IGV are removed, the struts are the only noise source. By reducing the number of noise sources, it is easier to get a better understanding of the benefits of TEB.

4.1.1.1 30,000 RPM Tests without IGV

The experiments performed without the IGV at 30,000 RPM (40 PNC) are the simplest to evaluate. The 30,000 RPM (40 PNC) case was chosen because the unsteady interaction between the rotor and stator is cut off. The radiation directivity plots for the BPT, the 1st harmonic of the BPT and the overall sound pressure levels are shown in figure 4.1. At 30,000 RPM (40 PNC) TEB is effective at reducing the BPT of the Boeing Translating Inlet. Table 4.2 shows that the tone was decreased by an average of 3.1 dB over the entire directivity. TEB is very effective between 20° and 90°, where the maximum reduction is 6.4 dB and the BPT is reduced by an average of 3.7 dB.

The 1st Harmonic of the BPT showed little noise reduction due to TEB. The average measurement position saw a decrease of 0.9 dB, with a maximum reduction of 4.6 dB. Table 4.3 shows the SPL reduction for the 1st harmonic of the BPT due to TEB.

In figure 4.1, the overall sound pressure level measurements at 30,000 RPM (40 PNC) shows a decrease in the measured noise. This is important because it shows that the TEB is actually reducing noise and is not redistributing the noise at different frequencies.

Table 4.2 Tone SPL Reductions for 30,000 RPM (40 PNC) without IGv

Microphone Angle	Tone Sound Pressure Level	Tone Sound Pressure Level	dB Reduction
	Without Blowing	With Blowing	
	dB	dB	dB
0°	94.3	96.5	-2.2
10°	94.7	96.3	-1.6
20°	93.8	91.9	1.8
30°	93.0	90.8	2.2
40°	93.7	90.2	3.6
50°	94.8	88.5	6.4
60°	92.9	87.8	5.1
70°	87.9	83.5	4.4
80°	80.1	78.4	1.7
90°	80.7	79.1	1.7
100°	78.1	77.5	0.6
110°	83.0	77.8	5.2
<u>Average dB</u>	91.89	90.78	3.10

Table 4.3: 1st Harmonic SPL Reductions for 30,000 RPM without IGv

Microphone Angle	1 st Harmonic SPL	1 st Harmonic SPL	dB Reduction
	Without Blowing	With Blowing	
	dB	dB	dB
0°	95.4	90.7	4.7
10°	90.4	91.4	-1.0
20°	101.3	98.0	3.2
30°	95.5	95.6	-0.1
40°	90.4	93.4	-3.1
50°	88.4	87.7	0.7
60°	85.0	85.1	-0.2
70°	77.4	76.4	1.0
80°	78.2	79.7	-1.5
90°	78.3	75.4	2.9
100°	77.8	81.6	-3.8
110°	75.9	76.4	-0.5
<u>Average dB</u>	92.98	91.24	0.89

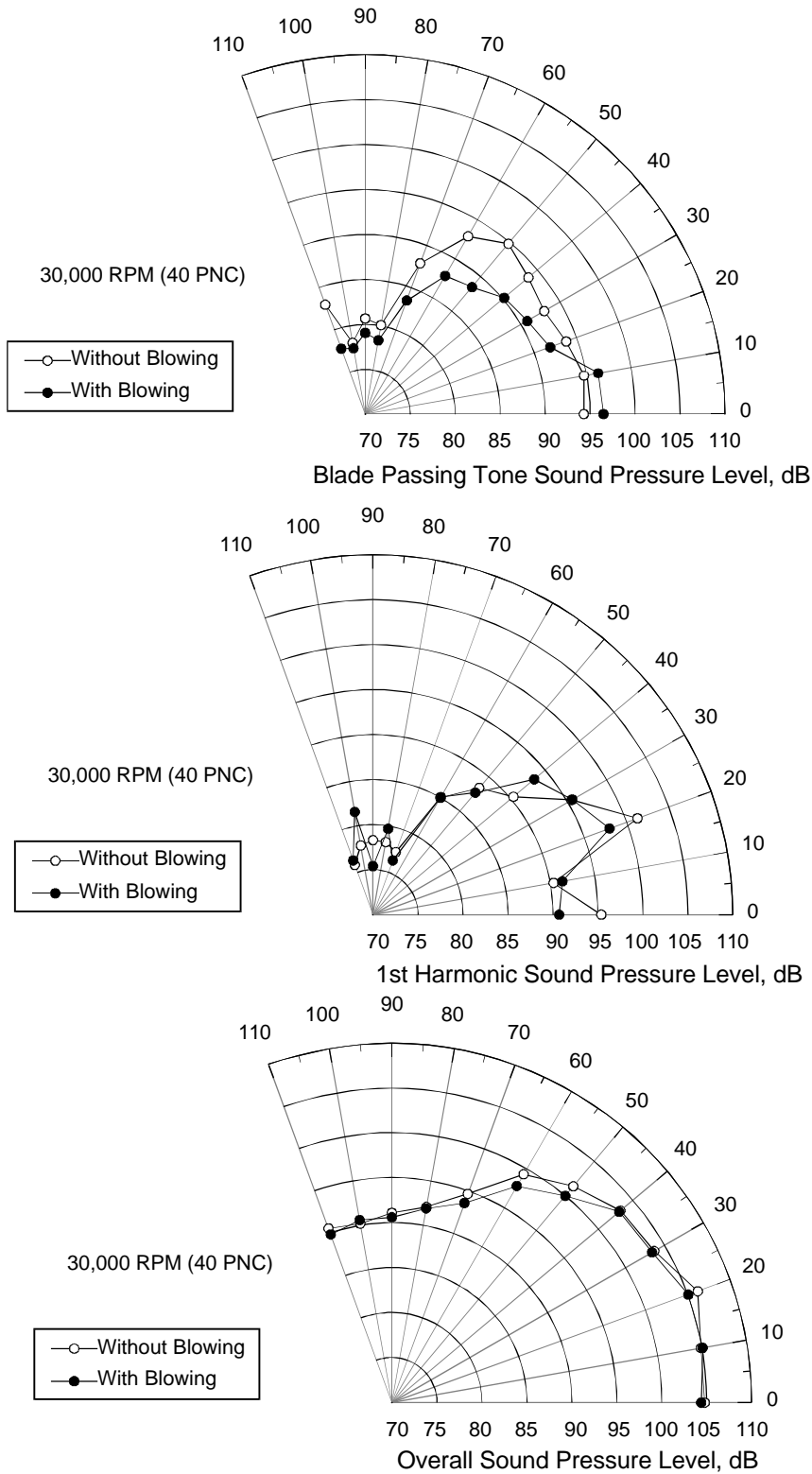


Figure 4.1: Directivity Plots of the Boeing Translating Inlet at 30,000 RPM without IGV

4.1.1.2 30,000 RPM Tests with IGV

The addition of IGV greatly reduced the effectiveness of TEB at 30,000 RPM (40 PNC). Figure 4.2 is the acoustic directivity plots of the BPT, the 1st harmonic of the BPT and the overall sound pressure level. The BPT was reduced from an average reduction of 2.5 dB to only an average reduction of 0.5 dB. The maximum BPT without IGV was 6.4 at 50° while the addition of IGV reduced the maximum SPL reduction to 2.4 dB at 20°. Table 4.4 displays the BPT SPL reductions at 30,000 RPM (40 PNC).

The 1st harmonic of the BPT at 30,000 (40 PNC) was increased by an average of 0.5 dB with the addition of IGV. The maximum SPL reduction is 1.8 dB, but the maximum increase is 2.9 dB. Table 4.5 displays the SPL reductions for the 1st harmonic of the BPT at 30,000 RPM (40 PNC).

The variation in overall sound pressure levels at 30,000 (40 PNC) with IGV was negligible.

Table 4.4: Tone Sound Pressure Level Reductions at 30,000 RPM (40 PNC) with IGV

Microphone Angle	Tone Sound Pressure Level	Tone Sound Pressure Level	dB Difference
	Without Blowing	With Blowing	
	dB	dB	dB
0°	96.0	93.6	2.4
10°	98.5	96.7	1.8
20°	96.3	93.9	2.4
30°	93.0	94.6	-1.6
40°	90.1	89.2	0.9
50°	91.6	91.3	0.3
60°	87.6	88.0	-0.3
70°	86.0	86.6	-0.7
80°	76.3	77.2	-0.9
90°	78.7	77.8	0.9
100°	85.5	84.9	0.6
110°	75.6	78.6	-2.9
<i>Average dB</i>	<i>92.47</i>	<i>91.26</i>	<i>0.50</i>

Table 4.5: 1st Harmonic SPL Reductions for 30,000 RPM (40 PNC) with IGV

	1 st Harmonic Sound Pressure Level	1 st Harmonic Sound Pressure Level	dB Reduction
	Without Blowing	With Blowing	
Microphone Angle	dB	dB	dB
0°	93.0	92.7	0.3
10°	102.1	100.3	1.8
20°	96.0	98.0	-1.9
30°	95.4	97.4	-2.0
40°	90.2	92.0	-1.9
50°	98.7	98.3	0.4
60°	98.6	97.7	0.9
70°	92.1	93.0	-0.9
80°	87.7	88.6	-1.0
90°	88.8	91.7	-2.9
100°	85.7	88.6	-2.9
110°	84.7	83.2	1.5
<i>Average dB</i>	<i>95.75</i>	<i>95.61</i>	<i>-0.43</i>

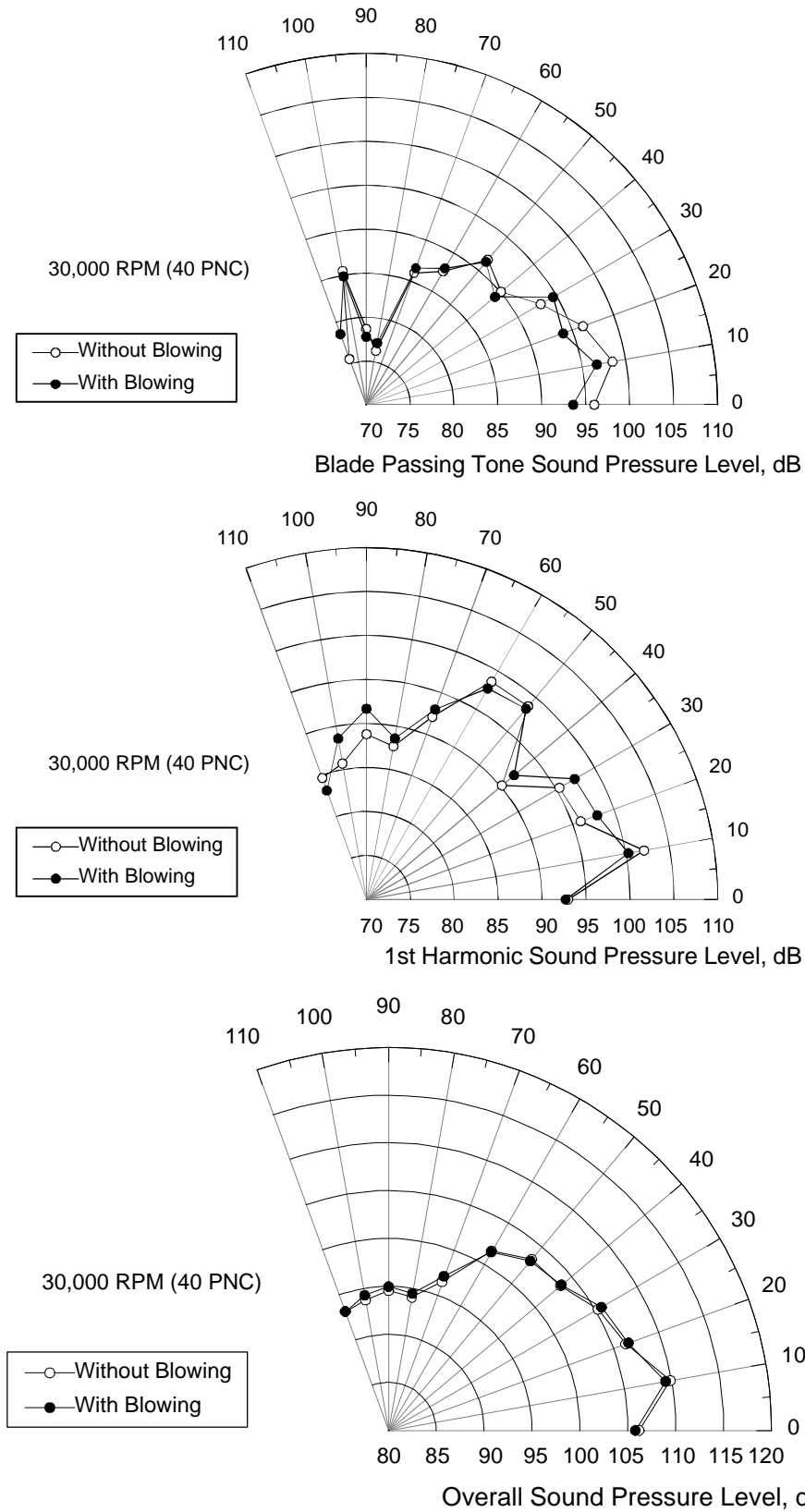


Figure 4.2 Directivity Plots of the Boeing Translating Inlet at 30,000 RPM with IGV

4.1.2 Acoustic Tests at 50,000 RPM

Acoustic tests were also performed at 50,000 RPM with and without IGV. The acoustic tests performed at 50,000 RPM have three noise sources. The noise caused by the interactions between the rotor / stator, the rotor / IGV and the rotor / strut are cut on.

4.1.2.1 50,000 RPM Tests without IGV

The next speed tested was 50,000 RPM (60 PNC) which corresponds to landing conditions. Figure 4.3 shows the acoustic directivity plots of the BPT, the 1st harmonic of the BPT and the overall sound pressure levels. At this speed, TEB also lowered the BPT by a maximum of 5.2 dB and an average of 1.9 dB. Since the rotor / stator noise is cut on at 60 PNC, the effects of TEB are reduced. At landing speed, the region of greatest reduction is between 0° and 30° which is most likely where rotor / strut noise is dominant. From 40° to 110°, TEB did reduce the BPT at some angles, but made others louder. The Tone SPL reductions for 50,000 RPM (60 PNC) without IGV is given in table 4.6.

The 1st harmonic of the BPT was reduced with TEB. The maximum reduction at 50,000 RPM is 2.6 dB with an average reduction of 1.2 dB. The 1st harmonic SPL reductions are given in table 4.7.

Table 4.6: Tone SPL Reductions for 50,000 RPM (60 PNC) without IGV

	Tone Sound Pressure Level		dB Reduction
	Without Blowing	With Blowing	
Microphone Angle	dB	dB	dB
0°	106.2	103.0	3.2
10°	108.6	103.9	4.7
20°	107.8	102.6	5.2
30°	104.5	103.1	1.5
40°	100.2	101.9	-1.7
50°	99.5	100.6	-1.1
60°	101.7	99.1	2.6
70°	98.5	97.1	1.5
80°	92.4	92.5	0.0
90°	96.3	96.0	0.3
100°	96.6	97.0	-0.4
110°	96.9	95.9	1.0
<u>Average dB</u>	<i>103.34</i>	<i>100.60</i>	<i>1.91</i>

Table 4.7: 1st Harmonic SPL Reductions for 50,000 RPM (60 PNC) without IGV

	1 st Harmonic Sound Pressure Level		dB Reduction
	Without Blowing	With Blowing	
Microphone Angle	dB	dB	dB
0°	100.1	100.3	-0.2
10°	102.5	101.0	1.4
20°	103.6	102.3	1.3
30°	102.1	102.2	-0.1
40°	107.5	106.5	1.0
50°	102.2	102.7	-0.5
60°	102.7	100.6	2.1
70°	96.6	96.2	0.4
80°	92.6	90.7	1.9
90°	92.7	91.5	1.2
100°	91.8	90.2	1.6
110°	91.1	88.5	2.6
<u>Average dB</u>	<i>101.50</i>	<i>100.67</i>	<i>1.17</i>

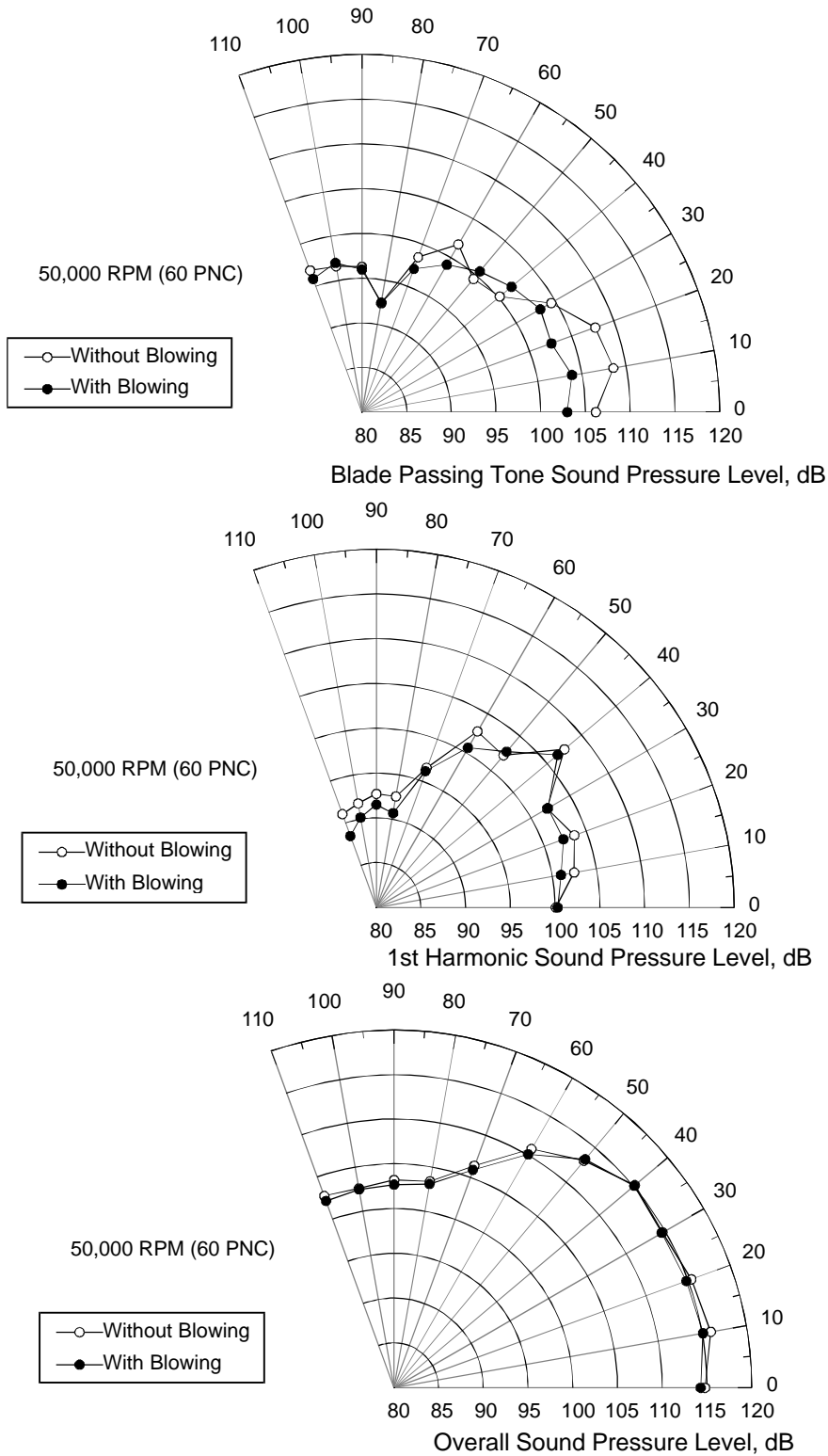


Figure 4.3: Directivity Plots of the Boeing Translating Inlet at 50,000 RPM without IGV

4.1.2.2 50,000 RPM Tests with IGV

The benefit of TEB at 50,000 RPM (60 PNC) was reduced with the addition of IGV. Figure 4.4 is the directivity plots of the BPT, the 1st harmonic of the BPT and the overall sound pressure level measured with the addition of IGV. The average reduction in tone was 1.10 dB with a maximum reduction of 3.3 dB. Similar to the tests without IGV, angles from 0° to 20° showed the greatest reductions. The Tone SPL reductions are given in table 4.8.

The 1st harmonic of the BPT also showed noise reductions at 50,000 RPM (60 PNC). The average reduction of the 1st harmonic of the BPT was 1 dB with maximum reduction of 2.7 dB. The reduction in the 1st harmonic of the BPT due to TEB is given in table 4.9.

Table 4.8: Tone SPL Reductions for 50,000 RPM (60 PNC) with IGV

Microphone Angle	Tone Sound Pressure Level	Tone Sound Pressure Level	dB Reduction
	Without Blowing	With Blowing	
	dB	dB	dB
0°	106.8	103.5	3.3
10°	112.0	111.0	1.0
20°	113.2	112.0	1.2
30°	104.5	104.8	-0.4
40°	103.5	104.2	-0.7
50°	106.4	103.5	2.9
60°	106.1	104.5	1.6
70°	105.9	105.9	0.0
80°	100.8	98.8	2.1
90°	95.1	94.3	0.8
100°	95.7	95.7	0.0
110°	92.2	93.4	-1.2
<i>Average dB</i>	<i>107.06</i>	<i>105.92</i>	<i>1.10</i>

Table 4.9: 1st Harmonic SPL Reductions for 50,000 RPM (60 PNC) with IGV

	1 st Harmonic Sound Pressure Level	1 st Harmonic Sound Pressure Level	dB Reduction
	Without Blowing	With Blowing	
Microphone Angle	dB	dB	dB
0°	111.6	110.4	1.1
10°	109.6	109.7	-0.2
20°	113.3	112.8	0.5
30°	111.1	109.9	1.2
40°	111.6	110.7	0.8
50°	109.4	106.7	2.7
60°	104.6	103.5	1.1
70°	98.6	97.5	1.0
80°	94.8	93.2	1.6
90°	92.0	92.2	-0.2
100°	90.5	89.9	0.6
110°	93.2	91.8	1.4
<i>Average dB</i>	<i>108.50</i>	<i>107.63</i>	<i>1.03</i>

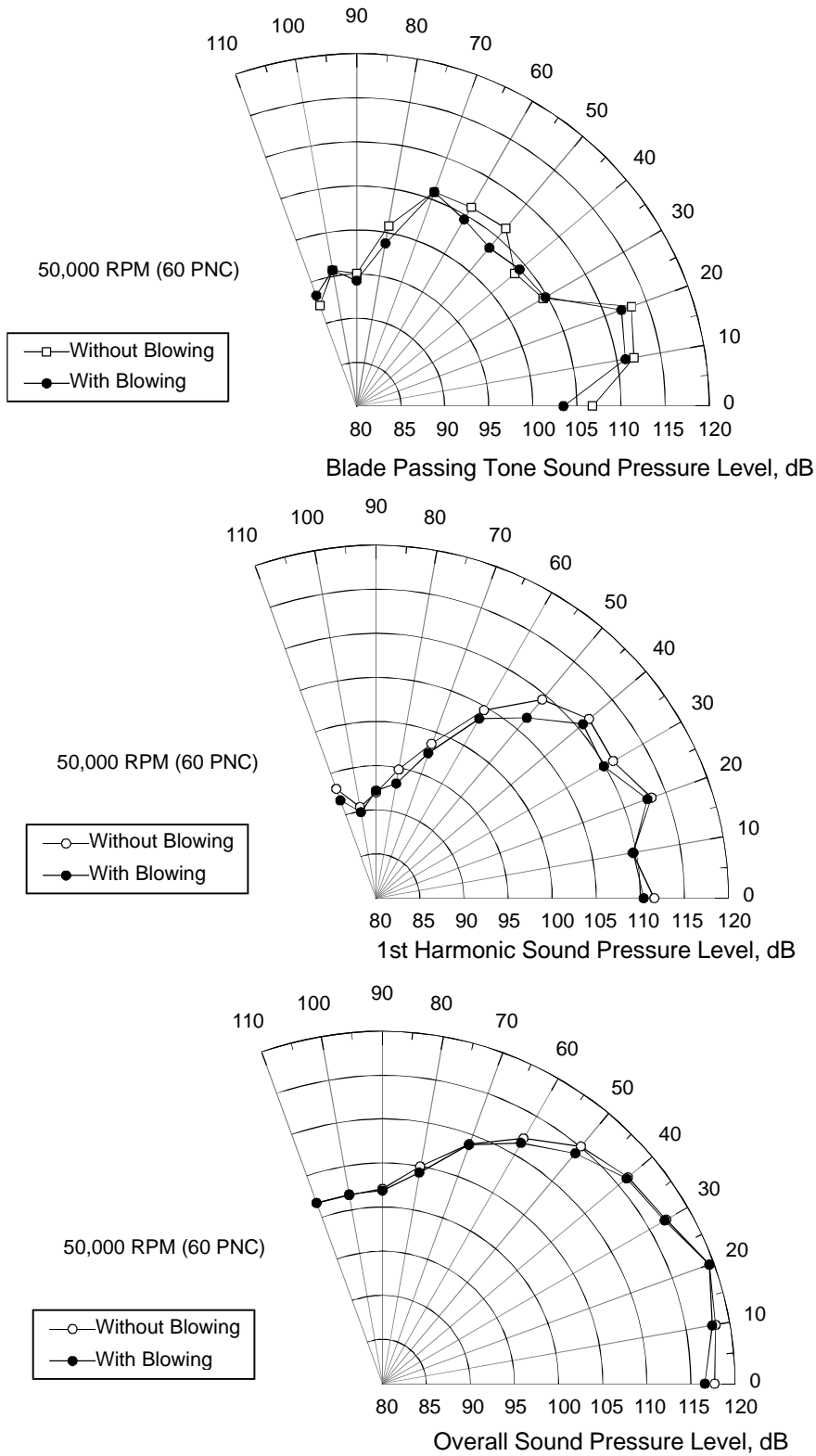


Figure 4.4: Directivity Plots of the Boeing Translating Inlet at 50,000 RPM with IGV

4.1.3 Acoustic Tests at 70,000 RPM

Acoustic Tests performed at 70,000 RPM have four noise sources: the rotor / stator, rotor / IGV, rotor / strut and multiple pure tones from shock waves are cut on.

4.1.3.1 70,000 RPM Tests without IGV

TEB had little effect on the sound pressure levels measured at 70,000 RPM (88 PNC). Figure 4.5 shows the acoustic directivity for the BPT, the 1st harmonic of the BPT and the overall sound pressure level. The average reduction in tone was 0.9 dB with a maximum reduction of 2.7 dB. The small reduction in the sound pressure levels is perhaps due to shock waves producing multiple pure tones. TEB will not reduce the noise generated as a results of shock waves at the blade tips. The BPT SPL reductions are given in Table 4.10.

Similar results are seen at the 1st harmonic of the BPT as at the BPT at 70,000 (88 PNC). The TEB did little to effect the tone. The largest reduction in the 1st harmonic is 2 dB, while the largest increase was 1.4 dB. Table 4.11 displays the SPL reductions in the 1st harmonic of the BPT at 70,000 RPM (88 PNC).

Table 4.10: Tone SPL Reductions for 70,000 RPM (88 PNC) without IGV

	Tone Sound Pressure Level	Tone Sound Pressure Level	dB Reduction
	Without Blowing	With Blowing	
Microphone Angle	dB	dB	dB
0°	113.6	110.9	2.7
10°	114.4	114.5	-0.1
20°	113.7	111.4	2.3
30°	112.5	111.8	0.7
40°	112.2	111.6	0.6
50°	111.7	111.8	-0.1
60°	115.2	115.0	0.2
70°	111.3	110.7	0.6
80°	111.2	111.1	0.1
90°	110.8	109.6	1.2
100°	109.2	110.3	-1.1
110°	114.3	112.5	1.8
<u>Average dB</u>	<i>112.84</i>	<i>112.07</i>	<i>0.87</i>

Table 4.11: 1st Harmonic SPL Reductions for 70,000 RPM (88 PNC) without IGV

	1 st Harmonic Sound Pressure Level	1 st Harmonic Sound Pressure Level	dB Reduction
	Without Blowing	With Blowing	
Microphone Angle	dB	dB	dB
0°	105.5	106.6	-1.1
10°	107.7	107.0	0.7
20°	107.1	107.4	-0.4
30°	109.5	109.4	0.1
40°	107.8	107.0	0.8
50°	110.0	108.0	2.0
60°	109.3	110.2	-0.9
70°	104.8	104.1	0.7
80°	101.2	99.7	1.5
90°	98.5	99.9	-1.4
100°	103.0	104.3	-1.3
110°	102.3	102.2	0.1
<u>Average dB</u>	<i>106.76</i>	<i>106.59</i>	<i>0.21</i>

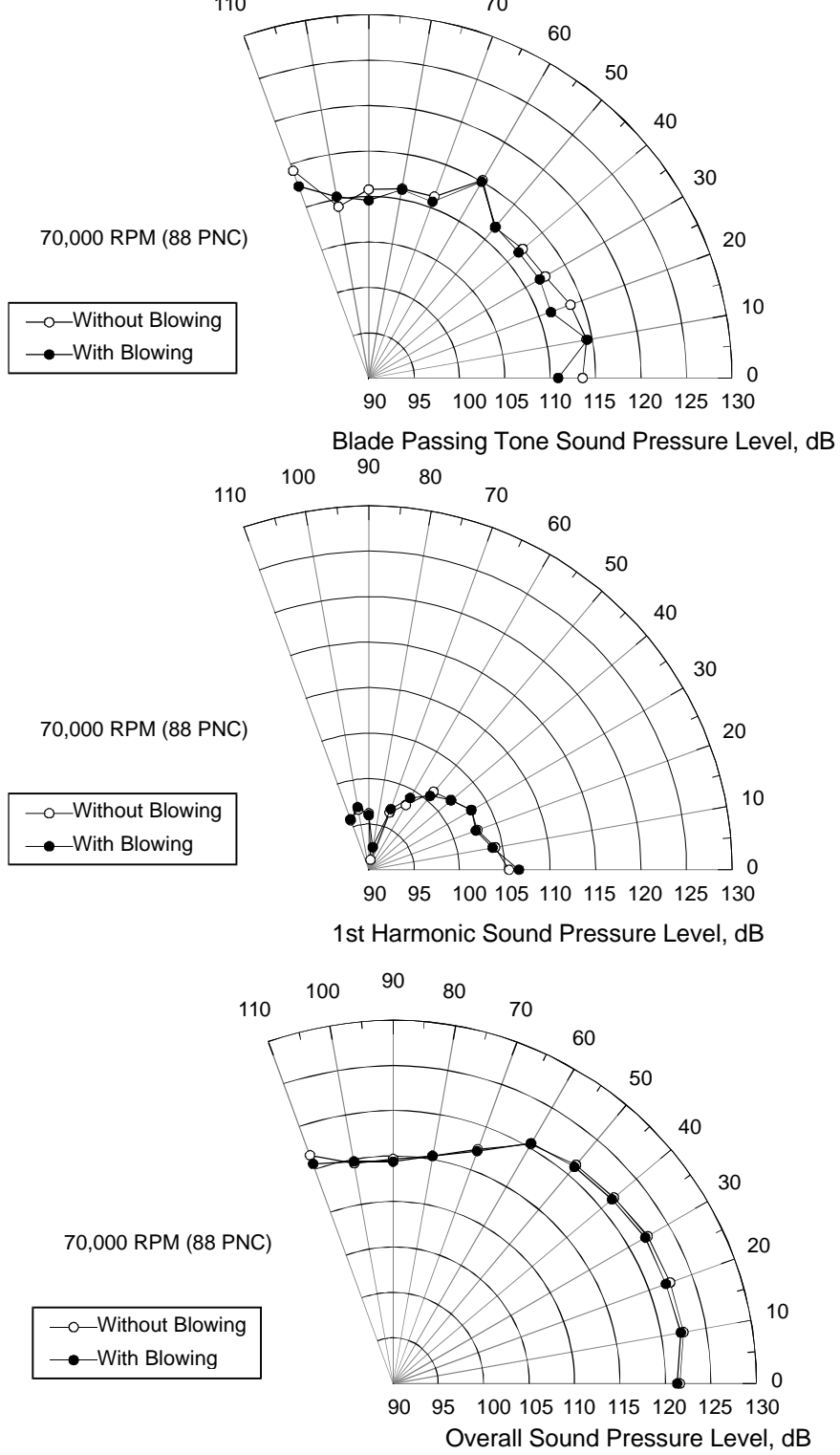


Figure 4.5: Directivity Plots of the Boeing Translating Inlet at 70,000 RPM without IGV

4.1.3.2 70,000 RPM Tests with IGV

Similar to the tests performed without IGV, TEB had little effect at 70,000 RPM (88 PNC). Figure 4.6 is the directivity plot of the BPT, the 1st harmonic of the BPT and the overall sound pressure level. At 70,000 RPM, the tone was not changed because of TEB. The BPT sound pressure level reductions are given in table 4.12.

The 1st harmonic of the BPT showed a small, but negligible sound pressure level reduction. The sound pressure level changes due to TEB are given in table 4.13.

The addition of the IGV did not have a substantial effect on TEB at 70,000 RPM. In the test with IGV and without IGV, the BPT and 1st harmonic of the BPT were unchanged.

Table 4.12: Tone SPL Reductions for 70,000 RPM (88 PNC) with IGV

Microphone Angle	Tone Sound Pressure Level	Tone Sound Pressure Level	dB Reduction
	Without Blowing	With Blowing	
	dB	dB	dB
0°	121.8	123.1	-1.3
10°	119.3	119.7	-0.4
20°	120.5	120.8	-0.3
30°	118.0	118.6	-0.6
40°	118.4	118.8	-0.4
50°	115.1	113.9	1.2
60°	110.4	111.8	-1.4
70°	107.0	106.5	0.5
80°	105.2	105.5	-0.3
90°	103.7	104.4	-0.7
100°	102.7	101.2	1.5
110°	103.3	103.6	-0.3
<i>Average dB</i>	<i>116.54</i>	<i>117.13</i>	<i>-0.11</i>

Table 4.13: 1st Harmonic SPL Reductions for 70,000 RPM (88 PNC) with IGV

	1 st Harmonic Sound Pressure Level	1 st Harmonic Sound Pressure Level	dB Reduction
	Without Blowing	With Blowing	
Microphone Angle	dB	dB	dB
0°	116.0	117.3	-1.4
10°	119.6	120.5	-0.9
20°	118.0	119.0	-1.0
30°	118.1	115.9	2.2
40°	119.7	119.0	0.7
50°	115.8	114.2	1.6
60°	109.8	109.0	0.7
70°	107.1	105.8	1.3
80°	102.9	102.7	0.2
90°	98.7	98.7	0.0
100°	97.8	96.1	1.6
110°	99.9	101.8	-2.0
<i>Average dB</i>	<i>115.33</i>	<i>115.31</i>	<i>0.44</i>

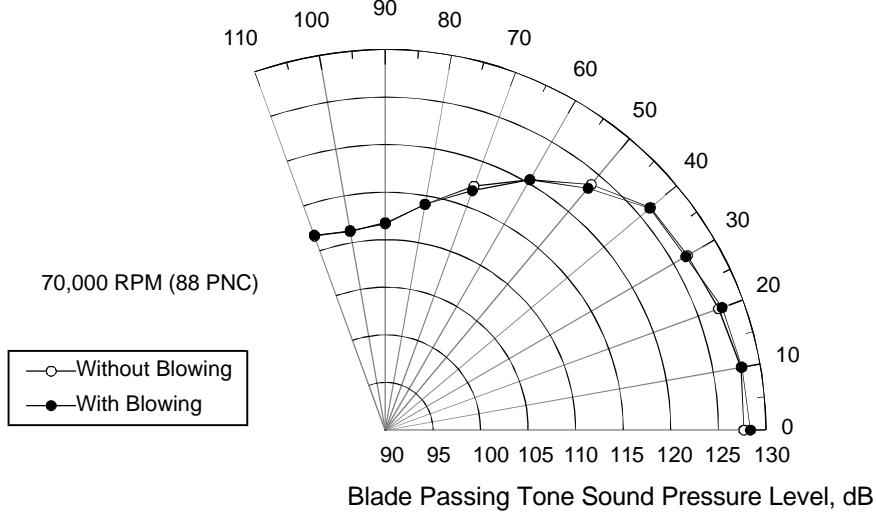
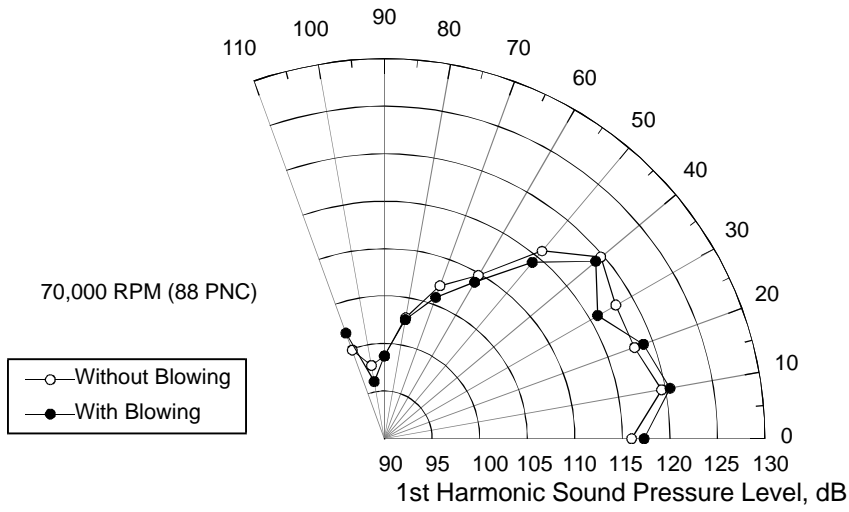
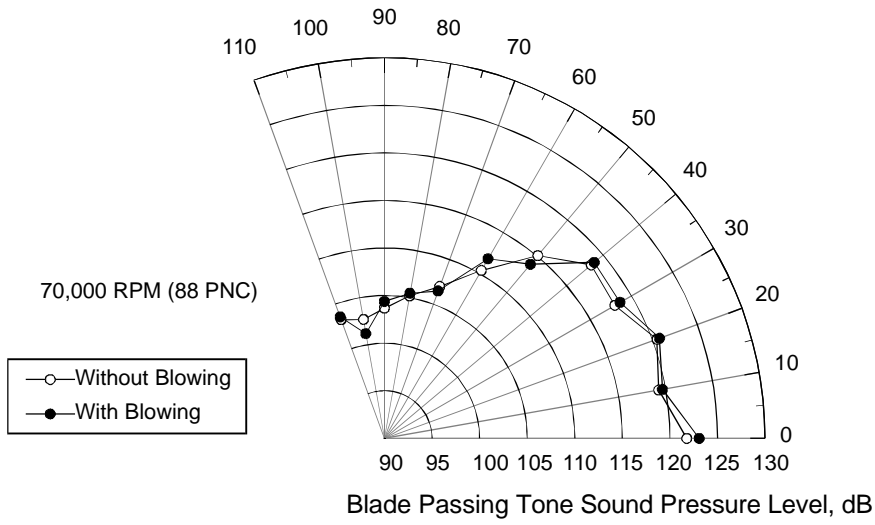


Figure 4.6: Directivity Plots of the Boeing Translating Inlet at 70,000 RPM with IGW

4.1.4 Discussion of Acoustic Results

TEB was effective at reducing the BPT and the 1st harmonic of the BPT at both 30,000 RPM and 50,000 RPM without IG. In particular, the TEB was effective in reducing the BPT when the rotor / stator noise was cut off and the rotor / strut noise was the only noise source. The addition of IG reduced the effectiveness of TEB at all speeds tested. Figure 4.7 shows the reductions seen in the BPT with IG and without IG. At 70,000 RPM, TEB did not change the measured sound pressure levels.

Figure 4.7 shows that the IG reduced the effectiveness of TEB in reducing the BPT over the range of angles between 30° to 80° at 30,000 RPM. The IG also reduced the reductions in the BPT seen between the angles of 10° and 30° at 50,000 RPM. Another noticeable impact of the IG is seen when comparing the 1st harmonic sound pressure levels at 70,000 RPM. The addition of the IG increased the measured sound pressure level at each angle. Figure 4.8 shows the acoustic directivity plot of the 1st harmonic sound pressure levels at 70,000 RPM with and without IG. Table 4.14 shows that the IG increased the 1st harmonic by an average of 8.6 dB.

It should also be noted that the elimination of a strut wake might not be the optimum in terms of noise reduction. The optimal blowing rate in terms of noise reduction might include some noise generation that cancels noise from other sources such as the IG or stators. Future testing which included the use of aerodynamic sensors to find the optimum blowing pressure as opposed to acoustic sensors would lend insight into this problem.

Table 4.14: Comparison of the effects of IGV on the 1st harmonic at 70,000 RPM

Microphone Angle	1st Harmonic SPL	1st Harmonic SPL	dB Difference
	Without IGV	With IGV	
	dB	dB	dB
0°	105.5	116.0	-10.4
10°	107.7	119.6	-11.8
20°	107.1	118.0	-11.0
30°	109.5	118.1	-8.6
40°	107.8	119.7	-11.9
50°	110.0	115.8	-5.8
60°	109.3	109.8	-0.4
70°	104.8	107.1	-2.2
80°	101.2	102.9	-1.7
90°	98.5	98.7	-0.2
100°	103.0	97.8	5.3
110°	102.3	99.9	2.4
<i>Average dB</i>	<i>106.76</i>	<i>115.33</i>	<i>-8.6</i>

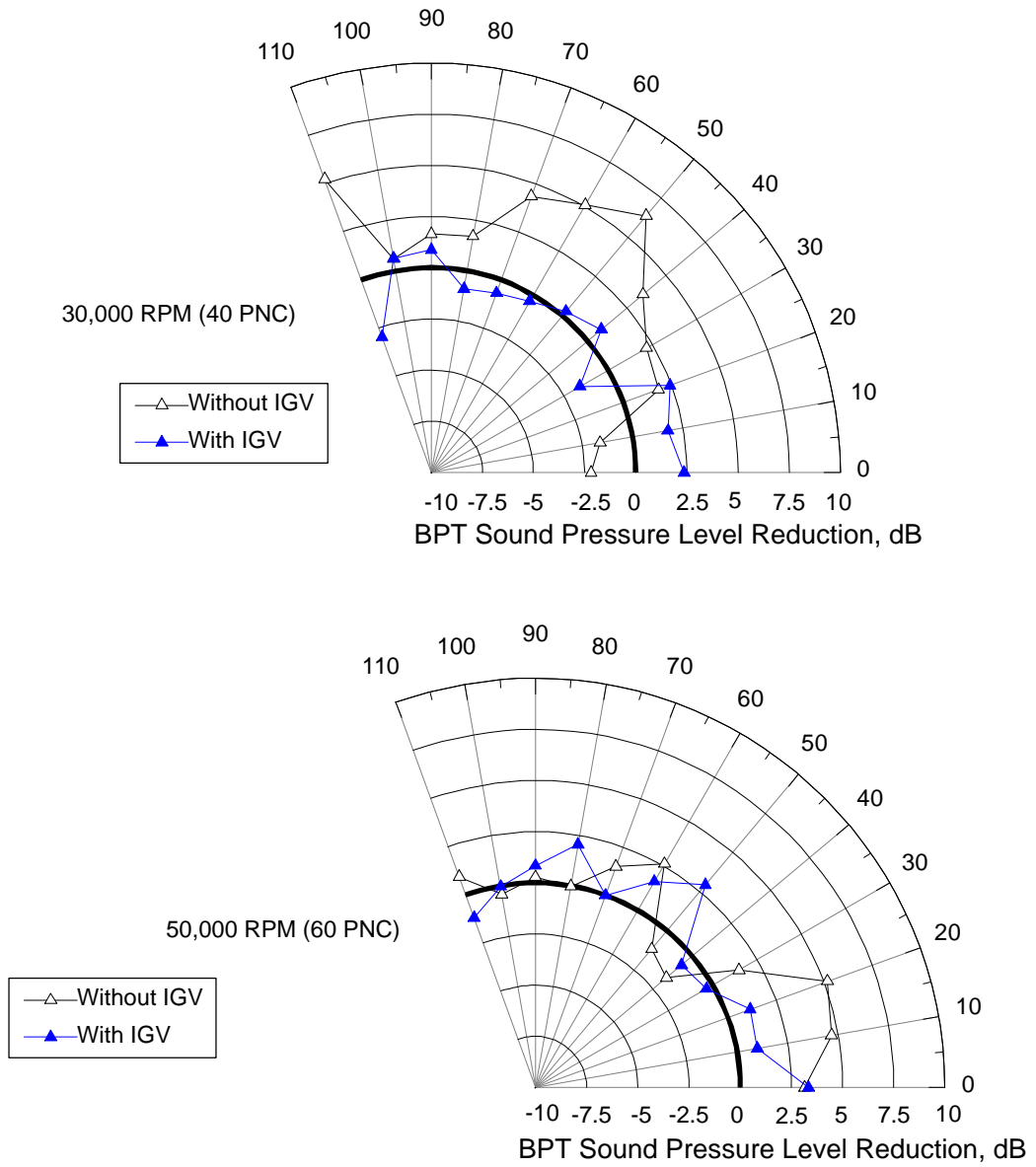


Figure 4.7: Comparison of the effect of IGV on TEB

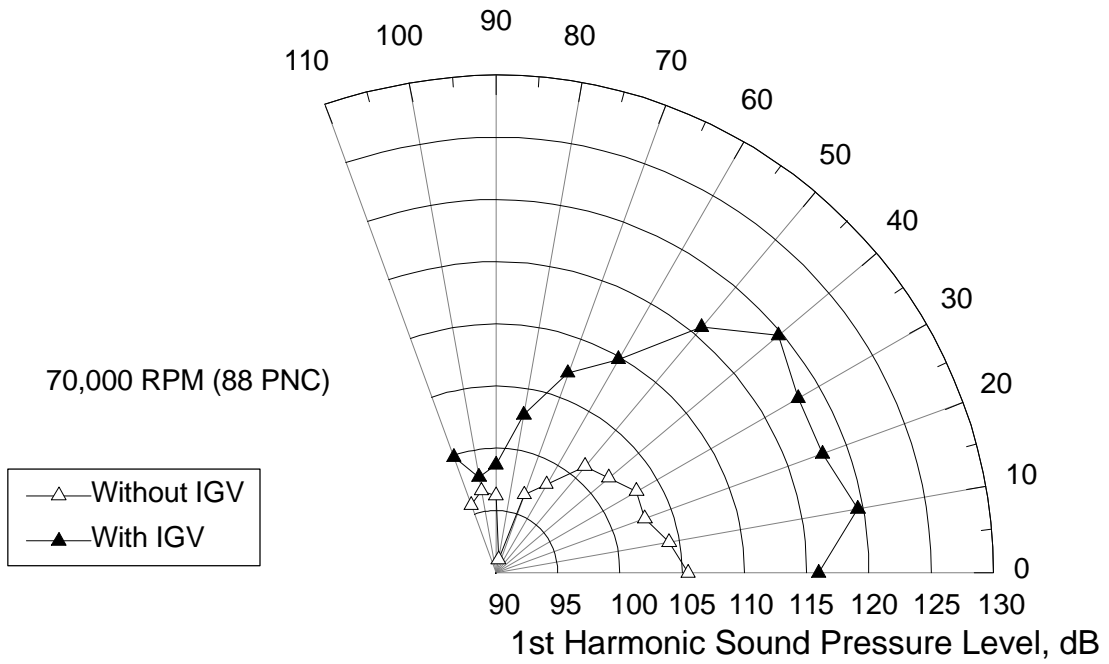


Figure 4.8: Impact of IGV on the 1st harmonic of the BPT at 70,000 RPM

4.1.5 Comparison with Previous Research

After examining the data taken using TEB with the Boeing Translating Inlet, it is interesting to compare the results to previous published results by Leitch (1997). Figure 4.9 is a directivity plot of both the Boeing Translating Inlet and the Experimental Blowing Inlet showing the reduction in the BPT at each angle due to TEB. The inlet used by Leitch in his research did not have IGV and therefore will be compared to the Boeing Translating Inlet without IGV. It should be noted that the bandwidth used by Leitch was 32 Hz as compared to 128 Hz used in this research. Previous data by Leitch (1997) showed a tone reduction at 30,000 RPM (40 PNC) was greatest between the angles of 60° and 100° where the average reduction was 6 dB. In the Boeing Translating Inlet, the maximum reduction was seen between 20° and 70° where the average reduction was 3.7 dB. At 50,000 RPM (60 PNC), Leitch (1997) achieved an average reduction in the tone of 2.6. This compares with an average reduction of 1.9 dB for the Boeing Translating Inlet at 50,000 RPM. The difference in the reduction in tone is most likely due to the blunt strut trailing edge used by Leitch (1997). The trailing edge in the current experiments is sharp and creates a smaller wake than blunt trailing edges. Figure E.1 shows the difference between the sharp crenulated and the blunt trailing edge. Figure 4.10 is a comparison of the wakes of blunt and sharp trailing edges of the Boeing strut taken on the strut design bench test. The bluntness of the strut trailing edge in the previous research likely gave Leitch a louder non-TEB blowing case to compare with his TEB. The current experiments compare favorably with the previous published research.

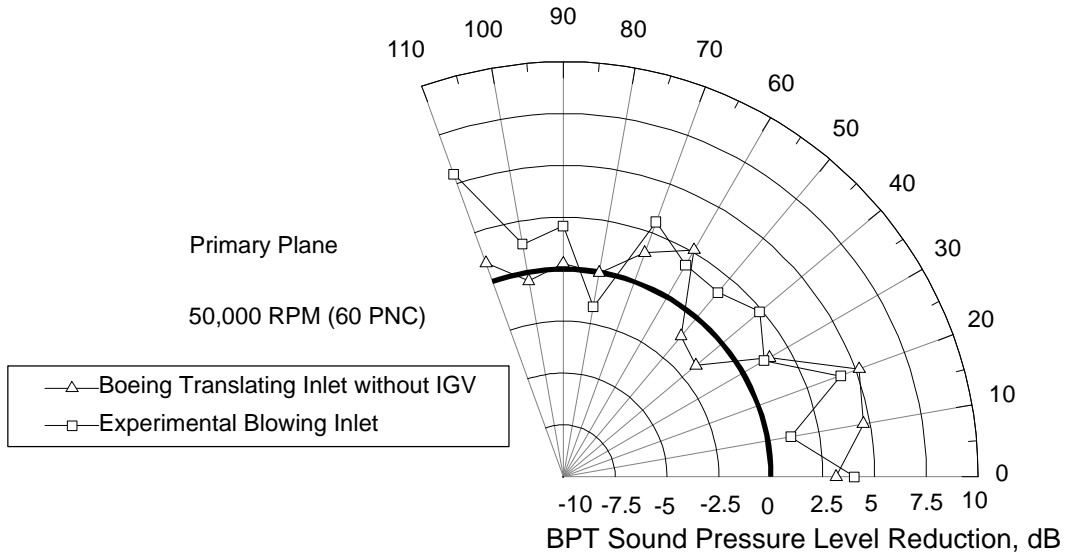
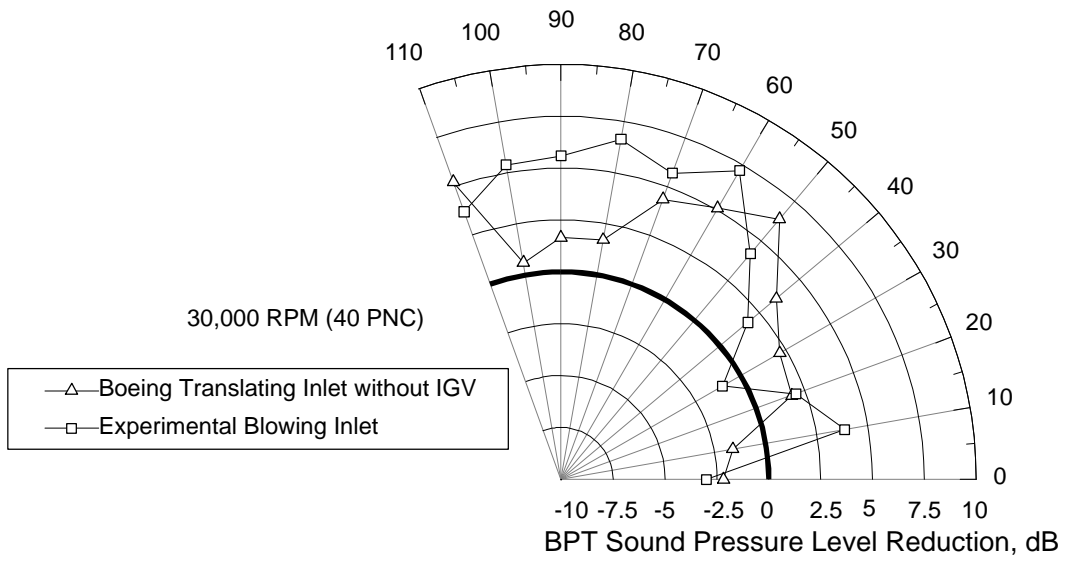


Figure 4.9: Comparison of reductions in the BPT due to TEB with previous research

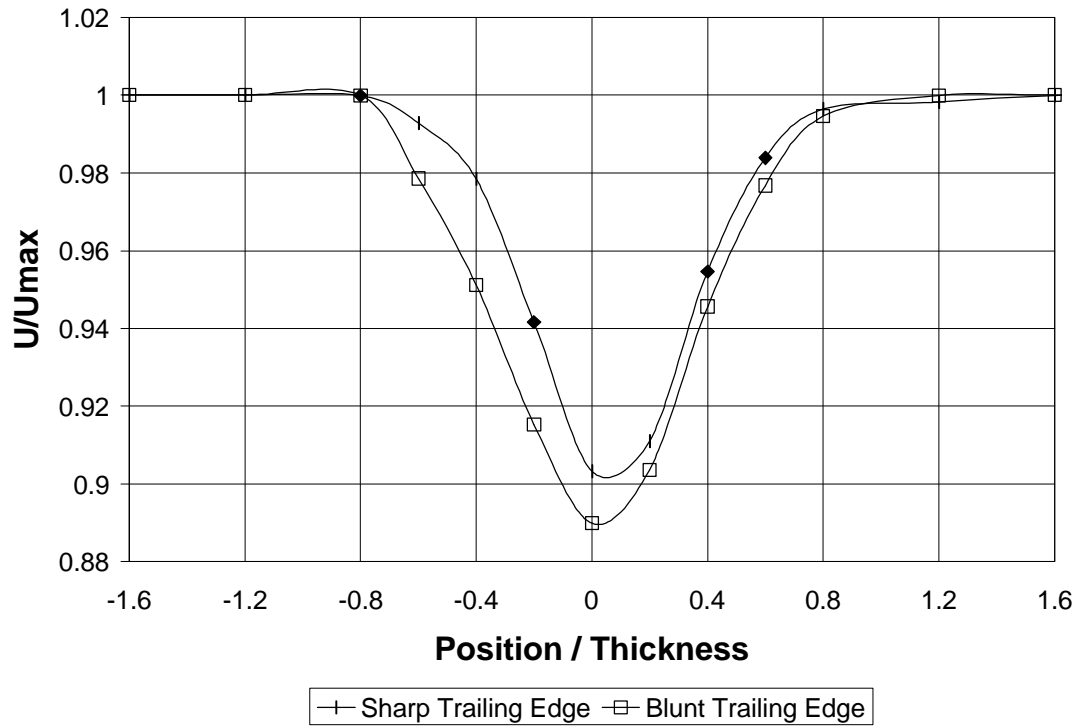


Figure 4.10: Comparison of the wakes of blunt and sharp strut trailing edges

4.2 Acoustic Analysis of the Boeing Translating Inlet

In an effort to better understand the acoustic radiation pattern of the inlet and why TEB had limited benefit, the noise sources were analyzed using procedures documented in chapter 2. In the Boeing Translating Inlet, there are three noise sources: the interaction between the rotor and the downstream exit guide vane or stator (called rotor / stator noise), the interaction between the rotor and the IGV (called rotor / IGV noise) and the interaction between the rotor and the strut (called rotor / strut noise). The interaction between the rotor and the stationary parts of the inlet can be directly related to the size and frequency of the wakes created by the inlet parts. This acoustic analysis will predict where concentrations of acoustic power will be radiated.

Although it is possible to calculate a complete radial directivity for each acoustic mode that propagates, only the location of the major lobe (ψ_p) is tabulated.

4.2.1 Analysis of the Rotor / Stator Interaction

The first source of noise is the unsteady interaction between the rotor blade and the downstream stator vanes, which is caused by wakes of the rotor blades hitting the downstream stator vanes. There are 18 rotor blades and 26 stator vanes, which leads to circumferential spinning modes of $m=8$ for the BPT and $m=10$ for the 1st harmonic. Table 4.15 is a compilation of the acoustic modes that are generated by the rotor / stator noise. The rotor / stator noise begins to propagate at 33,500 Hz.

Table 4.15: Modal Analysis of Rotor / Stator Interaction

	Summary of Acoustic Analysis					
	30,000 RPM		50,000 RPM		70,000 RPM	
	M	ψ_p	M	ψ_p	M	ψ_p
BPF			(8,0)	41°	(8,0)	28°
			(8,1)	71°	(8,1)	42°
					(8,2)	55°
1st Harmonic	(10,0)	43°	(10,0)	24°	(10,0)	17°
	(10,1)	71°	(10,1)	34°	(10,1)	24°
			(10,2)	43°	(10,2)	29°
			(10,3)	54°	(10,3)	35°
			(10,4)	70°	(10,4)	42°
					(10,5)	49°
					(10,6)	58°

4.2.2 Analysis of the Rotor / IGV Interaction

The unsteady interaction between the rotor and the IGV is caused by the wakes of the IGV hitting the downstream rotor. The pattern of the wakes produces spinning acoustic modes at the fan face that propagate down the inlet. The propagating modes for the rotor / IGV noise is given in Table 4.16. Figure 4.11 shows the calculated effects of the IGV on BPT at 30,000 RPM (40 PNC) and 50,000 RPM (60 PNC).

The directivity plots along with the modal analysis can be used to understand the effects of IGV of TEB. At 30,000 RPM, the only Rotor / IGV mode that propagates is (4,0) which has a principal lobe angle of 37°. Figure 4.11 does not show that the IGV increased the tone SPL at either 30° or 40°. There is an increase at 10° and 20° and most likely this is where the acoustic energy of mode (4,0) is concentrated. The shift in principal lobe angle could be due to the acoustic mode shape changing as the waves propagate through the inlet. It is also interesting to note that angles from 20° to 90° showed little noise reduction with the addition of IGV. Without IGV, the same angles showed large reductions in the BPT. Figure 4.11 shows that for the angles from 40° to 90°, the IGV actually reduced the sound pressure level.

At 50,000 RPM, the largest reductions in the tone due to TEB were seen at the angles of 0° to 30°. Figure 4.11 shows that the IGV increase the baseline measured sound pressure level at those angles. This is most likely due to modes (4,0) and (4,1) which have a principal lobe angle of 21° and 38°. However, it has already been shown that the acoustic wave is changing shape as it propagates down the inlet and most likely these modes are being shifted more towards the inlet axis. With the presence of modes (4,0) and (4,1) closer to the inlet axis, which is where the effects of TEB are seen most without IGV, the effectiveness of TEB at 50,000 RPM is diminished.

Table 4.16: Modal Analysis of the Rotor / IGV Interaction

	Summary of Acoustic Analysis					
	30,000 RPM		50,000 RPM		70,000 RPM	
	M	ψ_p	M	ψ_p	M	ψ_p
BPF	(4,0)	37°	(4,0)	21°	(4,0)	15°
			(4,1)	38°	(4,1)	26°
			(4,2)	62°	(4,2)	39°
			(10,0)	53°	(4,3)	58°
					(10,0)	35°
					(10,1)	51°
					(10,2)	68°
1st Harmonic	(8,0)	34°	(8,0)	20°	(8,0)	14°
	(8,1)	54°	(8,1)	29°	(8,1)	20°
	(6,0)	26°	(8,2)	37°	(8,2)	25°
	(6,1)	41°	(8,3)	47°	(8,3)	31°
	(6,2)	60°	(8,4)	62°	(8,4)	39°
			(6,0)	15°	(8,5)	47°
			(6,1)	23°	(8,6)	58°
			(6,2)	31°	(6,0)	11°
			(6,3)	42°	(6,1)	16°
			(6,4)	56°	(6,2)	22°
					(6,3)	28°
					(6,4)	36°
					(6,5)	45°
					(6,6)	56°

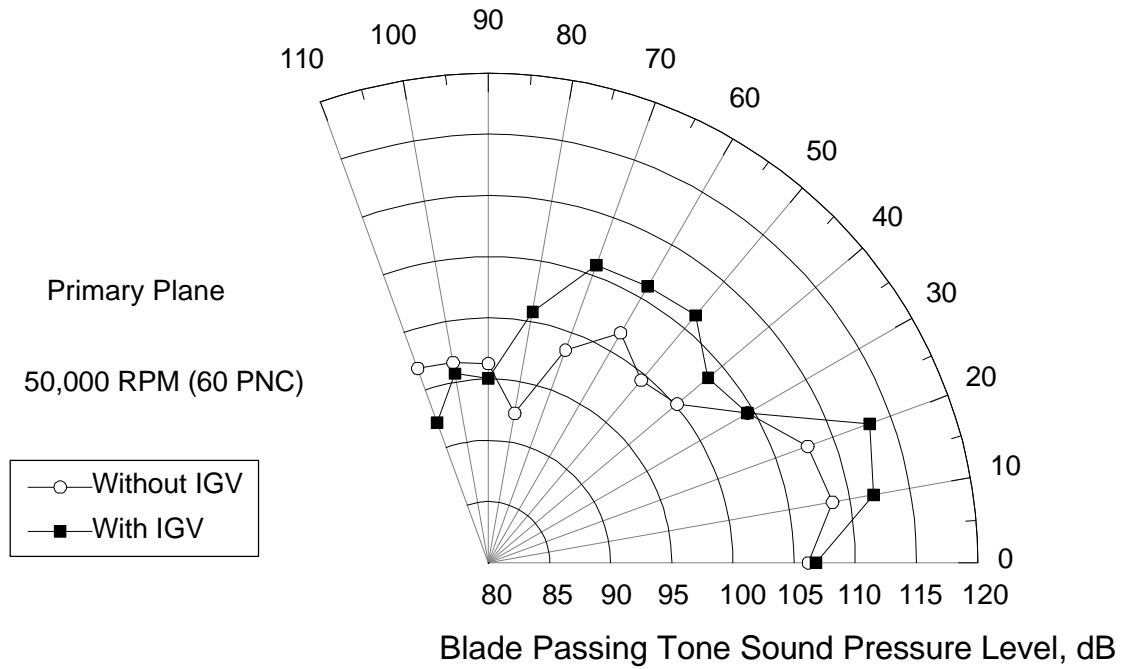
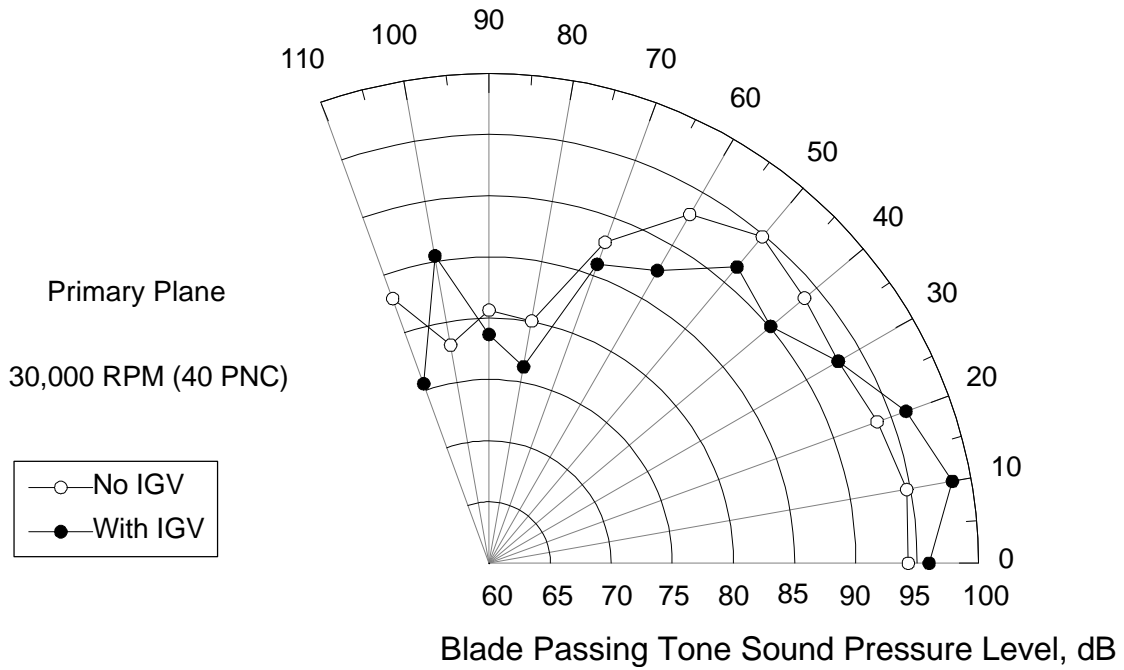


Figure 4.11: Acoustic Comparison of the influence of IGV on Acoustic Radiation Patterns

4.2.3 Analysis of the Rotor / Strut Interaction

The noise caused by the unsteady Rotor / Strut interaction is not as easy to understand as the IGV or stator noise. Due to the asymmetry of the strut pattern, there are many possibilities for the acoustic modes that could propagate. The only mode that will not propagate is the axisymmetric mode ($m=0$). The best way to understand the acoustic radiation pattern caused by the struts is to analyze the baseline directivity plot without TEB at 30,000 RPM (40 PNC). Without IGV at this speed the rotor / strut noise is the only noise that propagates. Figure 4.12 shows the directivity plot for this speed. While it very difficult to estimate which rotor / strut mode is dominant, it is easy to examine the directivity plot in figure 4.12 and see one or more modes at 10° and 50° . Since the major lobe for the mode appears to be near 10° , it is most likely a lower order mode because the location of the acoustic energy is near 50° . As the acoustic mode is cut on, the acoustic energy moves from the side plane into the front plane. The mode or lobe seen at 50° could be a higher order circumferential mode or it could be the same circumferential mode with a different radial mode. If there are two modes caused by the rotor / strut interaction, then we should see reductions in the BPT due to TEB near those values. At 30,000 RPM, near 10° , we do not see any reduction in the BPT due to TEB. However at 50° we see the largest reduction in the BPT at 30,000 RPM. This further backs up the hypothesis that a mode with a principal lobe angle of 50° at 30,000 RPM is caused by rotor / strut interaction. At 50,000 RPM, the principal lobe would have moved towards the inlet axis. The largest reduction in BPT at 50,000 RPM is seen between 0° and 30° . This is most likely the same mode that was reduced at 30,000 RPM.

The acoustics of the asymmetric strut pattern in the baseline design were compared to a symmetric strut design in appendix C. While definite conclusion about the modes excited by the rotor / strut interaction cannot be defined, it has been shown that the rotor / strut interaction excites a mode that is very sensitive to reductions in tone noise due to TEB.

4.3 Aerodynamic Test Results

To better understand the difference between the IGV and strut wakes, a bench setup was used to measure the wakes of the two structural members of the inlet. The details of the experimental setup are given in chapter two. Pitot Static measurements were taken every 1° over a 25° arc to measure in detail the flow field at the fan face. Figure 4.13 shows that the wakes of the IGV are significant contributors to the flow distortion at the fan face. Although the struts are larger than the IGV, the blunt leading and trailing edges of the IGV combined with the proximity to the fan face make the IGV wakes deeper than the strut wakes. The IGV are much thinner and have a smaller chord length than the struts, which makes the IGV the primary noise source in the Boeing Translating Inlet, and reduces the effectiveness of TEB.

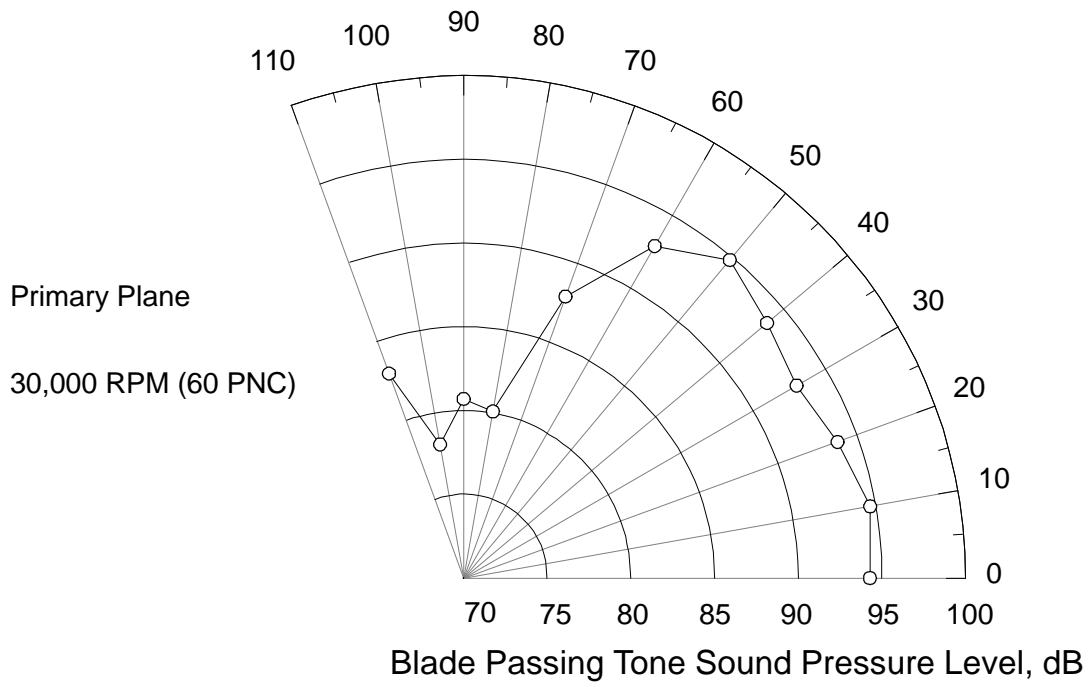


Figure 4.12: Acoustic Radiation Pattern of Rotor / Strut Noise

Aerodynamic Data: Boeing Translating Inlet

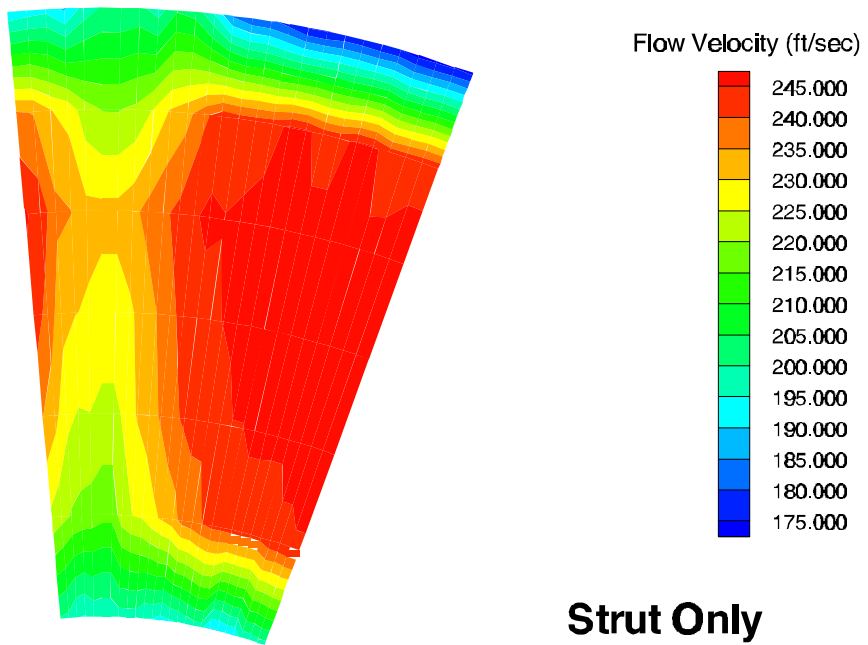
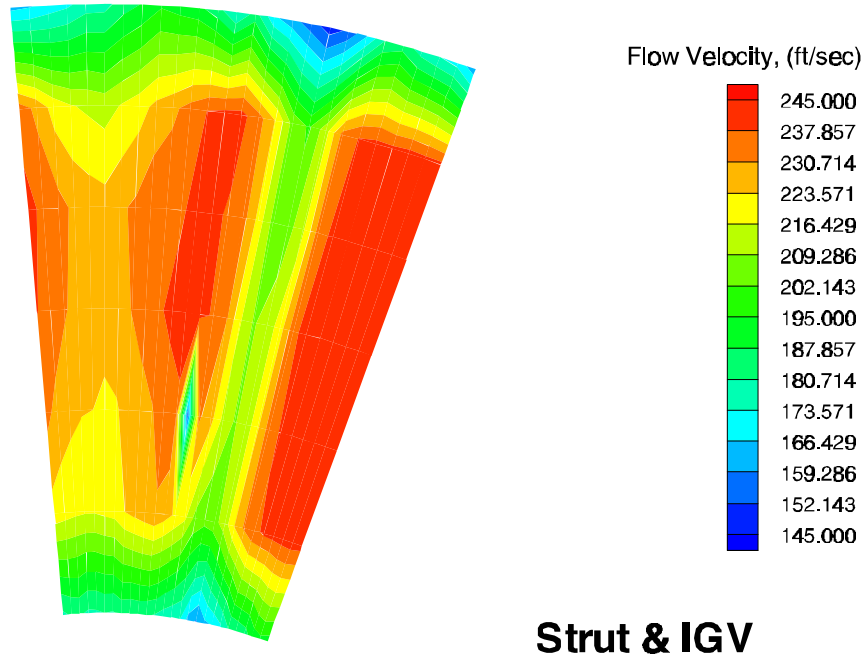


Figure 4.13: Contour Plot of Fan Face Velocity

5.0 Conclusions

The research performed in this thesis examined the effectiveness of trailing edge blowing (TEB) for the reduction of fan noise in supersonic commercial aircraft engines. TEB was utilized in these experiments to re-energize the wakes of upstream flow disturbances and thereby reduce the flow distortion at the fan face. Previous work has already shown that decreasing the fan face circumferential distortion will reduce the tone noise. The focus of the experiments is a candidate inlet for the High Speed Civil Transport (HSCT) aircraft. The inlet is an axisymmetric supersonic inlet with upstream struts for structural support from which TEB is implemented. The struts were designed to allow for the ejection of high pressure air from the trailing edge of the strut. The purpose of the TEB is to re-energize the wake of the strut to reduce the fan face distortion seen by the engine. Acoustic tests were performed with and without IGV in the Virginia Tech Anechoic Chamber at speeds of 30,000 RPM (40 PNC), 50,000 RPM (60 PNC) and 70,000 RPM (88 PNC). The test speed of 50,000 RPM corresponds to landing speed, and 70,000 RPM corresponds to landing speed.

The experiments can be classified into two categories. The first case did not include the IGV in the inlet. For this case, TEB reduced the Blade Passing Tone (BPT) at 30,000 RPM and 50,000 RPM. At 70,000 RPM, TEB did not significantly reduce the sound pressure levels due to multiple pure tones from blade tip shock waves. The second case included the IGV in the inlet. The IGV reduced the effectiveness of TEB in

reducing the BPT at both 30,000 RPM and 50,000 RPM. At 70,000 RPM (88 PNC), TEB did not change the sound pressure levels measured. Table 5.1 is a summary of the noise reductions due of TEB from the strut.

Table 5.1: SPL Reductions due to TEB

	30,000		50,000		70,000	
	Without IGV	With IGV	Without IGV	With IGV	Without IGV	With IGV
Tone	3.1	0.5	1.9	1.1	0.9	-0.1
1st Harmonic	0.9	0.0	1.2	1.0	0.2	0.4
Overall	0.6	0.0	0.4	0.4	0.3	0.0

In these experiments it important that the struts were chosen for the TEB. The addition of the IGV added a third and dominating noise source to inlet. The IGV reduced the effectiveness of TEB from the struts because the wakes that were being removed by TEB were not as large as the wakes created by the IGV. This problem is easily seen by aerodynamic surveys of the wakes behind the struts and the IGV at the fan face of the inlet. Due to manufacturing restraints it was not possible to modify the IGV for TEB. If the Boeing Translating Inlet was being considered for full scale implementation of TEB for fan noise reduction, the strength of the fan face distortion caused by the IGV would make the IGV a prime candidate for TEB. Although full scale IGV would turn the flow, Waitz et al. (1995) have shown that the velocity defect does not have to be fully re-energized to see reductions in turbulence and therefore acoustic benefits.

The effectiveness of trailing edge blowing for use in supersonic aircraft inlets to reduce fan noise generated at the blade passing frequency has been shown with a 1/14th scale model acoustic test. Future research into trailing edge blowing as a method of fan noise reduction can be focused to take advantage of the conditions where TEB is most effective. Trailing edge blowing was very effective when the struts were the only source of fan noise. The addition of other strong noise sources in the inlet reduced the reductions seen in the blade passing tone.

Trailing edge blowing in 1/14th scaled model of an aircraft engine inlet validates the capabilities of the technology for noise reduction under the right circumstances. The scaled model tests do not take into consideration the complexities of implementing a technology in a working gas turbine. Therefore, the end goal of these and any future experiments would be to modify a working gas turbine with trailing edge blowing on rotors or stators to examine the noise reduction capabilities of TEB in full scale.

References

Corcoran, Timothy, "Control of the Wake from a Simulated Blade by Trailing Edge Blowing," Masters Thesis, Mechanical Engineering Department, Lehigh University, 1992.

Detwiler, K.P. "Reduced Fan Noise Radiation from a Supersonic Inlet," Masters Thesis, Mechanical Engineering Department, Virginia Polytechnic Institute & State University, Blacksburg, Virginia, April 1993.

Johnson, R. T., Fleeter, S., "Inlet Guide Vane Wakes, Including Rotor Effects", ASME 95-GT-436, June 1995.

Kinsler, L.E., Frey, A.R, Coppens, A.B., and Sanders, J.V. Fundamentals of Acoustics. 3rd ed. New York: John Wiley & Sons, 1982.

Lakshminarayana, B., Davino, R., "Mean Velocity and Decay Characteristics of the Guidevane and Stator Blade Wake of an Axial Flow Compressor", ASME 79-GT-9, April, 1979.

Miller, K. C., "Comparison of the Aeroacoustics of Two Small-Scale Supersonic Inlets", Masters Thesis, Mechanical Engineering Department, Virginia Polytechnic Institute and State University, August 1996.

Model 460 Turbofan Propulsion Simulator Products Specification, Tech Development Inc., U.S. Patent 3434679.

Naumann, R. Georg, "Control of the Wake from a Simulated Blade by Trailing Edge Blowing," Masters Thesis, Mechanical Engineering Department, Lehigh University, 1992.

Nuckolls, W. E., Ng, W. F., "Fan Noise Reduction from a Supersonic Inlet during Simulated Aircraft Approach", ASME 93-GT-279, May 1993

Pande, A., Ng, W. F., "Effects of Struts on the Aeroacoustics of Axisymmetric Supersonic Inlets," Masters Thesis, Mechanical Engineering Department, Virginia Polytechnic Institute and State University, November 1994.

Trefney, C.J., Wasserbauer, J.W. "Low-Speed Performance of an Axisymmetric, Mixed-Compression, Supersonic Inlet with Auxiliary Inlets," NASA TP-2557, February 1986.

Tyler, J. M., and Sofrin, T.G., "Axial Compressor Noise Studies," SAE Transactions, Vol. 70, 1962.

Wagner, R. "Aeroacoustics of the Bifurcated 2D Supersonic Inlet," Masters Thesis, Mechanical Engineering Department, Virginia Polytechnic Institute & State University, Blacksburg, Virginia, December 1994.

Waitz, I. A., Brookfield, J. M., Sell, J., Hayden, B., J., "Preliminary Assessment of Wake Management Strategies for Reduction of Turbomachinery Fan Noise", CEAS/AAIA-95-102, June 1995.

Appendix A: Comparison of Strut Shapes and their Effects on Far Field Noise Levels

In evaluating the geometric model used in the experiments, several questions were raised. The first question is quantifying the acoustic impact of using of faceted shaped struts instead of airfoil shaped struts. The faceted struts are easier and cheaper to manufacture, however, the airfoil shape is the profile found in a working aircraft engine. An isometric view of each strut is found in figure A.1. Two sets of struts were manufactured. Acoustic tests were performed using each set of struts in the Boeing Translating Inlet without the presence of inlet guide vanes (IGV). Acoustic measurements were taken at all twelve radial positions at 50,000 RPM (60 PNC) and 70,000 RPM (88 PNC). While the modal analysis of the struts is not defined, these tests provide an insight into the use of faceted struts to simulate airfoil shaped struts.

Experiments were performed in the Virginia Tech Anechoic Chamber to evaluate the acoustic impact of the strut shape. The experiments were run at a speed of 50,000 RPM (60 PNC) and 70,000 RPM (88 PNC) to examine the effects of subsonic and supersonic blade tip speeds. Figure A.2 shows the radiation directivity of the faceted and airfoil struts at 50,000 RPM (60 PNC). Figure A.3 shows the radiation directivity of the faceted and airfoil struts at 70,000 RPM (88 PNC).

At 50,000 RPM, the faceted struts generated higher sound pressure levels. Table A.1 shows that the tone and 1st harmonic were increased by an average of 2.4 dB and 1.5

dB respectively. The increases were not at every location, but at angles where the struts have been seen to be a dominant noise source.

At 70,000 RPM, the struts made very little difference to the tone and 1st harmonic sound pressure levels. The BPT was increased by an average of 0.14 dB while the tone decreased by an average of 1.5 dB.

The experiments performed with the faceted and airfoil shaped struts indicate that the struts have a stronger influence on the tone noise levels at 50,000 RPM than at 70,000 RPM. The BPT was increased 2.4 dB at 50,000 RPM because of the strut shape, the BPT was only increased by 0.14 dB at 70,000 RPM. The comparison of the far field acoustics of the strut shape indicate that faceted struts are not acoustically the same as airfoil struts at 50,000 RPM, but are very similar at 70,000 RPM.

Table A.1: Acoustic comparison of Faceted and Airfoil Struts at 50,000 RPM

Faceted - Airfoil	Tone SPL	1st Harmonic SPL	Overall SPL
Microphone Angle	dB	dB	dB
0°	2.2	-6.0	-0.1
10°	5.0	5.8	3.8
20°	0.1	1.6	1.5
30°	2.3	0.5	1.4
40°	2.8	2.5	1.9
50°	-5.4	1.7	-1.3
60°	-0.2	3.3	0.3
70°	-7.0	-1.5	-3.3
80°	0.9	-1.4	-2.5
90°	7.5	-2.1	-2.5
100°	2.4	0.6	-1.1
110°	1.9	2.8	-3.8
<i>Average dB</i>	<i>2.43</i>	<i>1.54</i>	<i>0.12</i>

Table A.2: Acoustic comparison of Faceted and Airfoil Struts at 70,000 RPM

Faceted - airfoil	Tone SPL	1st Harmonic SPL	Overall SPL
Microphone Angle	dB	dB	dB
0°	-3.0	-0.9	0.8
10°	-0.3	-1.9	0.7
20°	1.6	-0.7	1.5
30°	2.5	-1.0	1.4
40°	1.7	-4.6	-2.4
50°	1.1	-1.5	0.6
60°	-3.4	-3.4	-0.1
70°	-4.1	-2.8	-2.2
80°	-7.4	-3.7	-3.0
90°	-9.3	-3.9	-4.0
100°	-2.4	2.7	-1.9
110°	5.1	-1.9	-2.4
<i>Average dB</i>	<i>0.14</i>	<i>-1.50</i>	<i>-0.55</i>

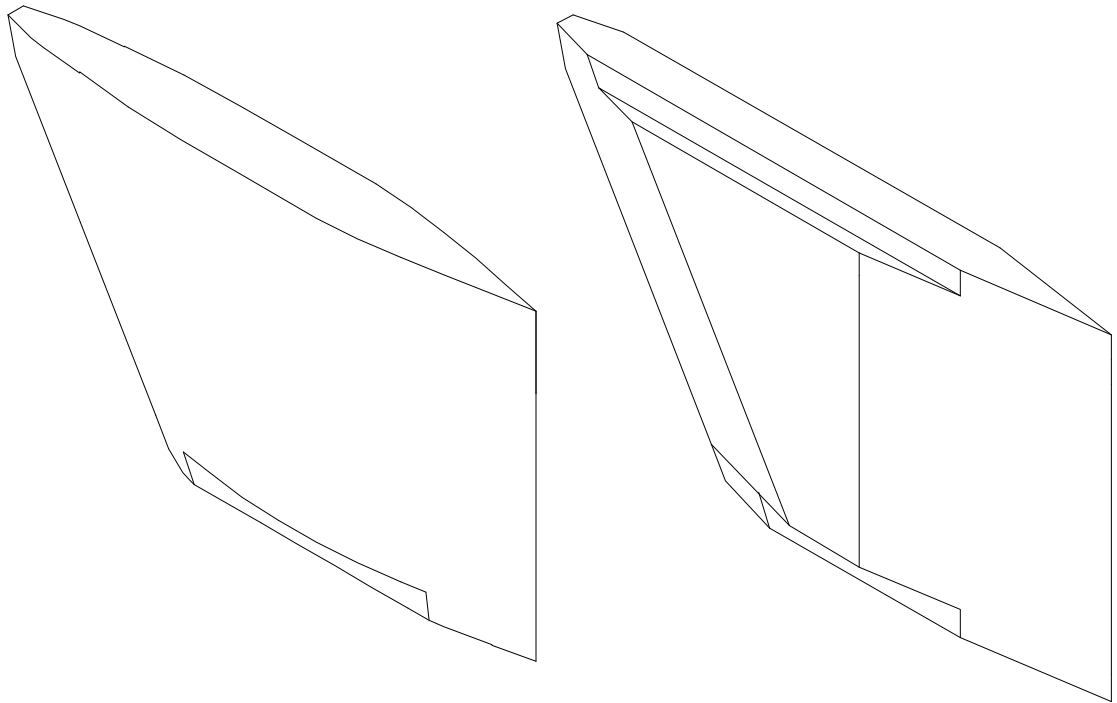


Figure A.1: Isometric views of the VPI Faceted Strut and the Boeing Airfoil Strut

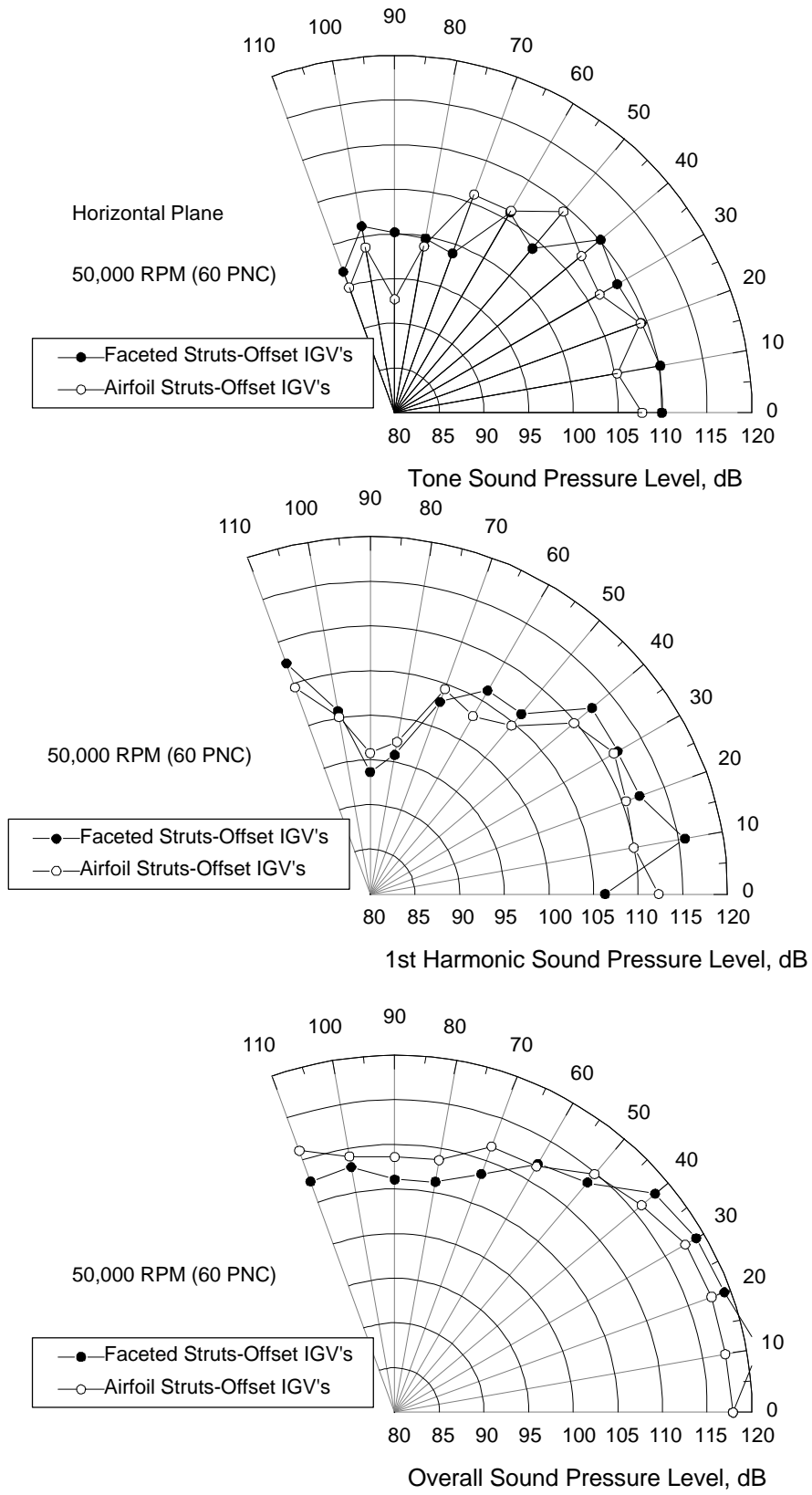


Figure A.2: Radiation Directivity of Faceted and Airfoil Struts at 50,000 RPM (60 PNC)

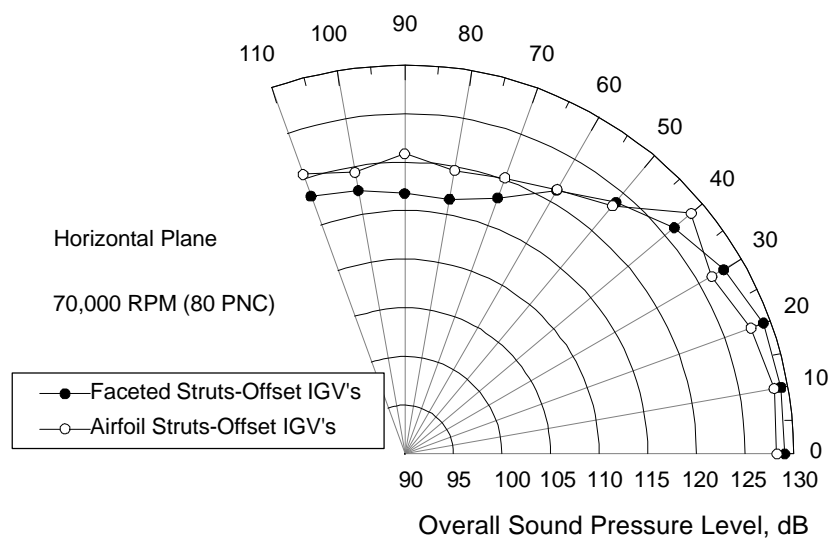
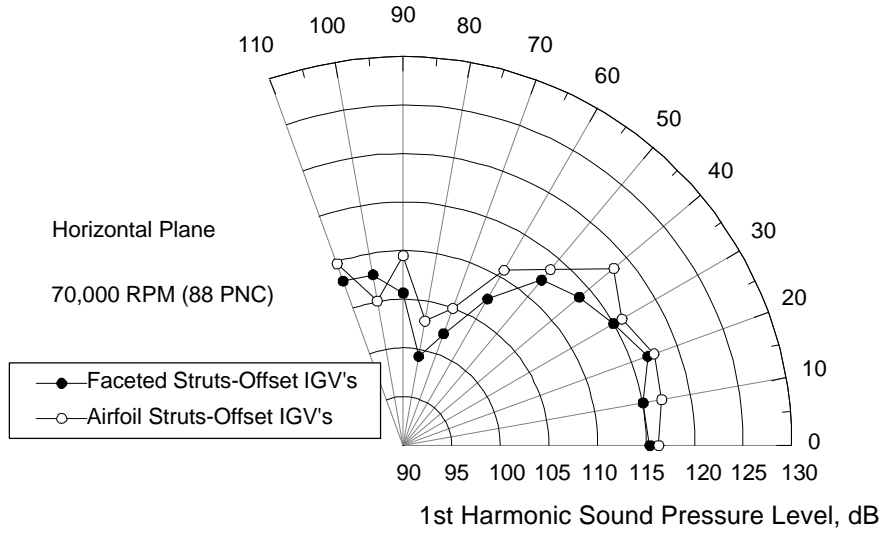
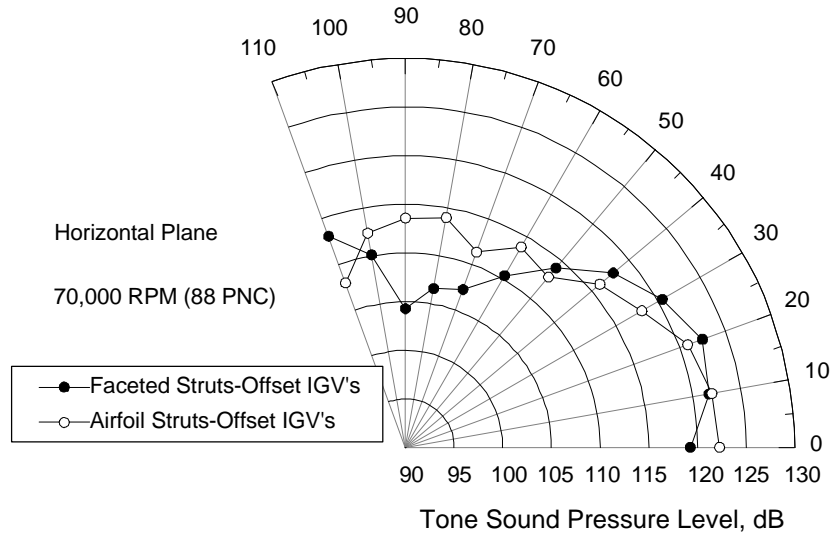


Figure A.3: Radiation Directivity of Faceted and Airfoil Struts at 70,000 RPM (88 PNC)

Appendix B: The Acoustic Effects of Struts and IGV Rotational Clocking

The experiments which were performed involved the wakes of two upstream flow disturbances. Because of the flexibility of the inlet model, the inlet guide vane (IGV) assembly is capable of being rotated or clocked to align or offset the strut wakes. Figure B.1 shows the two extreme cases of IGV / Strut Clocking. Acoustic experiments were performed at speeds of 50,000 RPM (60 PNC) and 70,000 RPM (88 PNC) with the Boeing Translating Inlet using the two IGV rotational arrangements.

At 50,000 RPM (60 PNC), the aligning of the strut and IGV wakes increased the measured sound pressure levels. Table A.1 catalogs the difference in the measure Blade Passing Tone (BPT) at each angle. By aligning the strut and IGV wakes, the BPT was increase by an average of 3.9 dB and a maximum of 10.7 dB. The 1st harmonic of the BPT saw similar increases in sound pressure levels. The 1st harmonic was increased by a maximum of 7.2 dB and an average of 2.2 dB. This increase likely due to the larger wakes created by the interaction between the wakes of the struts and IGV. It is also interesting to note that at some angles, the BPT was decreased. This is possibly due to the breakup of the IGV symmetry which caused some modes to be less present in the acoustic radiation directivity.

Table B.1: BPT SPL increases at 50,000 RPM due to strut and IGV aligning

Microphone Angle	Tone SPL	Tone SPL	dB Difference
	Offset IGV	Aligned IGV	
	dB	dB	dB
0°	107.7	107.8	-0.1
10°	105.3	109.5	-4.3
20°	109.3	109.4	-0.1
30°	106.5	107.2	-0.8
40°	107.3	109.2	-1.9
50°	109.4	101.5	7.9
60°	106.1	104.0	2.1
70°	106.0	102.0	4.0
80°	98.9	101.9	-3.1
90°	92.7	103.3	-10.7
100°	98.8	96.4	2.5
110°	94.9	103.0	-8.1
<i>Average dB</i>	<i>105.87</i>	<i>106.12</i>	<i>-3.88</i>

Table B.2: 1st Harmonic SPL increases at 50,000 RPM due to strut and IGV aligning

	1st Harmonic SPL	1st Harmonic SPL	
	Offset IGV	Aligned IGV	dB Difference
Microphone Angle	dB	dB	dB
0°	112.3	107.9	4.5
10°	110.0	115.6	-5.6
20°	110.5	116.3	-5.8
30°	111.5	108.2	3.3
40°	109.8	111.0	-1.1
50°	104.6	111.8	-7.2
60°	103.0	104.1	-1.1
70°	104.4	99.7	4.8
80°	97.3	94.9	2.4
90°	95.8	99.1	-3.3
100°	100.1	97.7	2.4
110°	104.6	99.1	5.5
<i>Average dB</i>	<i>107.95</i>	<i>110.20</i>	<i>-2.21</i>

At 70,000 RPM (88 PNC), the combining of the wakes of the struts and IGV have less of an effect. The BPT is increased by only an average of 1.35 dB. Also, the maximum increase measured was 5.4 dB while the sound pressure levels were reduced at one angle by 9.1 dB. The first harmonic showed very little effect of aligning the stators and IGV with an decrease of 0.6 dB. The effects of aligning the strut and IGV wakes are minimal at 70,000 RPM because there are other larger factors affecting the tone noise.

Similar to the comparing of the strut shape in appendix A, the aligning of the wakes of the struts and IGV increased the measured BPT and 1st harmonic of the BPT at 50,000 RPM. The effects of the wakes was decreased at 70,000 RPM. in both the BPT and the 1st harmonic of the BPT.

Table B.3: BPT SPL increases at 70,000 RPM due to strut and IGV aligning

	Tone SPL	Tone SPL	dB Difference
	Offset IGV	Aligned IGV	
Microphone Angle	dB	dB	dB
0°	122.3	117.7	4.6
10°	122.0	122.9	-0.9
20°	120.9	119.8	1.2
30°	118.1	118.9	-0.9
40°	116.1	118.6	-2.5
50°	112.9	113.0	0.0
60°	113.8	113.8	0.0
70°	111.4	112.9	-1.5
80°	114.0	104.9	9.1
90°	113.6	116.4	-2.8
100°	112.4	117.9	-5.4
110°	108.0	111.2	-3.2
<i>Average dB</i>	<i>117.57</i>	<i>117.56</i>	<i>-1.35</i>

Table B.4: 1st Harmonic of BPT SPL increases at 70,000 RPM due to strut and IGV aligning

	1st Harmonic SPL	1st Harmonic SPL	dB Difference
	Offset IGV	Aligned IGV	
Microphone Angle	dB	dB	dB
0°	116.3	116.6	-0.2
10°	117.0	116.8	0.2
20°	117.5	117.2	0.3
30°	116.0	114.8	1.2
40°	118.3	114.8	3.5
50°	113.6	113.4	0.2
60°	110.8	108.1	2.7
70°	105.0	104.8	0.2
80°	103.0	103.6	-0.6
90°	109.5	106.6	3.0
100°	105.1	109.6	-4.5
110°	109.9	108.7	1.2
<i>Average dB</i>	<i>114.25</i>	<i>113.37</i>	<i>0.06</i>

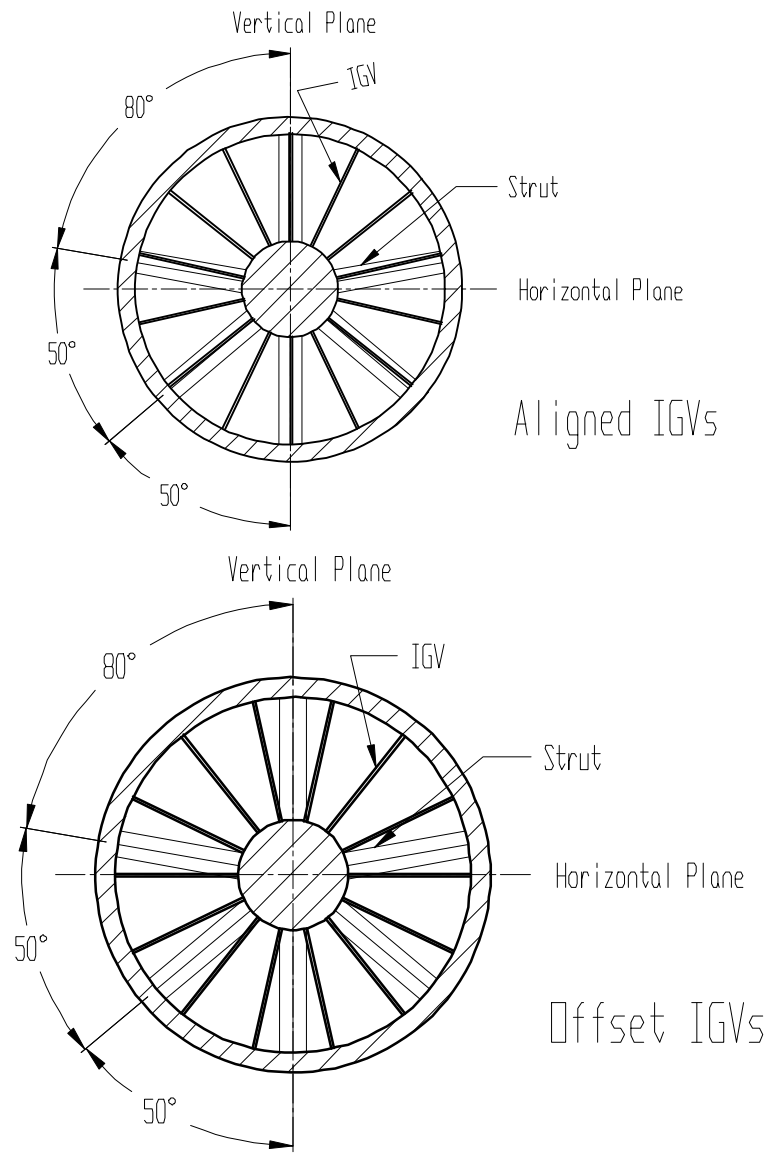


Figure B.1: Inlet Guide Vane / Strut Clocking positions

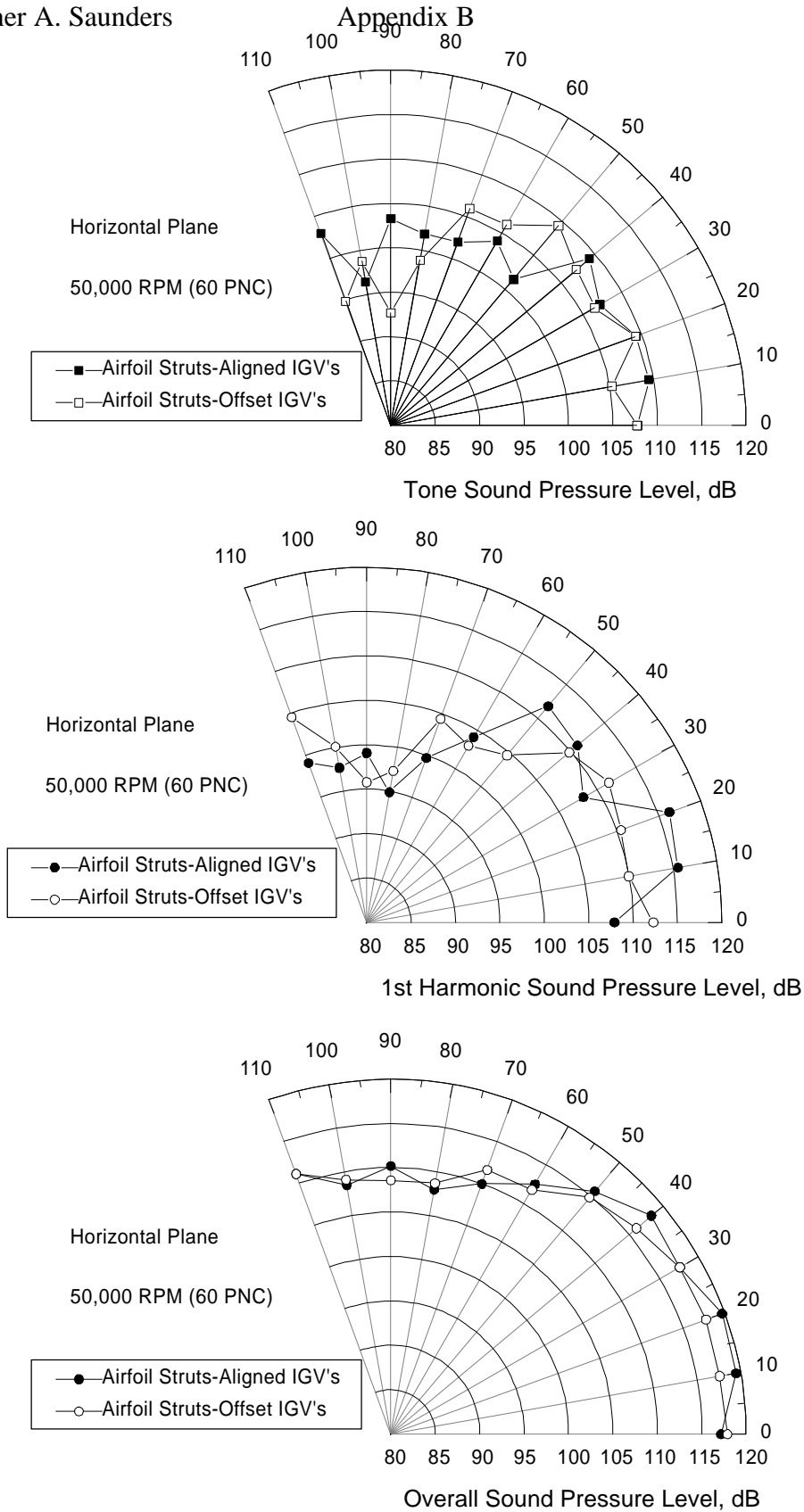


Figure B.2: Acoustic Radiation Directivity of Aligned and Offset IGVs at 50,000 RPM

Appendix B

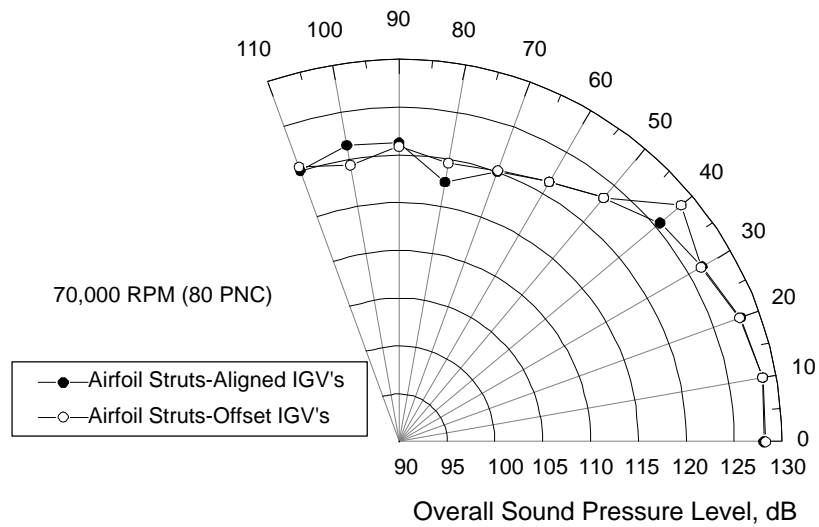
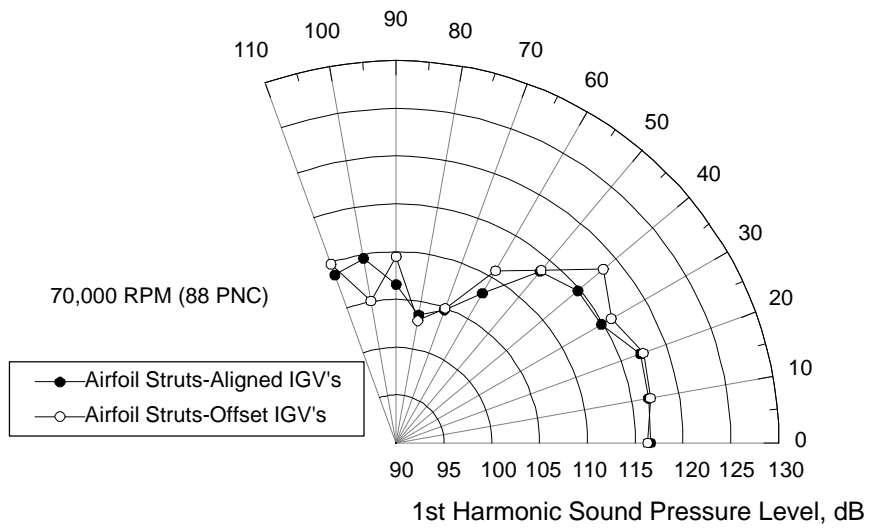
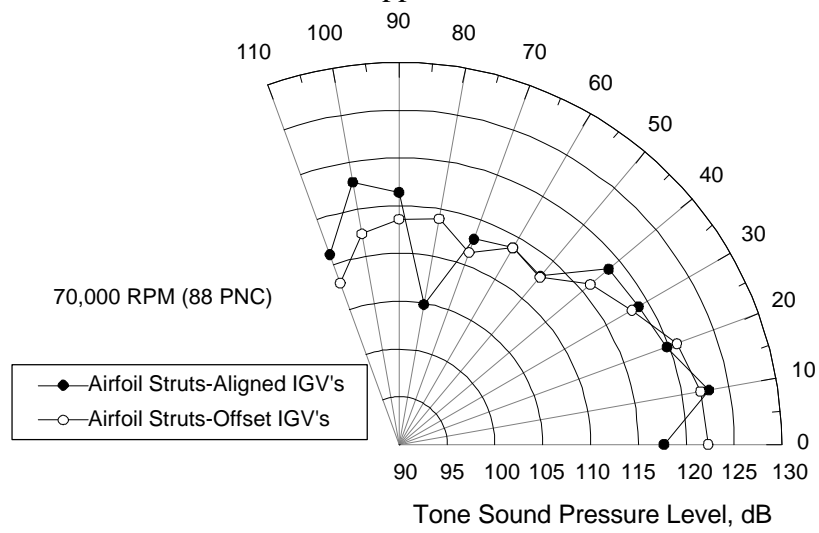


Figure B.3: Acoustic Radiation Directivity of Aligned and Offset IGV's at 70,000 RPM

Appendix C: Comparison of Symmetric Strut Patterns to Asymmetric Strut Patterns

In order to understand the effects of the asymmetric strut pattern, the Boeing Translating Inlet was tested in the Anechoic chamber with a symmetric strut pattern. The strut patterns are shown in figure C.1. The tests were conducted at 50,000 RPM (60 PNC) with Inlet Guide Vanes (IGV). The symmetric struts are advantageous to use since they can be used with the exact same hardware as the asymmetric struts.

The modal analysis of the symmetric strut / rotor interactions is straightforward. The modes that can be produced according to the Tyler and Sofrin model are $m = 0$, $m = 6$ and $m = 12$. Table C.1 details the modes present and the major lobe angles predicted.

Acoustic tests were conducted in the anechoic chamber at 50,000 RPM for both the symmetric strut pattern and the asymmetric strut pattern. The directivity plots for the Blade Passing Tone (BPT) is shown in figure C.2. The sound pressure levels measured at the BPT are very similar except for several angles where there is a distinct difference. The first angle that is noticeably different is the axisymmetric mode, $m = 0$. The asymmetric strut pattern reduced the axisymmetric mode as is seen in the reduction of 8.2 dB in the BPT at 0° . While the asymmetric strut pattern reduced the 0° location, it increased the BPT at 20° , 50° and 60° . The increases are most likely due to modes that the asymmetric strut pattern is exciting. Although the exact circumferential modes that are being radiated are not determined by this experiment, it is possible to see that at 20° ,

50° and 60°, the axisymmetric strut pattern is exciting acoustic modes that are not excited with the symmetric strut pattern.

Table C.1: Summary of Acoustic Analysis of the Symmetric Strut Pattern

	Summary of Acoustic Analysis for Symmetric Struts					
	30,000	RPM	50,000	RPM	70,000	RPM
	M	ψ_p	M	ψ_p	M	ψ_p
BPF	(6,0)	60°	(6,0)	31°	(6,0)	22°
			(6,1)	51°	(6,1)	34°
					(6,2)	46°
					(6,3)	65°
1st Harmonic	(6,0)	26°	(6,0)	15°	(6,0)	11°
	(6,1)	41°	(6,1)	23°	(6,1)	16°
	(6,2)	60°	(6,2)	31°	(6,2)	22°
			(6,3)	42°	(6,3)	28°
			(6,4)	56°	(6,4)	36°
					(6,5)	45°
					(6,6)	56°

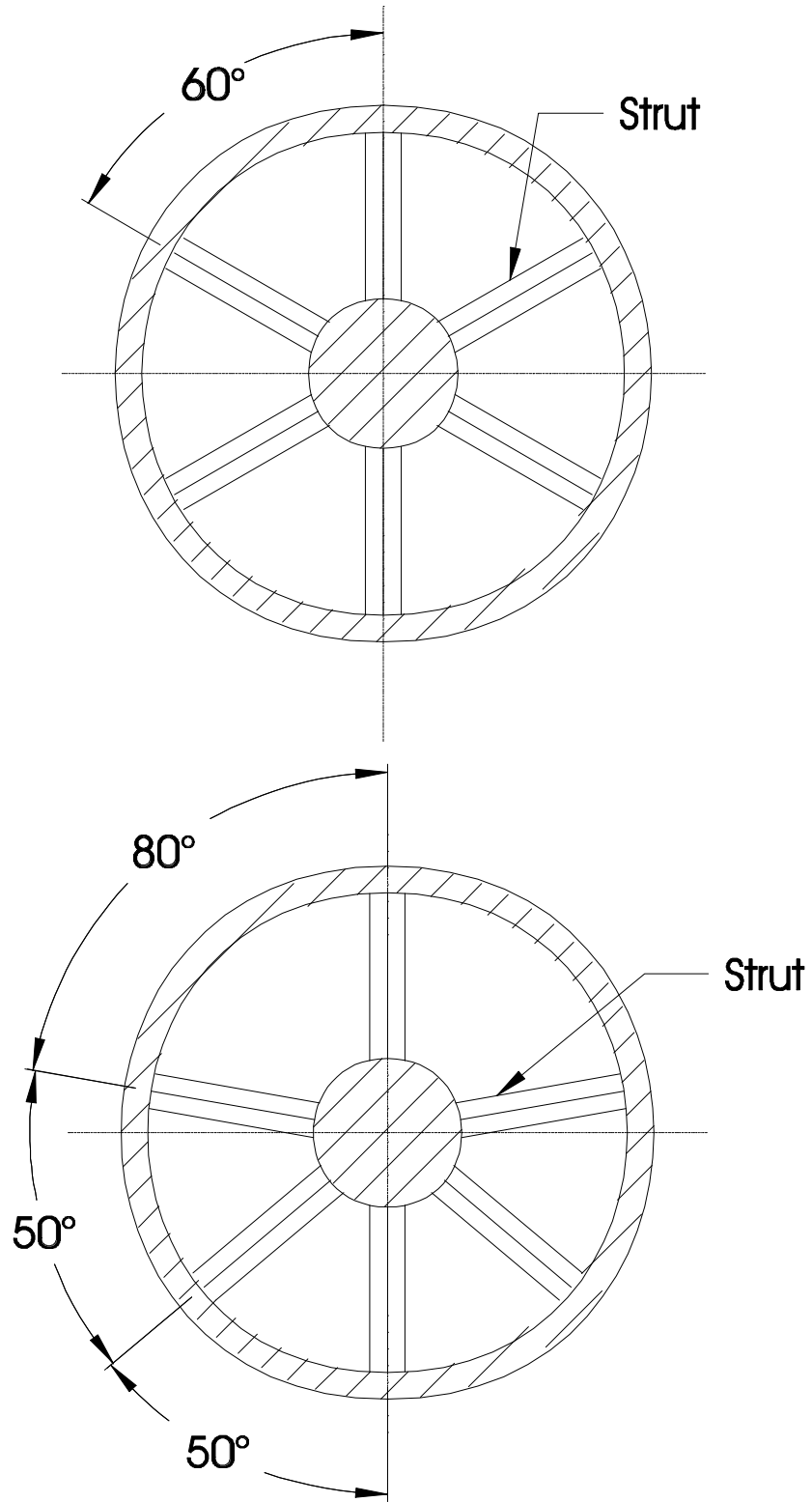


Figure C.1: Symmetric and Asymmetric Strut Patterns

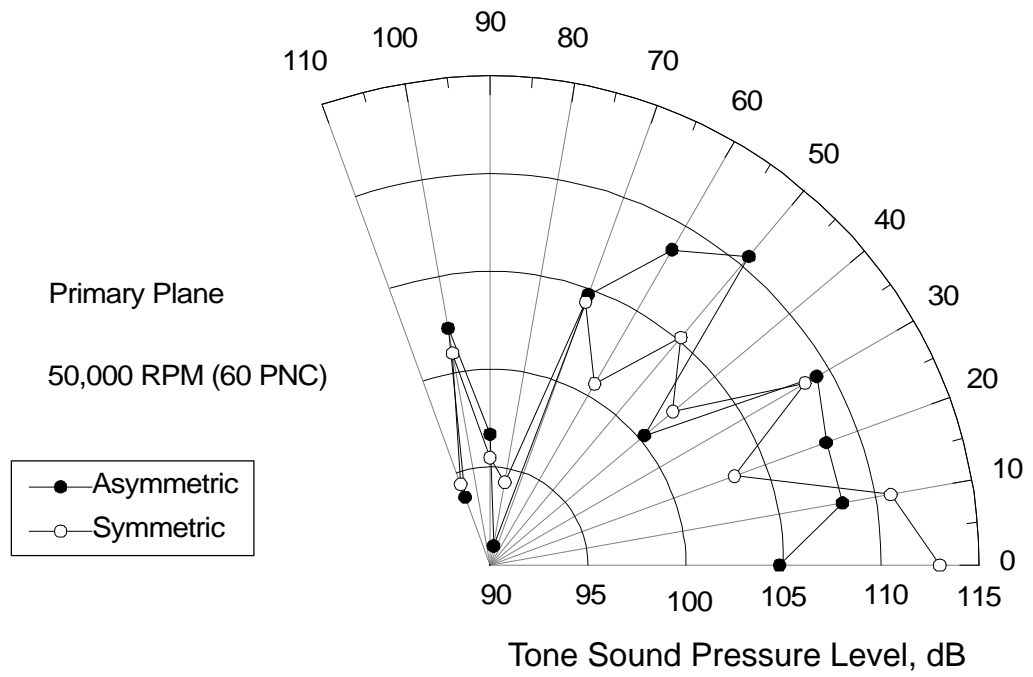


Figure C.2: Acoustic Comparison of Asymmetric and Symmetric Strut Patterns

Appendix D: Anechoic Chamber Aerodynamic Measurements

Aerodynamic measurements were taken in the anechoic chamber to examine the reduction in fan face distortion due to trailing edge blowing (TEB). The Boeing Translating Inlet was modified to allow a 0.125 in. (0.318 mm) diameter pitot static probe to radially traverse in the inlet during testing. The measurements taken with the pitot static probe can be used to calculate a flow velocity. The testing speeds used were 30,000 RPM (40 PNC), 50,000 (60 PNC), and 70,000 RPM (88 PNC). The locations of the radial traverses behind the strut are shown in figure D.1. Seven radial measurement positions were used for each circumferential traverse. Three circumferential traverses were also performed at 25%, 50% and 75% of the strut height as shown in figure D.2. Each traverse was conducted with TEB and without TEB. The inlet guide vanes (IGV) were removed for the anechoic chamber aerodynamic tests.

Figure D.3 shows the results of the radial traverse behind a strut at 30,000 RPM, 50,000 RPM and 70,000 RPM. Each of the testing speeds shows that near 70% of the strut height, the probe is directly behind a TEB jet and picks up the high velocities from the jet. Figure D.4 shows the three circumferential traverses at the 25%, 50% and 75% of the strut height. The mixing of the flow behind the strut because of TEB was very complicated. During the aerodynamic survey, it was apparent that the six discrete jets did not mix well with the wake. Due to limited data points taken and a spatial resolution

problem, the aerodynamic measurements did not fully capture what was happening at the fan face of the inlet.

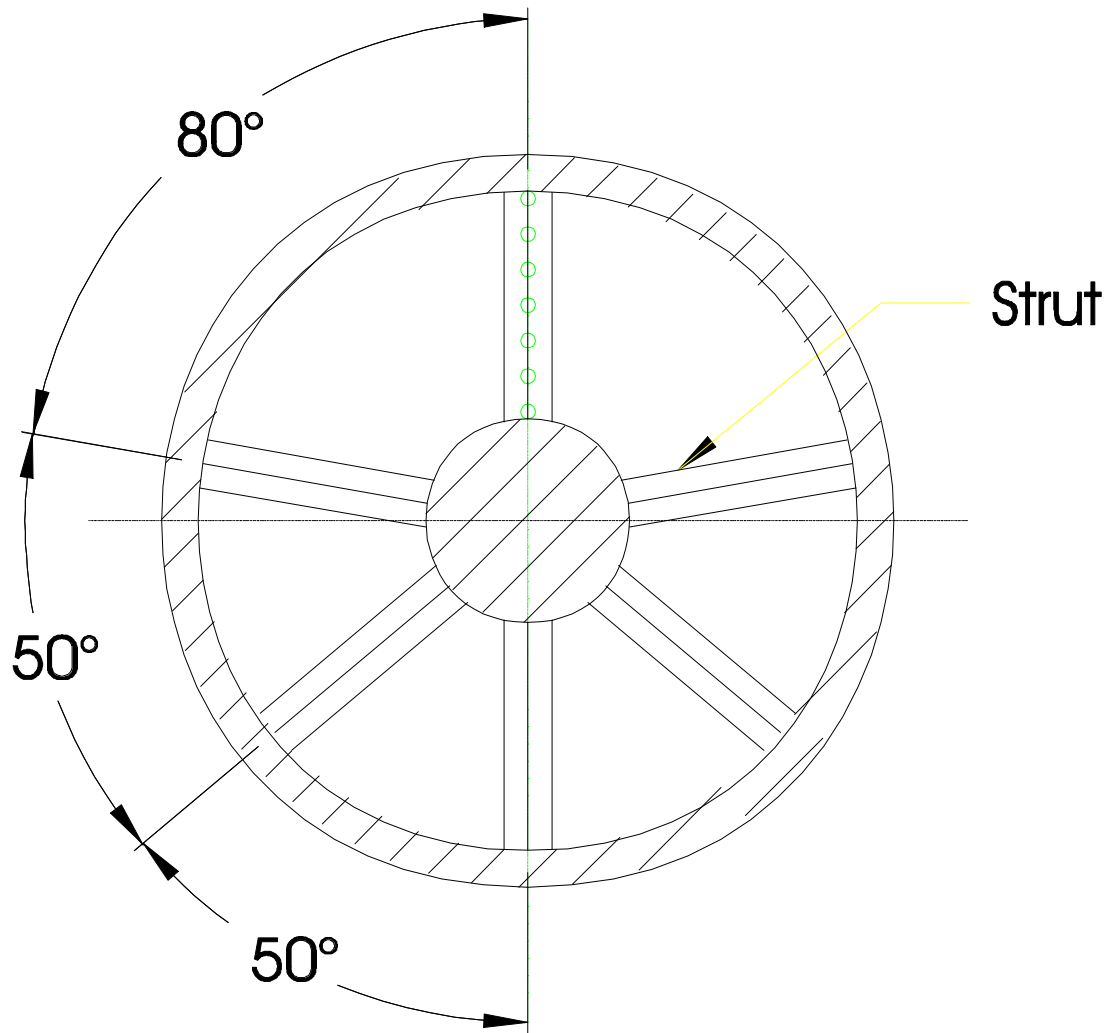


Figure D.1: Aerodynamic Measurement Locations

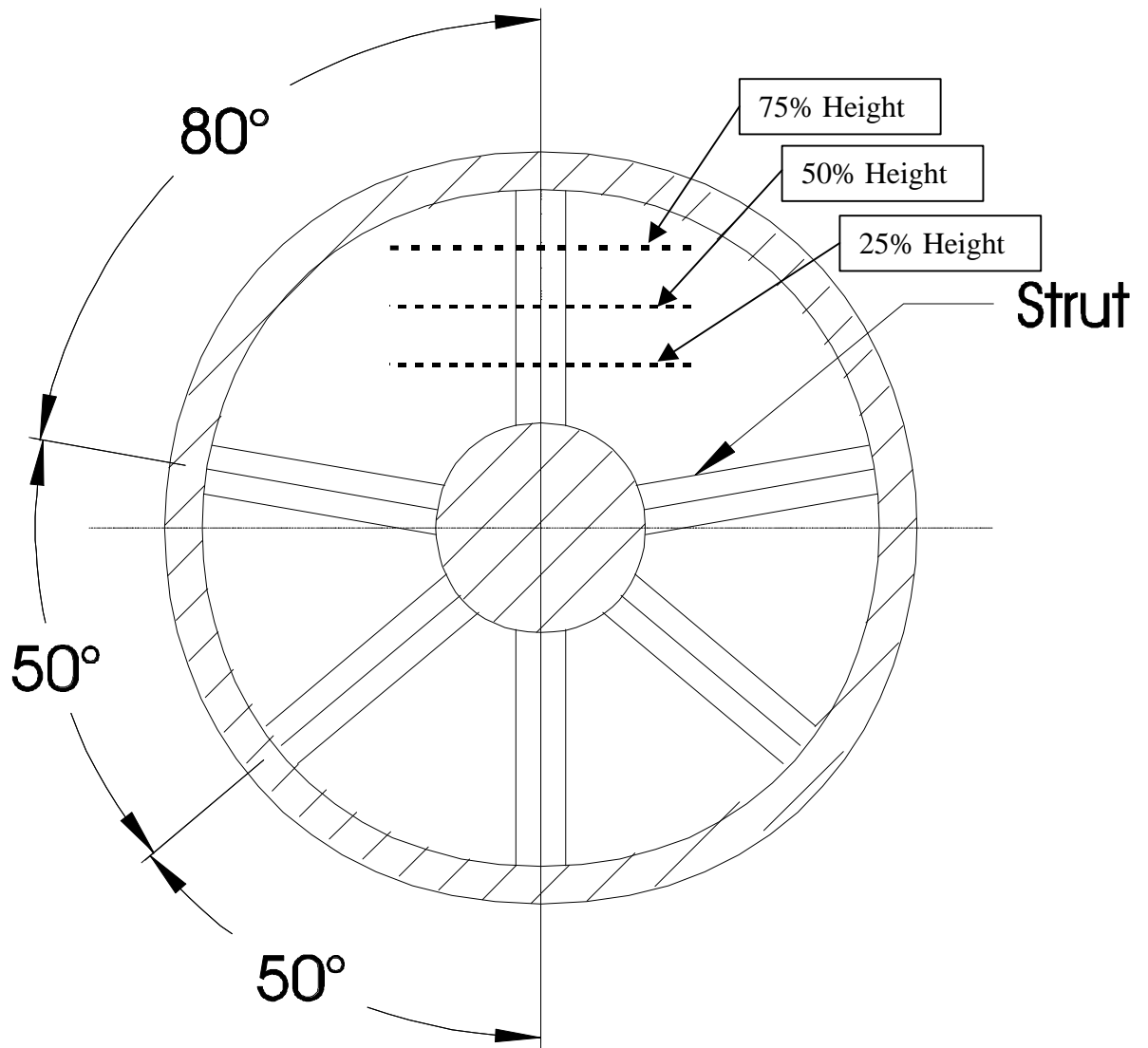


Figure D.2: Circumferential Aerodynamic Measurement Positions

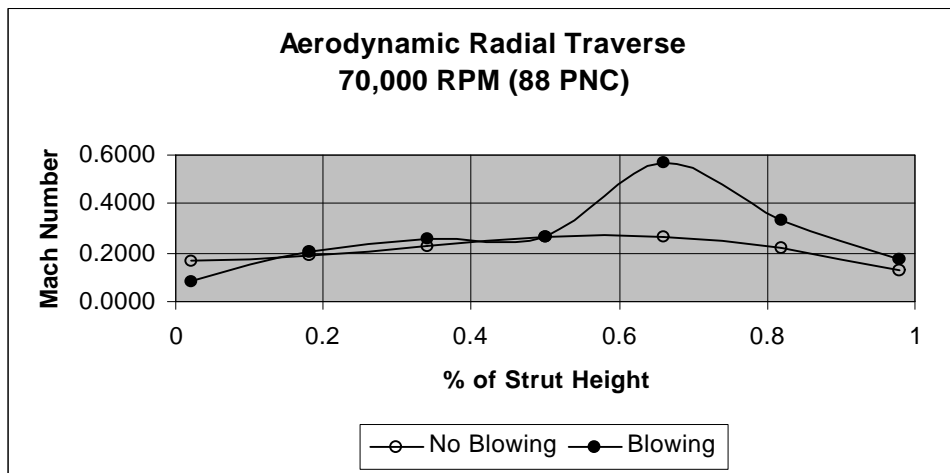
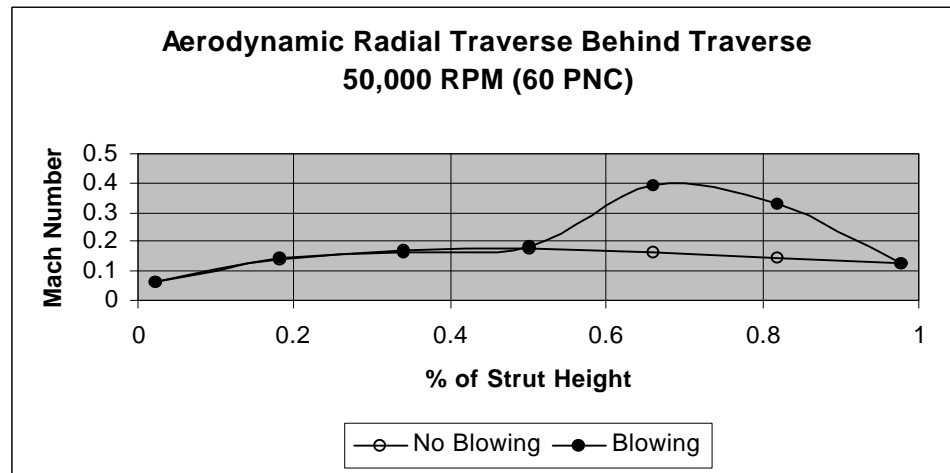
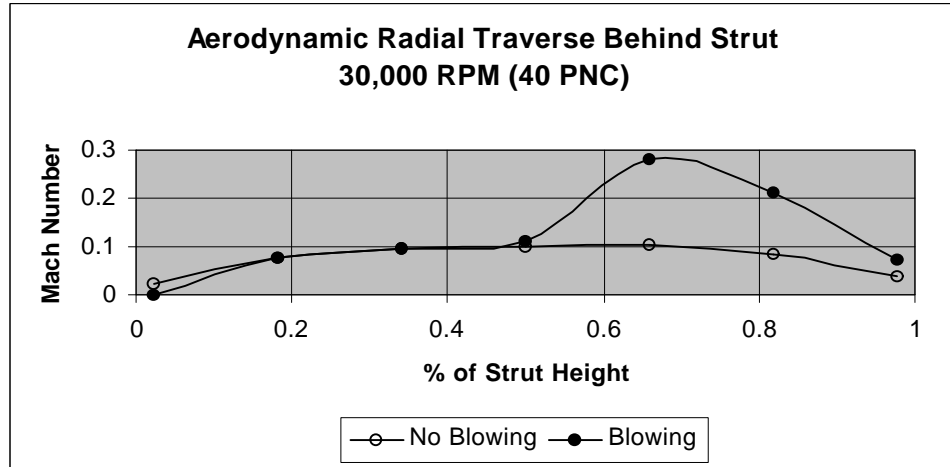


Figure D.3: Aerodynamic Radial Traverses

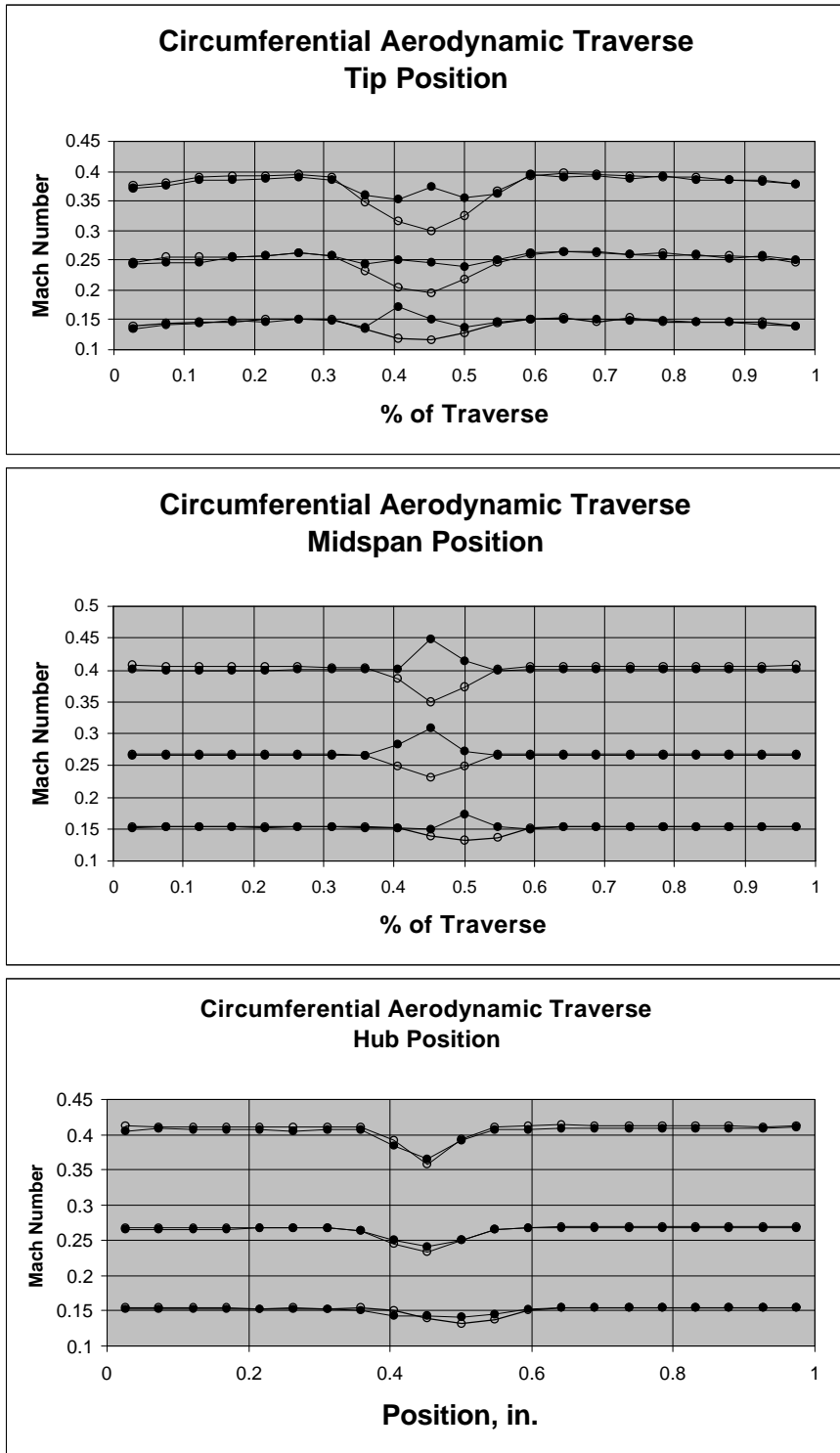


Figure D.4: Circumferential Aerodynamic Traverses

Appendix E: Bench Design Tests

A bench setup was used to evaluate the designs for implementing the trailing edge blowing (TEB) on the Boeing Translating Inlet. The design evaluation process consisted of using a low speed fan to generate a flow field simulating the inlet environment. Pitot static probes were used to measure the wake generated by the strut. The jet created by the TEB was measured separately from the fan induced flow field. Finally, the strut jet and flow field were combined and measured. Leitch (1997) demonstrated that the upstream blowing pressure is not related to the shape of the jet flow created. Therefore, an arbitrary blowing pressure was used to evaluate the strut blowing designs.

Three basic design were tested that deviated from previous designs. The first design, referred to as strut #1, is shown in figure E.1a. The blowing strategy is the same as was used by Leitch (1997). It has a cylindrical cavity in the strut body and 6 varying exit holes sizes, utilizing larger holes at the tip of the strut than at the hub. The trailing edge was machined blunt. The second strut design is the previous strategy used by Leitch except with a crenulated sharp trailing edge. This strut design, referred as strut #2, is shown in figure E.1b. The crenulations are created in the trailing edge when the exit hole is drilled. The third strut design used the crenulated trailing edge and six uniform holes with the same strut cavity as the first two strut designs. This strut, referred to as strut #3, is shown in figure E.1c.

Each strut was tested with in three conditions. First, the strut was tested with the fan blower on to measure the wake. Second, the jet created by TEB was measured without the fan blower on. Third, the blower was turned on with the TEB jet and the resulting flow field was measured. Figure E.2 is a radial traverse comparison of the three designs. Figure E.3-5 are circumferential traverses comparing the re-energizing of the strut wakes on the strut design bench test.

Strut # 3 was the strut chosen for the Boeing Translating Inlet. This strut was chosen because it gave a more uniform radial velocity profile, as seen in figure E.2, and a more wake filling at the hub measurement location. The uniform blowing at the trailing edge of strut #3 is due to an increased inlet flow area to exit flow area ratio. The larger this ratio is, the more uniform the discrete jets will be. For Strut #3, the inlet area to exit area ratio is 6.26. The inlet area to exit area ratio of struts #1 and #2 is 2.2.

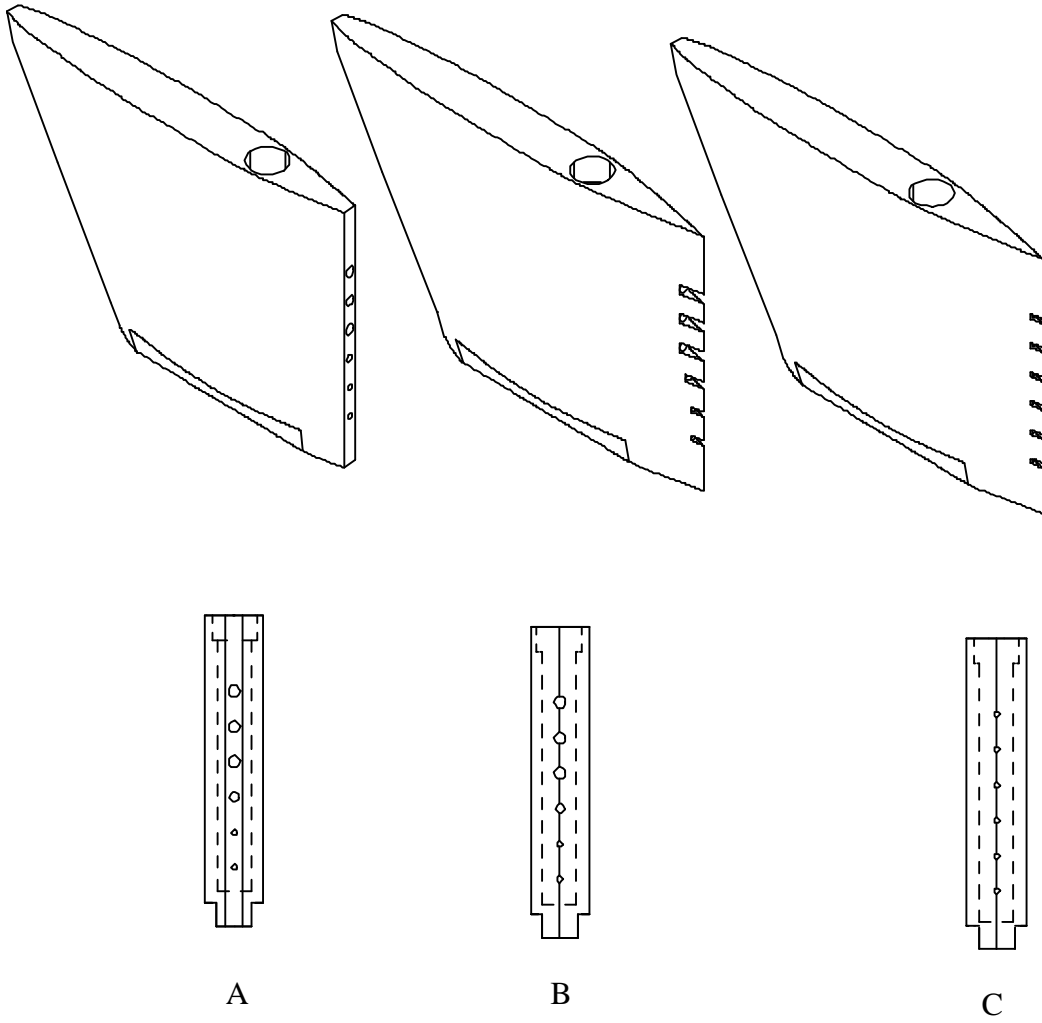


Figure E.1: Previous Strut Designs for TEB

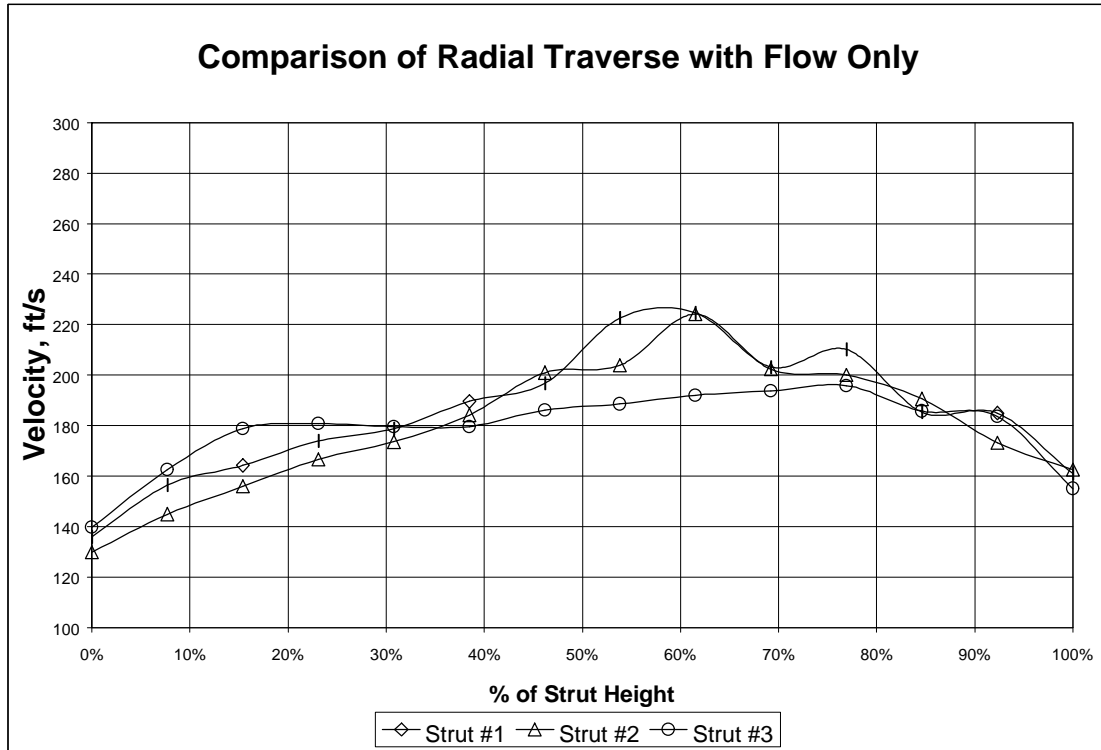


Figure E.2: Radial Traverse

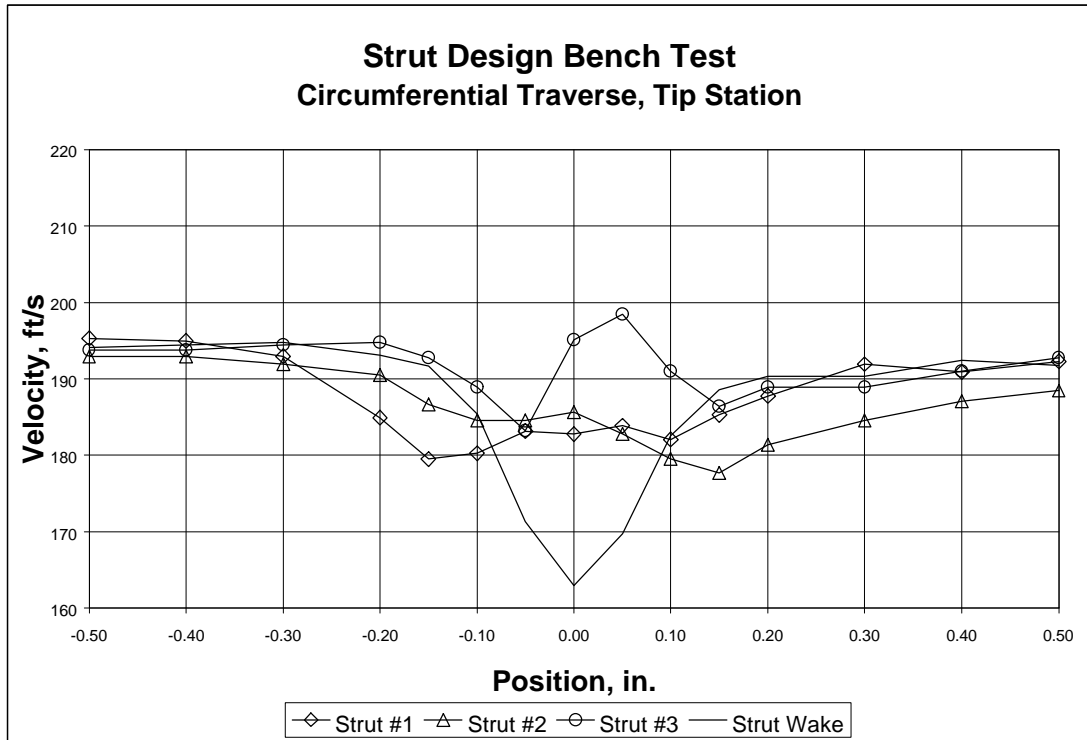


Figure E.3: Tip Circumferential Traverse

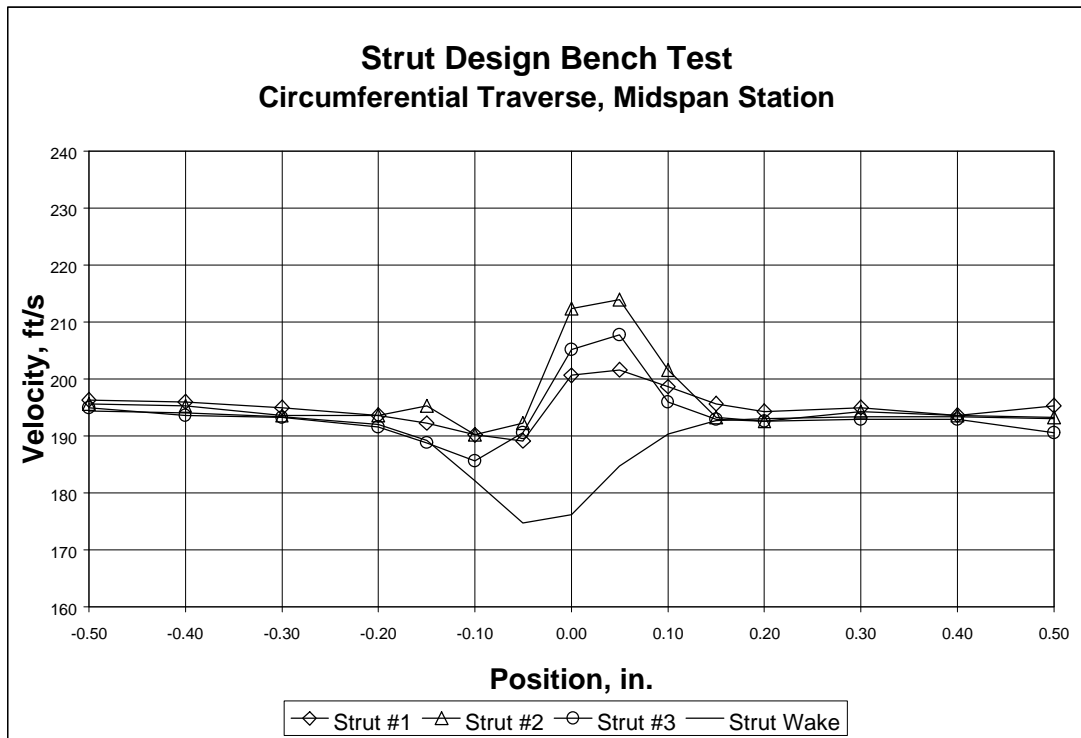


Figure E.4: Midspan Circumferential Traverse

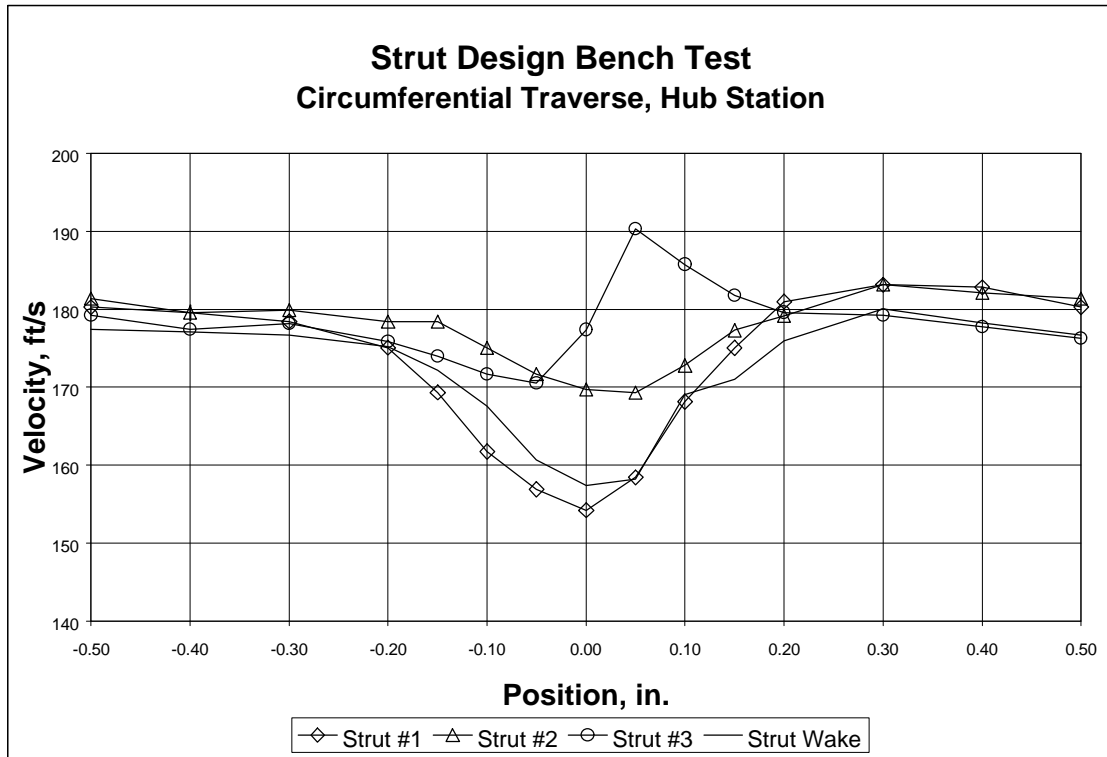


Figure E.5: Hub Circumferential Traverse

Vita

Christopher A. Saunders was born on August 17, 1973, in Arlington, Massachusetts. In 1978 after living in Ann Arbor, Michigan, for three years, he moved to Hyattsville, Maryland. After graduating from Springbrook High School in Silver Spring, Maryland, in June of 1991, Mr. Saunders began his undergraduate career at Virginia Polytechnic Institute and State University in Blacksburg, Virginia. During his undergraduate career, Mr. Saunders worked as a Mechanical Engineering Co-op for the Heat Transfer Group of the National Institute of Standards and Technology in Gaithersburg, Maryland. There he published three technical papers on moisture transfer in building envelopes and innovative testing methods for non-homogeneous insulation panels. In June of 1995, Mr. Saunders married the former Patricia Ann Kiefer of Richmond, Virginia and has loved every minute of the following years. Mr. Saunders graduated Cum Laude with a Bachelor's of Science in Mechanical Engineering from Virginia Tech in May of 1996. He then began his graduate studies under the direction of W. F. Ng. Upon completion of this degree, the author will be employed as an associate engineer by Lexmark International, Inc., in Lexington, Kentucky. The author defended his work on January 21, 1998.

Christopher A. Saunders